2017

Application of stone columns in foundations of transportation infrastructure

Pei Tai
University of Wollongong

APPLICATION OF STONE COLUMNS IN FOUNDATIONS OF TRANSPORTATION INFRASTRUCTURE

A thesis submitted in fulfilment of the requirements

for the awards of the degree

Doctor of Philosophy

from

University of Wollongong, NSW, Australia

by

Pei Tai

School of Civil, Mining and Environmental Engineering

Faculty of Engineering and Information Sciences

2017

CERTIFICATION

I, Pei Tai, declare that this thesis, submitted in fulfilment of the requirements for the award of Doctor of Philosophy, in the School of Civil, Mining, and Environmental Engineering, University of Wollongong, is wholly my work unless otherwise referenced or acknowledged. The document has not been submitted for qualifications at any other academic institution.

Pei Tai

November 2017

PUBLISHED WORK

The following publications are related to this thesis.

Tai, P., Indraratna, B., and Rujikiatkamjorn, C. (2017). "Experimental Simulation and Mathematical Modelling of Clogging in Stone Column". Canadian Geotechnical Journal, Published on the web 25 August 2017, *https://doi.org/10.1139/cgj-2017-0271.*

In preparation:

Tai, P., Indraratna, B., and Rujikiatkamjorn, C. "Laboratory assessment of the performance of stone column under partially drained cyclic loading".

Tai, P., Indraratna, B., and Rujikiatkamjorn, C. "Consolidation analysis of soft ground improved with stone column between Equal Strain and Free Strain".

ABSTRACT

Modern transportation infrastructure such as highways or high-speed railways is being built worldwide under very different ground conditions. Sometimes the foundation needs to be treated to ensure the safety of structures and vehicles. Use of stone columns, as one of the favourite ground improving methods, can shorten the drainage paths while immediately increasing the stiffness of the entire ground. They have already been proven to be effective under low to medium loads. In this thesis, the performance of ground improved by stone column under transportation infrastructure was assessed, and several issues related to the long-term behaviour were discussed through soil consolidation analysis. The effects of clogging in stone column and foundation stiffness were analysed through laboratory tests and a fully instrumented field trial in comparison with the proposed consolidation theory. Laboratory tests were also carried out to investigate the performance of stone column in a unit cell (physical model) under cyclic loading.

Clogging in stone column was assessed quantitatively using computed-tomography (CT). It is observed that the extent of clogging is substantial in the upper part of the column, but diminishes rapidly with depth. The soil properties in the clogged zone were determined indirectly, based on a series of tests of clay-aggregate mixtures with various clay contents. An “equal strain” consolidation model was developed to capture both the initial and time-dependent clogging. The model accounts for a reduction in permeability and an increase in compressibility of the column. This model offers identical results to some previous studies if clogging is ignored. Furthermore, load-settlement predictions

using the proposed model were also compared to the existing model under ‘free strain’ condition.

The stiffness of the foundation above the unit cell was included in a consolidation model to reflect the real state of ground improved with stone column, which is between “equal strain” and “free strain”. The stress distribution at the top of the unit cell varies as the shear stress in foundation layer develops. The shear stress is generated due to the occurrence of differential settlement and can be calculated through a method similar to classic “trapdoor” theory. Closed-form solutions were derived via the variable separation method for cases of equal strain, free strain, and conditions in between, respectively. Under equal strain or free strain condition, the results agree with previous models. It also indicates that the initial consolidation degree is higher for free strain, but the consolidation rate under equal strain condition is faster after a short time.

Parametric studies were carried out to assess the influence of foundation stiffness on the consolidation rate, stress concentration ratio, and differential settlement under different modular ratio (E_c/E_s), radius ratio (r_s/r_c) and permeability ratio (k_c/k_s). Generally, it shows that when the foundation become stiffer, the consolidation rate of the whole unit cell becomes faster, the resulted stress concentration ratio increases, while the differential surface settlement between column and surrounding clay decreases. It is also found that the time needed to achieve 90% of consolidation degree decreases as modulus ratio increases, or radius ratio decreases, or permeability ratio increases. Monitoring data of a fully instrumented field test was also presented and compared with the predictions using this proposed model. It is concluded that this model can predict the development of total and differential settlement and the average stress on top of the

surrounding soil, but the predictions of pore water pressure and total stress on top of the column show some discrepancies.

The results of a series of laboratory model tests were also presented to study the performance of stone column under cyclic loading, where miniature sensors were installed to monitor the variations of total stress and pore water pressure. The repeatability of these model tests was verified. The comparison with previous model tests demonstrates that stone column reduces settlement considerably compared to the ground without improvement or after being improved by PVD. The influences of cyclic stress ratio (CSR), loading frequency and confining pressure were also described: the critical cyclic stress ratio (CCSR) had an upper limit of 0.8 in the model tests; the permanent axial strain and excess pore pressure increased significantly when the loading frequency increased to 10 Hz; the samples became more vulnerable as the confining pressure decreased. A relationship was established between the number of cycles corresponding to the peak excess pore pressure and that corresponding to the maximum slope of axial strain curve in logarithm scale. Finally, a test including multiple loading-resting stages was conducted, and the result indicated that, after experience loading and rest period, behaviour similar to “overconsolidation” was experienced by the sample.

ACKNOWLEDGEMENT

First of all, I would like to thank my supervisor, Professor Buddhima Indraratna, for his invaluable academic guidance and supervision throughout my PhD. This thesis would not have been completed without his support. His kind encouragements, critical suggestions, great enthusiasm and patience help complete this journey.

Then I would like to thank my co-supervisor, Associated Professor Cholachat Rujikiatkamjorn, for his valuable comments and meticulous reviewing on my writings. I would also like to thank Dr. Ana Heitor, for her great help in the preparation of my first paper. I am also grateful to Mr Ritchie Mclean, Mr Alan grant, and other technical staffs for their assistance and humour in the laboratory. I would also like to thank Dr. Sudip Basack for his effort on the preliminary work on the field test in Ballina.

I would like to thank the Australian Research Council and University of Wollongong, who provides funds for my PhD scholarship. Without this assistance, I may never have come to Australia.

Last but not least, I would like to thank my family for their understandings and supports, and all my friends, who bring laughter into my life and always make me accompanied.

Table of content

List of Figures

List of Tables

Chapter 1 Introduction

1.1 Background

A considerable amount of time and money can be saved if structures can remain stable on a natural foundation, but in most instances, natural ground of soft soil does not have sufficient bearing capacity or meet the serviceability requirements upon the construction of new infrastructure. Proper ground improvement methods would be required to avoid these issues (Indraratna et al., 1992).

The ground improvement methods selected must satisfy different requirements including site conditions, types of structures, as well as budgetary consideration. At present there are four methods commonly used in practice (Sivakumar et al., 2004):

1. Installing piles is efficient and usually save time, albeit being expensive;
2. Vertical drains associated with embankments or vacuum preloading can accelerate consolidation, but they are always time-consuming;
3. Chemical stabilisation by mixing lime, cement, or other chemicals into soft clay with a high water content; it is not environmentally friendly, and sometimes may lead to adverse environmental issues delaying the construction decision;
4. Stone columns which increase the overall stiffness and shear strength of soft ground; they are typically used when loads are at low or medium levels (Hughes and Withers, 1974, Black et al., 2007).

Regardless of the limitation in the application, stone columns usually provide a relatively cost-effective and environmentally friendly option compared to other ground improvement methods.

The principal concept of stone column is replacing some of the original soft clay with an array of compacted columns made of a coarse granular material such as gravel or sand. To some extent, stone columns act as piles that ‘shoulder’ the load from surrounding soil and serve as vertical drains that allow excess pore pressure to dissipate. This method increases the bearing capacity, reduces total and differential settlements, accelerates consolidation, improves stability, and enhances the control of liquefaction (Hu, 1995, Guetif et al., 2007, McCabe et al., 2009).

The demand for highways and high-speed rails in coastal regions has been constantly increased worldwide due to the increasing needs of modern transportation, so the challenge is to improve the thick deposits of soft soil so that the transportation infrastructure can be built. The traffic load induced by highways or railways usually is at a low level compared to high-rise buildings, and as stated above, stone columns performed well under low to medium loads, hence, installing stone columns is likely to be an appropriate choice for improving soft ground under transportation infrastructure.

1.2 Statement of the problem

Both static and cyclic loading conditions must be considered when stone columns are used to improve ground under transportation infrastructure as they experience static overburden and cyclic stress from traffic loads.

Accurate prediction of the consolidation of the ground improved with stone columns is often difficult in practice. The consolidation theories for stone column are usually modified from the traditional consolidation theory of vertical drains (Lekha et al., 1998, Han and Ye, 2001, Han and Ye, 2002, Zhang et al., 2006, Wang, 2009, Xie et al., 2009, Lu et al., 2010, Deb and Shiyamalaa, 2015, Lei et al., 2016). By all the research mentioned above, finding a more realistic prediction is always a challenge, and efforts

on theoretical development are still needed to be made. This thesis attempts to clarify two particular issues in associate with the consolidation of ground improved with stone columns: (a) clogging in stone column, and (b) differential settlement between the column and the surrounding soil.

The settlement of ground improved with stone columns usually stabilises after consolidation, but this equilibrium is broken when traffic loads are applied, so the performance of this composite ground under traffic loading must be re-evaluated. However, despite the fact that effort has been made over the last 40 years to understand the behaviour of ground reinforced with stone column theoretically and empirically, much of the past research (Hughes and Withers, 1974, Balaam, 1978, Mitchell and Huber, 1985, Priebe, 1995, Christoulas et al., 2000, Wood et al., 2000, McKelvey et al., 2004, Black et al., 2011, Cimentada et al., 2011) focuses on ground improved with stone column under static loading, while studies on the dynamic responses of stone column are often limited to mitigating liquefaction in silty soil (Madhav and Arlekar, 2000, Adalier and Elgamal, 2004). Only a few studies (Wang, 2009, Kolekar et al., 2012) have emphasised on the role of repeated loads (Hansbo et al., 1981). The behaviour of subgrade improved by stone columns under cyclic loading of highway or high-speed rail is one of crucial factors during design process. Therefore, comprehensive laboratory investigation focused on the ground improved with stone columns under dynamic loads is still highly desirable in practice.

1.3 Limitations

Stone columns are typically used as a group to improve soft ground, so to analyse an array of columns, the group effect needs to be evaluated. The group effect considers interaction between adjacent columns which obviously depends on column spacing.

Due to the complexity of group effect, current design technology is only based on the "unit cell" condition. A unit cell includes a single stone column and its peripheral soil where no friction force or flow occurs at its radial boundary. The work presented in the following chapters is based on this concept, where the detailed effect of column groups is not examined in this thesis.

1.4 Objectives and Scopes

In this thesis, the performance of soft ground improved with stone columns under static and cyclic loading is assessed. Under static loading, consolidation is of primary concern, so the objective is to develop a realistic consolidation model that can capture some features of stone columns, i.e., clogging and stress concentration. Under cyclic loading, laboratory model tests have been subjected to repeated loading to study the behaviour of stone column. Principal stress rotation and its effects are beyond the scope of this thesis. The detailed objectives are summarised below:

1. A laboratory investigation of clogging in a model stone column where the extent of clogging is defined through computer-tomography (CT) scanning, and the properties of soil in the clogged zone is determined by testing mixtures of various clay content.
2. Development of a consolidation model which includes the initial and time-dependent clogging. Investigation of the influence of clogging on the settlement of a unit cell has been carried out by comparing model tests and analytical prediction, and then the sensitivity of clogging related parameters is evaluated.
3. Development of a consolidation model that is between "equal strain" and "free strain". Discussion of the theoretical differences between solutions of equal strain and free strain is presented to examine the effect of foundation stiffness

on the consolidation of stone column unit cell. An application of this model is then employed to predict a field case.

4. A field study is reported where the monitoring data during consolidation stage was obtained from a fully instrumented embankment built on a soft ground improved with stone columns.
5. Laboratory assessment of the performance of stone column unit cell under cyclic loading has been conducted followed by comprehensive discussion of the effect of governing parameters, including the cyclic stress ratio (CSR), the loading frequency and the confining pressure.

The new knowledge about stone column technique obtained in this thesis is listed below.

1. A new consolidation model can be used to predict the consolidation rate of ground improved with stone columns, considering the process of clogging;
2. The stiffness of foundation is included in a general consolidation model, which gives a more practical solution between “equal strain” and “free strain” assumption;
3. The behaviour of stone column unit cell under long term cyclic loading is studied, the results would be useful if stone column is adopted under transportation structures;
4. A field embankment improved with stone columns is given with detail, it can be used as a high-quality case example when models need to be verified. In fact, this field trial has served well in studying the effect of foundation stiffness in this thesis.

1.5 Thesis outline

This thesis is divided into seven chapters, which are organised as follows:

Chapter 1 introduces the research background, the statement of the problem, and the limitations, objectives and scopes.

Chapter 2 presents a literature review of research in relation to the application of stone columns. It reviews some general factors affecting the performance of stone columns, such as the geometry of stone columns, the area replacement ratio, and the stress level and development of column deformation, etc. Particular attention is given to previous laboratory tests, consolidation theory and the cyclic effect.

Chapter 3 gives an example of a clogged model stone column where the extent of clogging is determined through CT scanning, and the properties of soil in the clogged zone are determined. This information on clogging is used as an input for a consolidation model including the effect of clogging. A stone column unit cell is compressed one-dimensionally and then compared to the prediction made using the proposed consolidation model.

Chapter 4 presents a consolidation model that can capture the foundation stiffness; consequently, solutions corresponding to equal strain and free strain, as well as general cases that lie in between are given. The effects of foundation stiffness on consolidation rate, stress concentration ratio and differential settlement are also discussed.

Chapter 5 gives details of laboratory model tests used to study the performance of stone column unit cell under cyclic loading. The experimental setup and testing procedure are discussed. Factors such as the CSR, loading frequency, and effective confining pressure are studied, and the development of excess pore pressure and stress redistribution on top of the unit cell is monitored.

Chapter 6 describes a fully instrumented embankment built above soft ground improved with stone columns and presents the monitoring data during consolidation stage. The

field data is compared to the prediction made by the consolidation model given in Chapter 4.

Chapter 7 provides the Conclusions and Recommendations, followed by a list of References, as cited in the body of the thesis.

Chapter 2 Literature Review

This chapter presents a review of stone column technique. Section 2.1 introduces the development of stone column as a ground improvement method since its first appearance, then it is followed by Section 2.2 which briefly describe the main installation methods at different field conditions. Section 2.3 concerns the previous research of performance of composite ground improved with stone columns, and these efforts lead to the stone column design methods as given in Section 2.4. Application of stone column under cyclic loading is rarely found in literature, therefore general knowledge of soil behavior under cyclic loading is reviewed in Section 2.5, where the difference of performance of soil under monotonic loading and cyclic loading is highlighted.

2.1 History of stone column

The earliest recorded application of stone columns was in 1830, in France, to improve the foundations of an ironworks situated above soft estuarine deposits (Moreau and Moreau, 1935). This method was not brought to the attention of industry for about one hundred years, but then it reappeared in 1933, in Germany, as a by-product of a vibro-flotation compaction method for granular material (Hughes and Withers, 1974). Due to the need to treat soft clay deposits during the late 1950s, stone column as a ground improving method was further developed when two different methods of installation, the "wet vibro-replacement" and "dry vibro-displacement" were introduced (Greenwood, 1975).

It is reported that field stone columns in the 1970s were up to 15 m long, with diameters from 0.5 m to 1.5 m, and a bearing capacity of more than 300 kN (Hughes et al., 1975).

Nowadays, due to the sophisticated equipment and advanced technology, stone columns can be installed to even deeper deposits with lengths of over 30 m (Black et al., 2007). In modern industry, the application of stone columns is more than improving soft cohesive soil, but it is also used to reduce the possible liquefaction of cohesionless soil under seismic loading (Adalier et al., 2003). However, this technique is only suitable for certain ground conditions and construction details (Adalier and Elgamal, 2004). According to past experience, when the shear strength of subgrade soil is between 10kPa and 50kPa, improvement with stone columns is considered to be appropriate (Hu, 1995). This suggestion agrees with the statement made by Greenwood and Kirsch (1983) that stone columns (vibro-displacement method) can be installed in stable but insensitive cohesive soils when the shear strength lies in the range of 30 to 60 kPa. The behaviour of ground improved with stone column has not been completely explored in literature; neither has the effects of disturbance due to installation, deformed columns, associated densification, cyclic loading, and column-soil interaction and so on.

2.2 Construction methods of stone column

No matter what kind of methods or tools are used, stone columns are normally installed using this procedure: initially a cylindrical cavity is created and sustained underground, and then granular materials are gradually filled in and compacted while the supports are extracted. This granular fill usually consists of gravel or crushed stone.

The construction of stone columns can be categorised into three methods.

1. Vibro-replacement

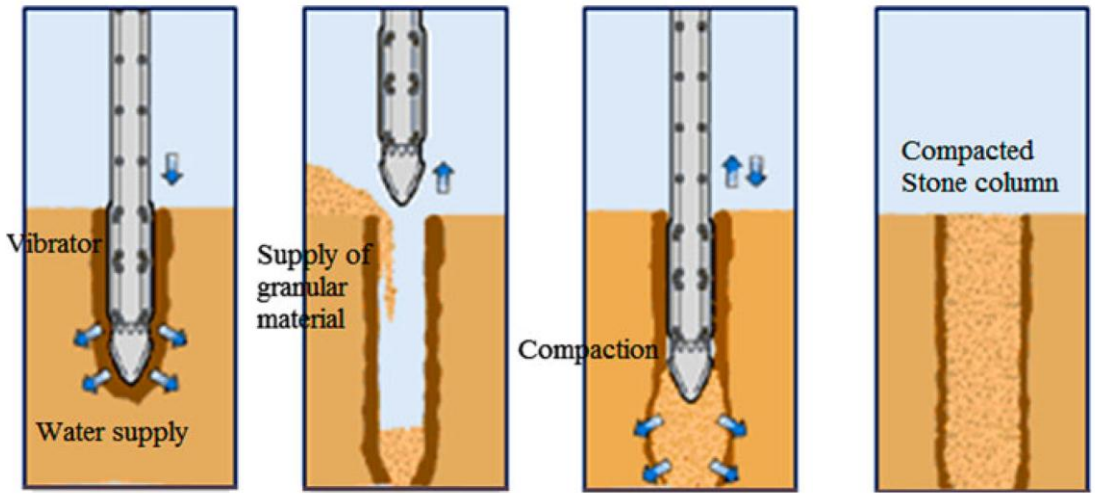

Figure 2.1 Vibro-replacement (Dheerendra Babu et al., 2012)

In this method, a cylindrical cavity is formed underground by jetting a probe down to the desired depth using water or oil. The key feature is that the material in the probe or case is flushed out in the liquid flows and replaced by granular material. The typical column diameter is between 0.8 m and 1 m. Figure 2.1 shows a schematic illustration of the vibro-replacement method.

2. Vibro-displacement

In vibro-displacement method, compressed air rather than liquid (water or oil) is used to assist the penetration of the probe into the ground. The soil underground is forced to form a cavity rather than being removed while making the borehole. The diameter of the stone column using this method is usually smaller (0.6 m) than that of vibro-replacement method. The vibro-displacement procedure is shown in Figure 2.2. A technique called "Vibro composer" (Dheerendra Babu et al., 2012) can also be categorised as wet vibro-displacement which is widely used in Japan to install sand compaction piles to stabilise soft clays with high water table (Aboshi et al., 1979).

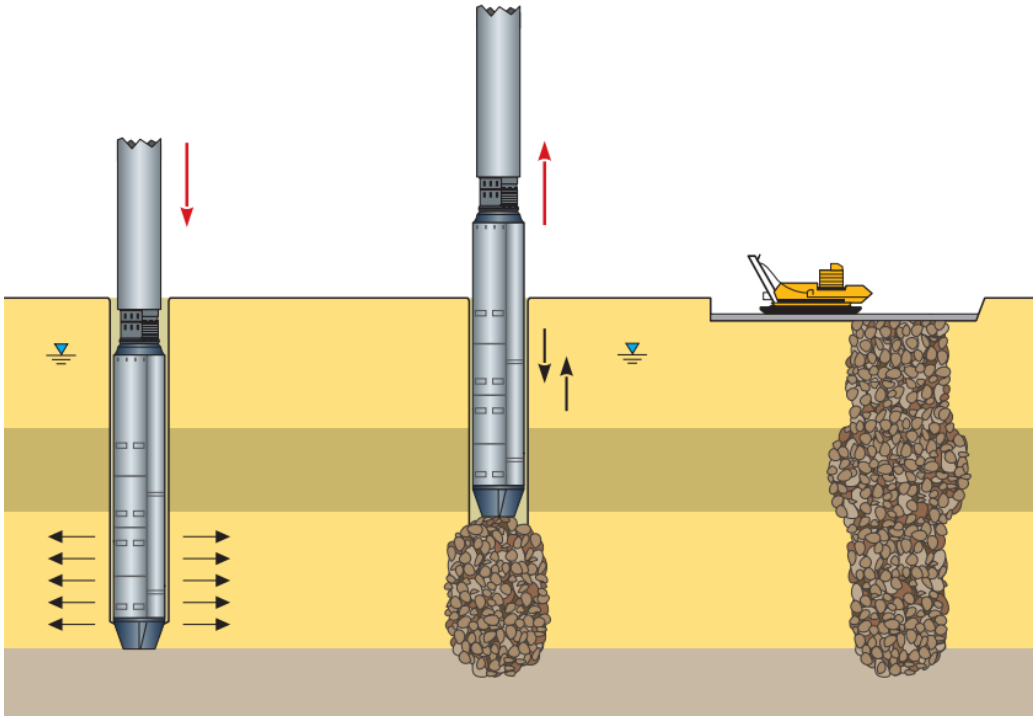

Figure 2.2 Vibro-displacement (Keller, 2017)

3. Rammed stone columns

The rammed stone column is an old-fashion method where stone column is installed in several stages. The compaction of granular materials in the pre-bored holes is achieved through heavy falling weight rather than vibration. The rammed stone column is cost effective due to the low requirement of equipment, but it may be relatively slow and uneconomical when the target depth exceeds 12-15m. Besides, it is not appropriate for improvement of sensitive soils. A sketch is presented below in Figure 2.3.

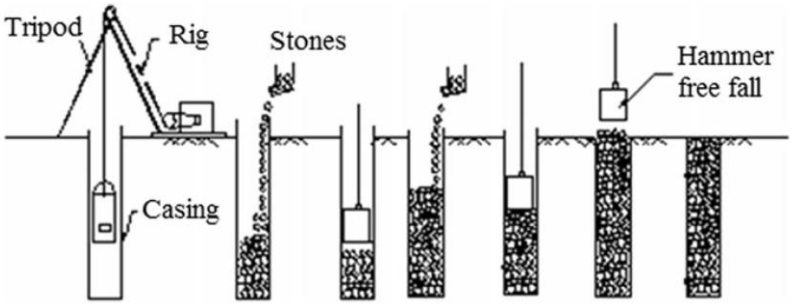

Figure 2.3 Rammed stone column (Dheerendra Babu et al., 2012)

For those different installation methods, the granular material is filled in by mainly two ways.

The first one is called bottom feed technique which means "the stone may be fed from a rig-mounted hopper through a permanent delivery tube along the side of the poker, which bends inwards and allows the stone to exit at the poker tip" (McCabe et al., 2007). The material used in the bottom feed system is between 15-45 mm (McCabe et al., 2007). The bottom feed technique is suitable for cases where the groundwater table is high, or the undrained shear strength is low, i.e. 15-50 kPa (Dheerendra Babu et al., 2012).

The granular material can also be introduced by the top feed technique, and the particles are slightly larger than that of the bottom feed system, i.e. 40-75 mm (McCabe et al., 2007). This technique is better suited to stable and insensitive cohesive soils with relatively high undrained shear strength, i.e. 30-60 kPa, or when the water table is low (Dheerendra Babu et al., 2012).

2.3 Previous research of stone column

The installation effect of stone column is similar as the one of pile installing, which is normally studied by cavity expansion theory as shown in Section 2.3.1. The bearing

capacity of stone column foundation depends on its failure mechanism, so the review which concerns stone column failure modes is presented in Section 2.3.2. The performance of stone column under static loading is closely related to several important parameters, which are the focus of previous research, such as L/d ratio (Section 2.3.3), area replacement ratio (Section 2.3.4) and stress concentration ratio (Section 2.3.5). Normally stone columns are configurated as a group, columns at various positions behaves differently, the group effect is introduced in Section 2.3.6. When assessing the long-term behaviour of stone column, the consolidation process has to be considered, basic consolidation theories for stone column is presented in Section 2.3.7.

2.3.1 Effect of installation

Because of disturbance due to installation, there may be an increase in the undrained shear strength of the surrounding clay (Randolph and Wroth, 1979), and other properties of peripheral soil may also be altered. The effect of installation is usually estimated using cavity expansion theory. Much work was carried out to verify the effectiveness and accuracy of this theory by comparing the results to experiments (normal gravity and multi-gravity environment) and field observations.

Cylindrical cavity expansion was used by Asaoka et al. (1994) to simulate the effect of installation from driven sand piles by comparing the results with a series of triaxial compression tests where the test sequence was disturbance, consolidation, and then shear. Although the similarity of this comparison is not evident, the theoretical and experimental analysis shows similar load-settlement curves.

A semi-empirical approach was proposed by Lee et al. (2004) based on cylindrical cavity expansion theory and then verified by the results of centrifuge tests where

variations of total stress and pore pressure were measured during the installation of sand compaction piles. It was suggested that the plain strain cavity expansion theory predicted the peak stress and the whole process well, but it may overestimate residual stress after the installation.

Field measurements were also carried out to study the effect of installation (Kirsch, 2006), from which both the individual and global effects were distinguished. The stress level ascended in each column installation, and a global enhancement zone was found around the column. Moreover, the concept of cavity expansion combined with increasing stiffness was used to model these effects using the finite element method.

Another field trial was conducted to estimate the lateral displacement in soft soil due to the installation of stone column (Kelly et al., 2011). The results were compared to the theoretical prediction by cavity expansion theory and showed consistency in the magnitude of lateral displacement.

Some numerical simulation with regards to the effect of installation was given by Guetif et al. (2007), who adopted a "composite cell model". The Mohr-Coulomb perfect plastic behaviour was assigned to the improved clay, and the zone of influence and the degree of improvement in terms of Young's modulus was predicted. However, these results must be validated by well-designed experiments.

Regarding Bothkennar clay, two constitutive models of Cam-clay type involving anisotropy and destructuration were compared with a traditional modified Cam-clay model in numerical simulation to estimate the effect of installation (Castro and Karstunen, 2010, Castro et al., 2014). The post-installation properties were adopted in the settlement analysis, and some design suggestions were presented.

Several model tests under 50 times gravity were carried out in a centrifuge with in-flight installation to reveal any observable disturbances (Weber et al., 2010). The microstructure of the smear zone was determined by environmental scanning electron microscopy and mercury intrusion porosimetry. The disturbance was divided to three zones, as shown in Figure 2.4: the penetration zone (also called clogging by Indraratna et al. (2013)) where the clay particles and granular particles are mixed; the smear zone which has been sheared and remoulded; the densification zone where there is a reduction in porosity but no structural changes.

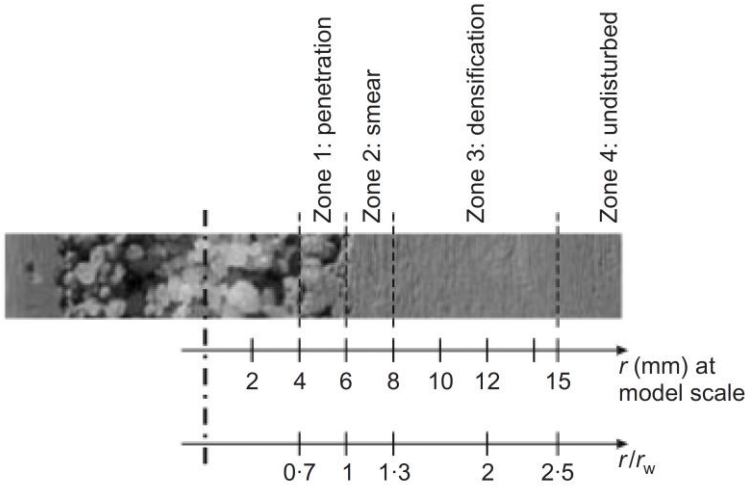

Figure 2.4 Microstructure of disturbance zone (Weber et al., 2010)

The frozen pile method was always used in physical model tests. This method was assessed by Parihar et al. (2011) through a comparison between installation at normal gravity (1g) and in-flight installation at high-gravity in a centrifuge. It indicated that no increase in pore pressure stress in 1g condition and centrifuge tests were similar to the previous study (Lee et al., 2004).

2.3.2 Failure types

There are two ways to obtain the bearing capacity for a pile in cohesive soils: both end bearing force and lateral frictional shaft resistance increases as settlement develops. A stone column is similar to a pile, but with some other features, i.e., it would bulge if the lateral confinement from the surrounding soil is not enough.

There are four different failure modes of stone column: bulging, punching, shearing, and bending (Wood et al., 2000). Many of these types of deformation above may happen at the same site or even for the same column, but the predominant deformation is always bulging (Kelly, 2014).

The geometry of stone columns such as length, diameter, spacing, and footing size may have some influence on their deformation (McKelvey et al., 2004). A common classification of stone column is based on their length, so if a stone column reaches the bearing stratum, it can be classified as “end bearing” or “fully penetrated”; otherwise it would be referred to as “floating” or “partially penetrated”.

2.3.3 L/d ratio

The L/d ratio is defined as the ratio of column length to its diameter. At low L/d ratios (less than 4-6), the load is transferred to the surrounding soil via frictional and end bearing modes. When friction reaches its limit, the end bearing capacity tends to carry more load, so the stone column is punched into the underlying stratum (Hughes and Withers, 1974, Black et al., 2007). For larger L/d ratios (6-13), loads are unlikely to transmit to the bottom of the column because of increased friction with depth (Black et al., 2007). There is no punching because the displacement of the footing is absorbed by compression and lateral deformation of the stone column at the upper position (Wood et

al., 2000). The bearing capacity of stone column is determined by the maximum lateral resistance that the surrounding soil can provide. If the L/d ratios are even higher than 13, the primary failure mode may be bending or shearing before bulging, or punching appears (Hu, 1995, Black et al., 2007).

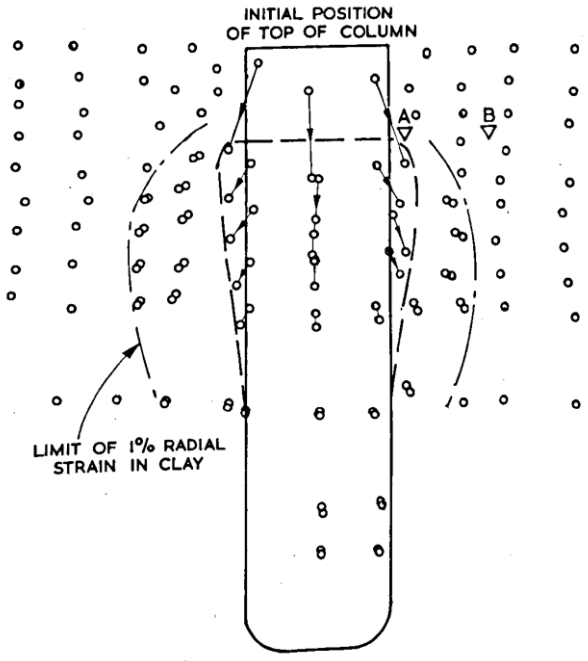

Figure 2.5 Displacement of lead shots in model column (Hughes and Withers, 1974)

An early laboratory test of a single stone column (Hughes and Withers, 1974), where the load was only applied beyond the column, showed that when the L/d values are less than 4, end bearing failure occurs earlier than bulging failure. It was also suggested that punching and bulging coincide at an L/d ratio of 4.1. For bulging failure, deformation only happened at the top of the column at a length of about four times the diameters of the columns, whereas at deeper depths there was no vertical or radial displacement. The authors also concluded that vertical stress decreased to zero at a depth of 6 times the column diameter, after which there was no increase in the bearing capacity from an

increase in the length. By plotting the radial strain in the soil model (Figure 2.5), an influence zone (more than 1% radial strain) was determined which is about 2.5 times bigger than the column.

Tests of columns in Speswhite kaolin were carried out to study their performance of in groups with a square grid configuration (Hu, 1995). The shortest column tests (L/d=5.7) showed a failure of punching and local bulging, while the column at the edge was compressed more and the column in the centre penetrated further into the clay. For an L/d ratio of 9.1, the bearing capacity increased by 15% compared to the shorter column (L/d=5.7) and the settlement of footing was 0.25 times the column diameter. The central column had the least deformation and only bulged at a shallow region, and the middle columns had a larger amount of deformation higher up the columns, while the columns closest to the edge bulged more above the shear planes. Moreover, a clear conical region appeared right below the footing where there was no noticeable bulging happened, but when the L/d increased to 14.5, there was a similar conical deformation profile, and the increase in the bearing capacity was negligible; furthermore, the middle columns failed by buckling rather than bulging or shearing.

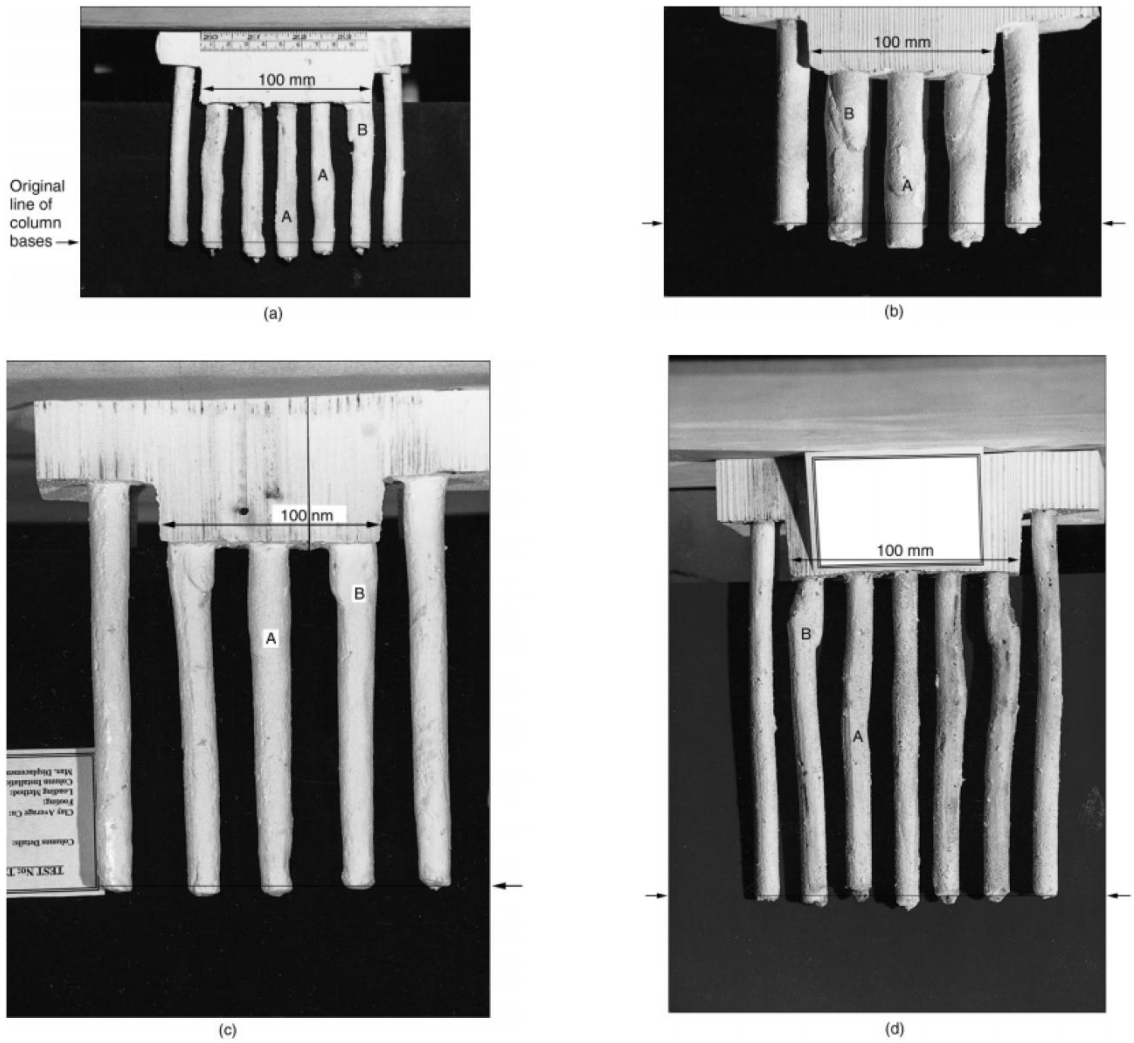

Figure 2.6 Exhumed Columns after test: (a) L/d = 9.1&L/D =1; (b) L/d = 5.7&L/D =1; (c) L/d = 9.1&L/D =1.6; (d) L/d = 14.5&L/D =1.7 (Wood et al., 2000)

When a low L/D (D means the length of strip footing) ratio of 1 was used, penetration still occurred, but it would have been prevented if the L/D ratio increased to 1.6-1.7. In addition to a critical column length of L/d ratio of 5.7-9.1 (Figure 2.6), an effective column length of 1.5D-2.5D is also proposed because the bearing capacity would not benefit from any increase in column length beyond this value, whereas the settlement of footing may still be reduced.

Transparent material rather than clay was introduced to give straightforward observations of the deformation of groups of floating columns (McKelvey, 2002).

These tests agreed with the tests where kaolin clay was used, and the influence of the L/d ratio regarding bearing capacity and failure mechanism could be observed.

Failure types including punching, bending, and bulging occurred where columns with L/d ratio of 6 were subjected to loading through a pad foundation; here the maximum punch-in depth was about 10mm while the column bent outwards and bulged along the entire length. When the L/d ratio increased to 10, punching did not occur, bending and bulging still occurred, but was only concentrated in the upper part, and shear planes could be seen. The ultimate bearing capacity increased by 5% while the footing settlement was 20mm, this means there was almost no increase in the load-bearing capacity with an increase in length beyond an L/d ratio of 6. However, if the settlement of all tests were compared at a working load which was 50% of the failure load, an increase in length beyond an L/d ratio of 6 resulted in a noticeable reduction in the settlement.

The effect of footing geometry was also studied. With circular footings (as shown in Figure 2.7), there was bulging along all the columns, 5 mm of punching for shorter columns and no penetration for the longer columns, but notable deformation occurred in the upper region of the columns. With strip footings, there was bulging but no penetration regardless of the column length, but deformation was smaller and more even in the central column while the columns at the edge were bulging and bending outwards.

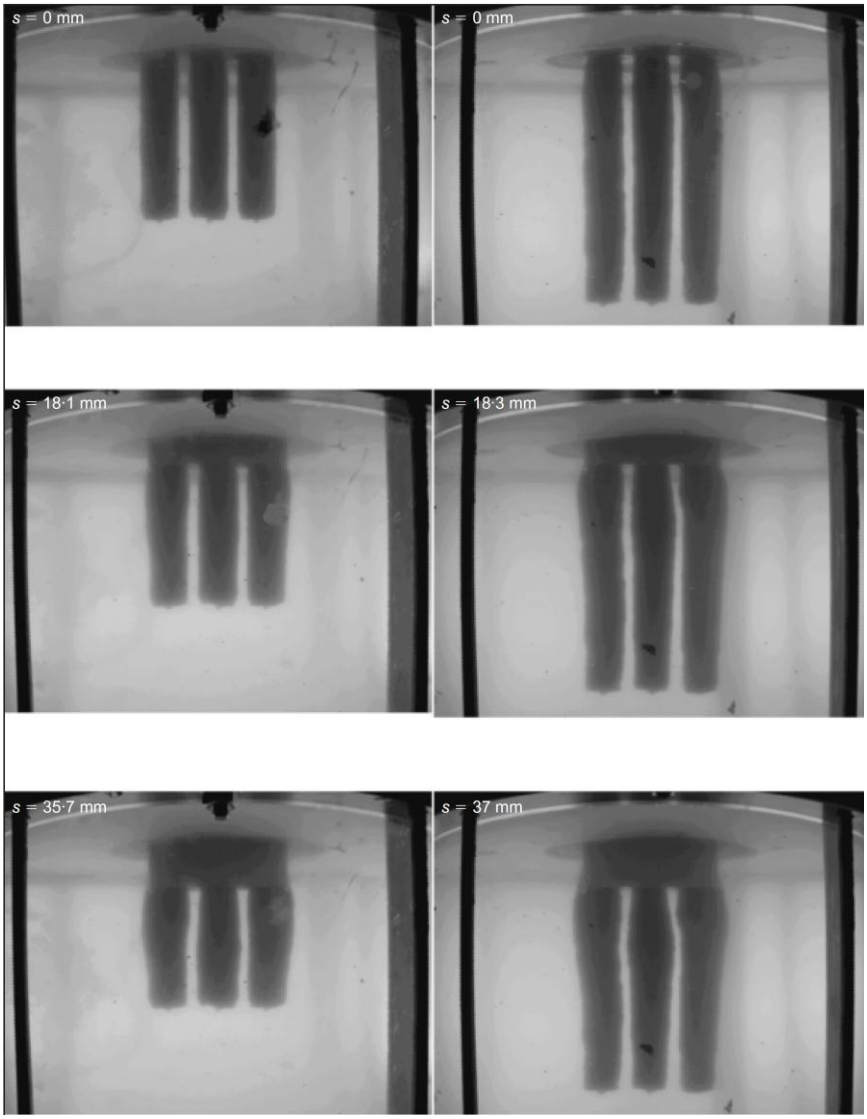

Figure 2.7 Model columns under a circular foundation (McKelvey et al., 2004)

A similar statement was made by Hu (1995) and Black et al. (2007) that overall instability may be induced if a particular column in group buckles or bends. This conclusion was made through stress control tests of three stone columns installed in a triangular pattern at an array of 120 ° under a circular footing with free drainage. Tests of single columns where the L/d ratios varied between 3.3 and 10.5 were also conducted in a unit cell. At L/d ratios of 2.5, 3.6, and 5.9, 50%-90% of the entire settlement came from tip penetration. Moreover, punching and bulging happened simultaneously for an L/d ratio of 6.5, but penetration started to decrease at an L/d ratio of 8 and became

negligible at an L/d ratio of 10. It was therefore concluded that a threshold value of L/d could not be found in terms of optimal reduction of settlement for a single column because any increase of L/d may reduce settlement without increasing the bearing capacity. However, when the L/d ratio reaches a significant value, stone columns act like end bearing rather than floating, so some reduction in the settlement may come from the rigid underlying layer. It is also noted that these results were obtained under certain loading platform, and the settlement and bearing capacity would depend on the geometry of the loading foundation.

2.3.4 Area replacement ratio (A_r)

The area replacement ratio, A_r, is defined as "the ratio of cross-sectional area of columns to the cross-sectional area of foundation soils" (Wood et al., 2000), and it was included in an elastic theoretical analysis by Balaam and Booker (1981) based on the unit cell concept. Charles and Watts (1983) proved through large-scale tests of a group of end bearing columns under a rigid raft that the elastic theory overestimated the reduction of settlement. Moreover, these large-scale tests also showed that only at a high area replacement ratio (33%) can elastic behaviour be observed whereas there was no volume change measured for a medium area replacement ratio (21%); however, an area replacement ratio of 30% can reduce settlement by 33%.

Centrifuge model tests were also carried out by Al-Khafaji and Craig (2000), where ground improved by 10 mm diameter stone columns set in a triangular pattern were used to sustain a 325 mm diameter model tank. The fluid in the tank generated a 160 kPa load when foundation drainage was permitted, and a settlement reduction ratio of 56% was obtained when the area replacement ratio was 40%. The density of sand was not measured during testing, but the friction angle was about 30 ° for stiff columns and

even less for loose columns; this was less than the friction angle of 35 ° - 45 ° for stone columns in practice.

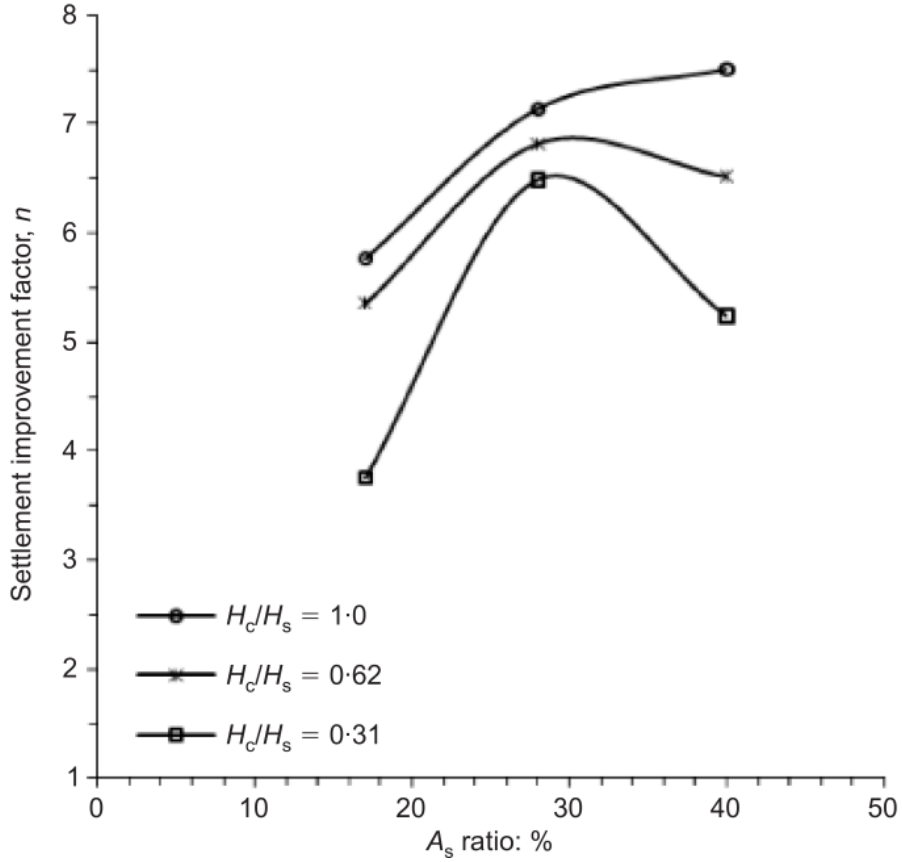

Figure 2.8 Settlement improvement factor plotted against A_r (Black et al., 2011)

Several model tests of isolated stone column were carried out (Black et al., 2007, Black et al., 2011), where the stiffness of soil reinforced with stone column increased as the area replacement ratio increased. The settlement improvement factor seems to have an upper limit as the area replacement ratio varies, but when the area replacement ratio was 28%, a maximum settlement improvement ratio of 7 was achieved for 160 kPa loading level. The optimal area replacement ratio was about 40% for a loading of 320kPa, and settlement increased as the area replacement ratio increased beyond this limit, as shown in Figure 2.8. The explanation given was when the area replacement ratio is between 25% and 30%, the surrounding clay is also densified, and the lateral

resistance increases to prevent bulging; but when the area replacement ratio is beyond this optimum value, improvement in the surrounding clay cannot generate enough resistance. However, the loading level in these model tests was not realistic compared to the field value (Kelly, 2014), and the footing area should be considered.

2.3.5 Stress concentration

Soft ground improved with stone columns means that the vertical stress generated by vertical load is always redistributed at the shallow depth because stone columns bear most of the upload than the surrounding soil due to arching. This uneven distribution of stress (stress concentration ratio) is defined as the ratio of vertical stress on the column to the average vertical stress on the surrounding soil at the same depth. Under a rigid footing, the magnitude of stress concentration ratio is directly related to the stiffness of the stone column and surrounding soil (Black et al., 2007).

The measured stress concentration ratio is usually in the range of 2-6 (Aboshi et al., 1979, Barksdale and Bachus, 1983, Hu, 1995, McKelvey et al., 2004). The stress concentration ratio increases during consolidation, and decreases with depth (Juran and Guermazi, 1988). The stress concentration ratio decreases as the applied load increases and the area replacement ratio decreases (Shahu et al., 2000). Ambily and Gandhi (2007) stated that the vertical stress tends to concentrate more on the column when the undrained shear strength of surrounding soil is lower, and the stress concentration ratios are at the same level between the cases of a single column and a group of columns.

2.3.6 Group effect

Deformation of a single stone column usually is axisymmetric bulging, but the failure mode is more complicated for a group of columns. It was observed that a group of

column resulted in more settlement reduction than a single column under the same L/d ratio and area replacement ratio (Black et al., 2007). The deformation is not axisymmetric around a group of columns, so there were non-uniform column distortions, and they bulged more towards the unrestrained direction (McKelvey et al., 2004). This group effect is attributed to the proximity between adjacent columns, which means it is affected by column spacing and the area replacement ratio.

A group failure mechanism, known as "conical wedge failure mechanism", was proposed by Hu (1995) from their observation that overall failure deepens along the centreline due to confinement between adjacent columns as well as the interaction between individual columns and the surrounding soil.

The behaviour observed in tests of a group of stone columns was compound, such that the stability of the entire system was decided by interactions between the columns, as well as the surrounding soil and structures. Since the group effects were uncertain, a unit cell assumption was widely adopted. This method was justified by the similar load-settlement responses and stress concentration ratio in tests of a single column and a group of columns (Ambily and Gandhi, 2007). It was also suggested that a reasonable prediction could be made based on the unit cell concept when the replacement area is between 6% and 44%. Moreover, the field performance of the central column of a group of columns can be represented by the unit cell model.

2.3.7 Consolidation theory of stone column

The analyses of consolidation for ground reinforced by stone column are usually developed on the basis of the traditional consolidation theories of vertical drains, which is a combination of vertical and radial consolidation. The traditional one-dimensional

consolidation theory proposed by Terzaghi (1943) is based on the effective stress principle, while the fundamental consolidation theory of vertical drains was initially proposed by Barron (1948). A simple method was given by Carrillo (1942) to combine vertical and radial consolidation. The following are some common assumptions in vertical and radial consolidation theory given above.

1. The soil is homogeneous and fully saturated.
2. Soil particles and water are incompressible.
3. Only small strain happens during consolidation.

The governing equation of combined consolidation is given in cylindrical coordinates as shown below:

$$\frac{\partial u}{\partial t} = c_v\left(\frac{\partial^2 u}{\partial z^2}\right) + c_h\left(\frac{\partial^2 u}{\partial r^2} + \frac{1}{r}\frac{\partial u}{\partial r}\right) \qquad \text{Eq 2.1}$$

In order to solve this equation, the two conditions proposed by Barron (1948) are known as “free strain” and “equal strain”. Details of these two hypotheses are given below:

- Equal strain

  Here the external load is applied by a rigid footing which results in an equal vertical strain at the soil surface. Arching means the redistribution of stress is considered to yield an extreme case where no differential settlement occurs, and for the foundation reinforced by stone column, the stress concentration which leads to a redistribution of stress should not be ignored.

- Free strain

  The vertical stress on the ground surface is uniform because of the flexible footing. There is no stress redistribution in the entire duration of consolidation,

so as consolidation progresses, the soil adjacent to the drainage will be compressed faster than the soil at the far side because of a shorter drainage path, and this leads to differential settlement.

Some solutions for the one dimensional and two-dimensional differential equations can be combined to furnish a simple solution to this three-dimensional problem with inspiration from heat conduction theory (Carrillo, 1942). The overall degree of consolidation, $\overline{U}$, can be expressed by the radial (U_r) and vertical (U_v) degrees of consolidation, which are solved separately through traditional consolidation theory.

$$1 - \overline{U} = (1 - U_r)(1 - U_v) \qquad \text{Eq 2.2}$$

The accuracy of Carrillo's method (Eq 2.2) was examined using rigorous solutions (Zhu and Yin, 2001, Zhu and Yin, 2004a, Zhu and Yin, 2004b). It was found that the average degree of consolidation is slightly overestimated by Carrillo's formula, but the discrepancy is less than 10%.

Previous researchers developed several consolidation theories for ground improved with stone columns. For example, the effect of gravel-clay modulus ratio was considered by Balaam and Booker (1981) who found that the rate of consolidation of clay increases as the column-clay modulus ratio increases under a rigid raft footing. A simplified solution for calculating the average degree of ground improved with stone column was proposed by Han and Ye (2001), who later included the well resistance and smear effect were (Han and Ye, 2002). A linear variation of horizontal permeability of soil in the disturbed zone was considered by Zhang et al. (2006) in a consolidation theory for a composite ground. A rigorous solution was found to estimate the average degree of consolidation for ground reinforced by stone column by considering column consolidation (Xie et al., 2008, Xie et al., 2009). A contradiction between "equal strain"

assumption and flow continuity at the soil-column interface was pointed out and solved by Lu et al. (2010) who combined both the radial and vertical flow within the column, whereby the variation of total vertical stress with depth and permeability variation in the disturbed zone were also included. To the best of the author's knowledge, only one theory has been proposed to estimate the consolidation under cyclic loading together with consideration of smear and swell resistance (Wang, 2009). The results showed that the rate of consolidation depends on the geometry of stone column, the magnitude of upload, the paths of cyclic loading, and so on.

2.4 Design of stone column

Currently, the design of stone column is often based on the unit cell concept. According to the requirements of bearing capacity and settlement control, the design can be divided into the ultimate limit state and serviceability limit state, respectively. Section 2.4.1 presents two simple, but useful design methods based on bearing capacity requirement, and a semi-empirical design method based on settlement control is briefly described in Section 2.4.2. A fundamental understanding of vibro-stone columns, which is normally obtained through reduced-scale physical model tests, also provides useful information in design practice.

2.4.1 Bearing capacity

Hughes and Withers (1974) found that based on their stress-controlled model tests, the ultimate bearing capacity of a unit cell was decided mainly by the maximum resistance provided by the surrounding soil against bulging. A straightforward method was also given to estimate the ultimate bearing capacity where the surrounding clay was considered as elasto-plastic and column bulging was modelled using cylindrical cavity

expansion theory. The maximum vertical stress that a unit cell can bear was determined using Eq 2.3. It is still the most commonly used equation in practice today to predict bearing capacity.

$$\sigma_v' = \frac{1 + sin\varphi_c'}{1 - sin\varphi_c'}(\sigma_{r0} + 4c - u) \qquad \text{Eq 2.3}$$

where φ_c' is the friction angle of column material, c is the cohesion of surrounding clay, σ_{r0} is the in situ lateral earth pressure, and u is the pore pressure.

By considering ground after treated as homogeneous, Priebe (1995) proposed a design method to predict the bearing capacity of a single stone column under strip foundations. This procedure was similar to standard methods of estimating bearing capacity, except that the modified friction angle and cohesion of this new homogeneous material were used. These modified soil parameters can be calculated using the equations below.

$$\tan\varphi_h = m \cdot tan\varphi_c' + (1 - m)tan\varphi_s' \qquad \text{Eq 2.4}$$

$$c_h = (1 - \frac{1}{A_r}) \cdot c \qquad \text{Eq 2.5}$$

$$c_h = (1 - m) \cdot c \qquad \text{Eq 2.6}$$

where c_h is the cohesion of composite material, φ_h and φ_s' are the friction angles of the composite material and the surrounding clay respectively, and m is the ratio of the load on the stone column to the total loads.

The stress concentration ratio can be treated as a function of the area replacement ratio and friction angle. The cohesion of this composite material can be obtained from Eq 2.5 or Eq 2.6 while noting that Eq 2.5 may lead to a more unsafe design because of column bulging.

However, the effectiveness of the Priebe (1995) method for estimating bearing capacity depends on the level of load applied to the stone columns. Bouassida et al. (1995) pointed out that the concept of equivalent material should be adopted where the reinforced soil is subjected to a triaxial loading, misleading results may occur if the principle stress direction is inclined. Bouassida et al. (1995) gave a general lower-bound estimate for bearing capacity of a foundation lying on a soil improved by a group of stone columns, and this solution can be rewritten using the equivalent material properties as given in the equations below.

$$\mathrm{Q} = 2\mathrm{A}(\mathrm{C} \cdot K_p^{eq} + \mathrm{C}^{eq}\sqrt{K_p^{eq}}) \qquad \text{Eq 2.7}$$

$$K_p^{eq} = 1 - A_r + \eta K_p \qquad \text{Eq 2.8}$$

$$\mathrm{C}^{eq} = \begin{cases} \dfrac{\left[C^c A_r\sqrt{K_p} + C(1-A_r)\right]}{\sqrt{K_p^{eq}}} & K_p \le 2 \\ \dfrac{\left\{C^c A_r\sqrt{K_p} + C\left[(1-A_r) + \frac{A_r}{2}g(\varphi)\right]\right\}}{\sqrt{K_p^{eq}}} & K_p \ge 2 \end{cases} \qquad \text{Eq 2.9}$$

$$g(\varphi) = \left(K_p - 1\right)\ln\left(K_p - 1\right) - (K_p - 2) \qquad \text{Eq 2.10}$$

where Q is the estimated bearing capacity, A is the area of top surface, C is the cohesion of the soft soil, Cc is the cohesion of the column material, K_p^{eq} and C^{eq} are the coefficient of passive stress and cohesion of the equivalent material respectively, Kp is the coefficient of passive stress of the column material.

This method were assessed by some experimental results which shows that the estimation is sufficiently close to the exact value of bearing capacity (Bouassida, 2016).

2.4.2 Settlement

A semi-empirical method for predicting settlement was also proposed by Priebe (1995) based on cylindrical expansion theory and the unit cell approach, where an extensive loading area on an unlimited column grid was considered. Moreover, some basic assumptions are made: the column is fully penetrated; the column material is incompressible; the bulk densities of the column material and surrounding soil are negligible compared to the upload; shearing is the only possible failure; the surrounding soil behaves elastically. In this method, an improvement factor was given as the settlement ratio of the untreated ground, s, to the treated one, s_t. Note that an area ratio was defined by Priebe (1995) as the reciprocal of the area replacement ratio in section 2.3.4. The expression where the common area replacement ratio is used and presented below (Hu, 1995).

$$\frac{s}{s_t} = 1 + A_r \cdot \left(\frac{0.5 + 2v \cdot \frac{1-A_r}{v+A_r}}{K_{ac} \cdot 2v \cdot \frac{1-A_r}{v+A_r}} \right) \qquad \text{Eq 2.11}$$

where K_{ac} and v are the coefficient of active earth pressure and Poisson's ratio of the column material respectively.

Figure 2.9 shows a widely used design chart provided by Priebe (1995), where μ_s is Poisson's ratio which is normally taken as 1/3.

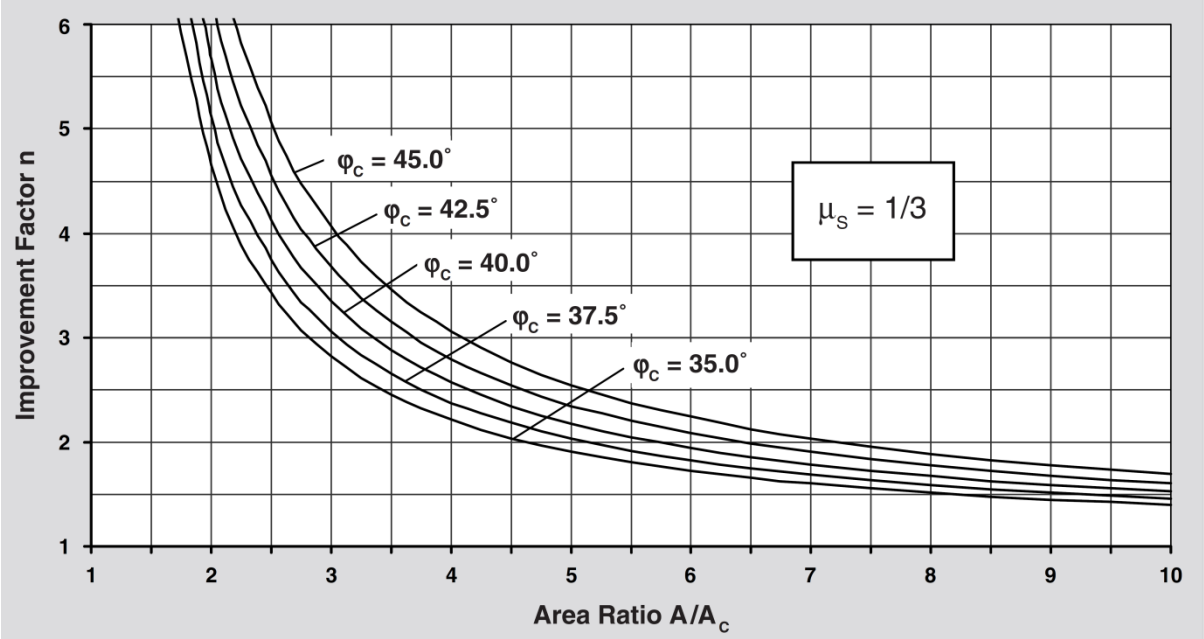

Figure 2.9 Design chart for vibro replacement (Priebe, 1995)

In this method, the benefit comes from the increase of effective stress in the surrounding soil is missing; therefore, it is usually considered as conservative or on the safe side. However, because of its simplicity and reasonable estimation, this method has been widely used in USA and UK since it was first proposed (Hu, 1995).

Another simple but effective settlement calculation method used in Japan is based on the equilibrium of column-clay interface proposed by Aboshi et al. (1979). The unit cell assumption was also assumed to be valid, and the settlement reduction ratio was given for a specific vertical stress increment as given in Eq 2.12 below:

$$\frac{s}{s_t} = \frac{\lg(\frac{\bar{\sigma}_0+\sigma}{\bar{\sigma}_0})}{\lg(\frac{\bar{\sigma}_0+\mu_c\sigma}{\bar{\sigma}_0})} \qquad \text{Eq 2.12}$$

where $\bar{\sigma}_0$ is the average initial effective stress, σ is the effective stress increment due to upload in the surrounding clay, and μ_c is the ratio of vertical stress in the clay to the one in the column.

Eq 2.12 indicates that the reduction in the settlement is related to the length of the column, which is reflected as the relationship between the average initial effective stress and depth. It is recommended that the stress ratio, μ_c, should come from in-situ tests and this method is more suitable for stiff to firm cohesive soils (Barksdale and Bachus, 1983).

2.5 Cyclic loading effect

The performance of ground improved with stone columns has barely been found in past research, therefore this section has to settle for the general performance of soft soil under cyclic loading. Dynamic stress induced by traffic loading is analysed in Section 2.5.1, it shows that change of stress magnitude and principal stress rotation is happening simultaneously during traffic. The change of principal stress magnitude is always quantified by cyclic stress ratio, and the effect of cyclic stress ratio is reviewed in Section 2.5.2. The performance of samples is influenced by train rate in both strain and stress controlled cyclic tests, relevant research is given in Section 2.5.3. For soft clay, the behaviour under cyclic loading also related to its overconsolidation ratio (Section 2.5.4).

2.5.1 Dynamic stress due to traffic

The real stress state of a certain soil element alternates with the position of the passing by vehicles. Within the plane of the wheel track, “there are pulses of vertical and horizontal stress accompanied by a double pulse of shear stress with a sign reversal on the vertical and horizontal planes” (Brown, 1996), as shown in Figure 2.10(b). It is obvious that not only the direction but also the magnitude of the principal stress is time-

dependent under traffic loading. The stress states of different soil elements and the principal stress rotation are shown in Figure 2.10(a).

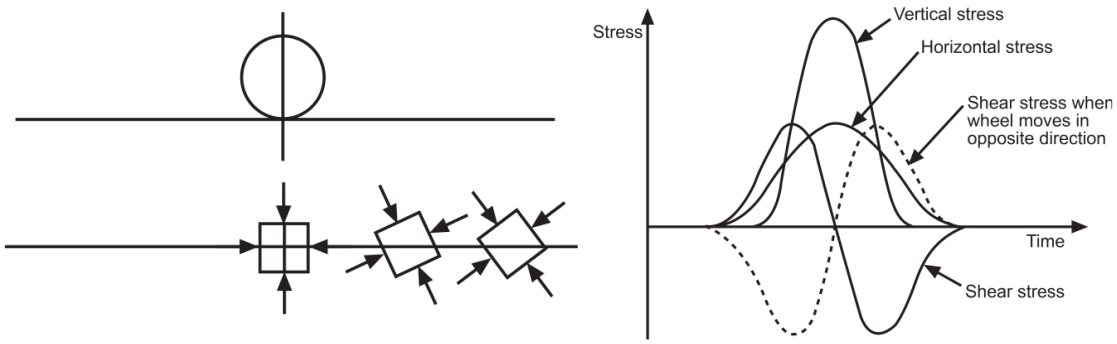

(a) (b)

Figure 2.10 (a) Principal stress rotation; (b) Stress conditions under a moving wheel load (Brown, 1996)

In conventional triaxial tests, a soil element is subjected to an axisymmetric stress state, so the effect that different magnitudes of principal stresses have on the behaviour of soil can be studied. The effect of the intermediate principal stress can be reflected by testing cubic specimens of soil in true triaxial tests because there is an independent control for all three principal stresses. However, to the author's knowledge, the rotation of principal stresses can be achieved in the laboratory only by using hollow cylinder apparatus.

The rotation of principal stress seems to induce an increase in excess pore pressure. It is also found that the effective friction angles, undrained shear strengths, stress-strain relationships, excess pore pressure, and stress paths can be expressed as functions of the angle or inclination of principal stress rotation (Broms and Casbarian, 1965, Ishihara and Towhata, 1983, Lin and Penumadu, 2005, Kumruzzaman and Yin, 2010).

I. The design axle load

The load input is needed to determine the dynamic stress. Various methods were developed to calculate the design axle load generated on the pavement or rail tracks, and the design axle load can be considered as proportional to the static vehicle weight with an empirical impact factor:

$$P_d = \phi P_s \qquad \text{Eq 2.13}$$

where P_d is the design axle load, P_s is the static wheel load, and ϕ is the dimensionless impact factor.

The magnitude of dynamic stress depends on the static weight and speed of the vehicle, and the in-situ intrinsic characteristics. As Eq 2.13 shows, factors other than the static weight are included empirically in the impact factor ϕ.

There are several typical methods for calculating the impact factor (Ni, 2012) and they are presented below in Table 2.1.

Table 2.1 Some types of formula for impact factor (Ni, 2012)

Source	Formula of impact factor ϕ	Note
AR*	$1+5.4\frac{v}{D}$	v is the vehicle speed(km/h), D is the wheel diameter(mm), P_s is static wheel load(kN), P_u is unsprung weight at one wheel(kN), D_j is track stiffness at the joints(kN/mm), g is gravitational constant(m/s^2), $\alpha_1+\alpha_2$ are total rail joint dip angle (radians).
AREA*	$1+5.21\frac{v}{D}$	
BR*	$1+\frac{8.784(\alpha_1+\alpha_2)v}{P_s}\sqrt{\frac{D_j P_u}{g}}$	
German	$1+\frac{v^2}{3\times 10^4}$	
	$1+\frac{4.5v^2}{10^5}-\frac{1.5v^3}{10^7}$	

* AR means Australian Railways; AREA means American Railroad Engineering Association; BR means British Railways.

A relationship was given by Indraratna et al. (2010) to describe the relationship existing between the rail speed, the loading frequency, and the loading amplitude for ballast layer under an axle load of 30 tons, as shown in Table 2.2.

Table 2.2 Relation of speed, stress and load frequency in ballast

Speed/km/h	73	145	218	291
Loading frequency/Hz	10	20	30	40
Dynamic stress/kPa	374	428	482	536

II. Stress in the subgrade

After obtaining the design load, the stress on top of the subgrade, which means the most to the performance of ground, can be determined. The process of propagation from the pavement to the subgrade is the key to determine the vertical stress on top of the subgrade.

Dynamic stress is first excited by the contact between the vehicles and the road or rail tracks, and then a stress wave is transmitted downwards. Especially for a railway, the subgrade stress is related to the type of train, the speed, track structure, track irregularity, ballast depth, the properties of soil in the subgrade, and the axle load.

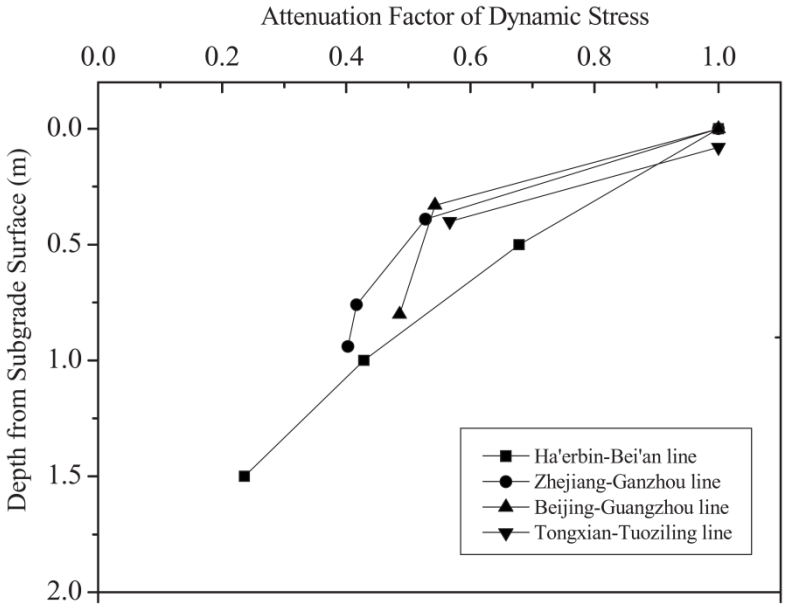

Figure 2.11 Attenuation factor of dynamic stress in the subgrade (Liu and Xiao, 2010)

While stress is being propagated, some degree of attenuation could occur due to both material damping and geometry damping. Geometry damping occurs because waves spread out from the source to a larger area, whereas material damping is induced because certain friction force is needed to overcome in the transmitting medium during propagation. The attenuation within the subgrade resulted from the damping was

approved by some field measurements (Liu and Xiao, 2010). As Figure 2.11 shows, the dynamic stress decreases rapidly with an increase in depth, with only 20% of the surface stress remaining at a depth of 2.5 m.

Some formulas were established for the estimation of dynamic stress in the subgrade in Chinese railroad subgrade design code. An empirical formula was proposed based on field measurements taken on the Guangzhou-Shenzhen railway and the Beijing circular railway (Liu and Xiao, 2010), where the dynamic stress is expressed as in Eq 2.14 below:

$$\sigma_d = 0.26P(1 + 0.0004v) \qquad \text{Eq 2.14}$$

where σ_d is the dynamic vertical stress (kPa) at the subgrade surface, P is the axle load of the train (kN), v is the train speed (km/h), 0.26 is the coefficient of axle load, 0.004 is the coefficient of speed.

Other measurements of newly constructed railways indicate that the coefficient of speed also depends on track quality and the type of soil in the subgrade, and the coefficient of axle load decreases as the thickness of ballast increases. A modified formula is given with different speed coefficients as shown in Eq 2.15 (Liu and Xiao, 2010):

$$\sigma_d = \alpha P(1 + \beta v) \qquad \text{Eq 2.15}$$

where α is the load coefficient which is recommended to be chosen as 0.21 for existing rail or thicker ballast (i.e., 0.35m), and 0.26 for new rail or thinner ballast, β is the speed coefficient which is suggested to be 0.005, 0.004, 0.003 for ordinary, quasi-high-speed, and high-speed rail, respectively.

III. Static deviator stress

The magnitude of total stress is a result of the superposition of static and dynamic stress. Because of the static deviator stress, there is only compressible principal stress on the soil element. As discussed in previous research (Wang and Chen, 2007, Ni, 2012), the static deviator stress consists of the initial static stress, σ_{ani}, which originates from the weight of structures such as embankments or ballast layer, and the mean static stress, σ_{mean}, upon which the cyclic stress, σ_{cyc}, changes. The former one results in an anisotropic consolidation while the latter one distinguishes the traffic loads from other dynamic loads such as earthquakes or waves. There is a sketch in Figure 2.12 that indicates the difference between those two parts.

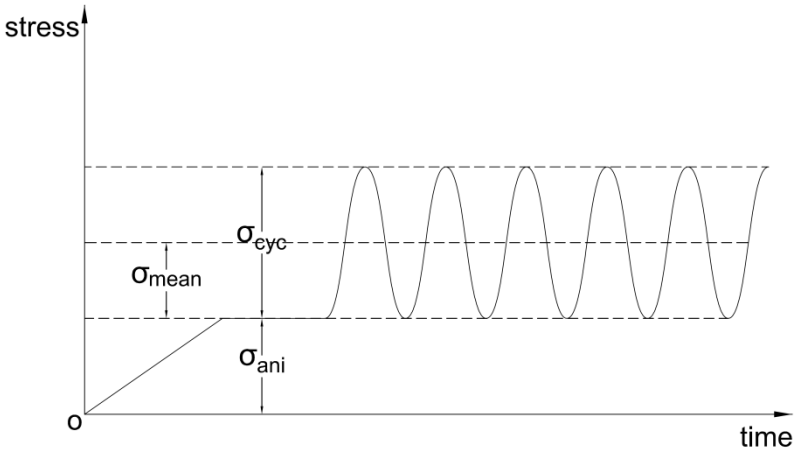

Figure 2.12 Typical terms of deviator stresses in cyclic loading

Previous studies of cyclic loading tests on anisotropically consolidated soft clay shows that the cyclic shear strength decreases as the initial static stress increases, but the total shear strength also increases, because it is the sum of the initial static shear strength and cyclic shear strength (Andersen et al., 1988, Hyodo et al., 1994).

Several undrained cyclic tests were conducted by Wang and Chen (2007) to study the effect of the mean static deviator stress, σ_{mean}, on the cyclic behaviour of soft clay. It

was concluded that the accumulation of deformation and excess pore water pressure was accelerated, and the cyclic strength decreased as the static deviator stress increased.

2.5.2 Cyclic stress ratio

The behaviour of soft clay under cyclic loading is quite different from that under monotonic loading. The differences were divided into two main aspects (Ni, 2012):

I. Cyclic loading may cause a much larger deformation than would be achieved in a single monotonic static loading, and then lead to failure, even if the cyclic stress level is obviously below the static failure stress.

II. There are some levels of cyclic stress at which collapse would happen only after a large number of cycles (10^6 or more).

Whether the sample fails or not, depends on the magnitude of cyclic stress. The critical cyclic stress was first defined by Larew and Leonards (1962) as the minimum repeated stress that could induce failure. This concept was later confirmed by a series of cyclic triaxial tests conducted by Sangrey et al. (1969) with samples of normally consolidated clay. Their tests showed that: at a high cyclic stress level (i.e., 0.8 times of the static failure stress), the excess pore pressure and axial deformation continued to increase with the number of cycles until failure; when the cyclic stress level is low (i.e., 0.5 times of the static failure stress), additional loading cycles caused no further noticeable increase in excess pore pressure and axial strain after the maximum value had been reached. The results of these tests are shown in Figure 2.13 below. The explanation was given: it depends on the level of cyclic stress that which one was dominant, the recoverable or non-recoverable pore pressure and deformation.

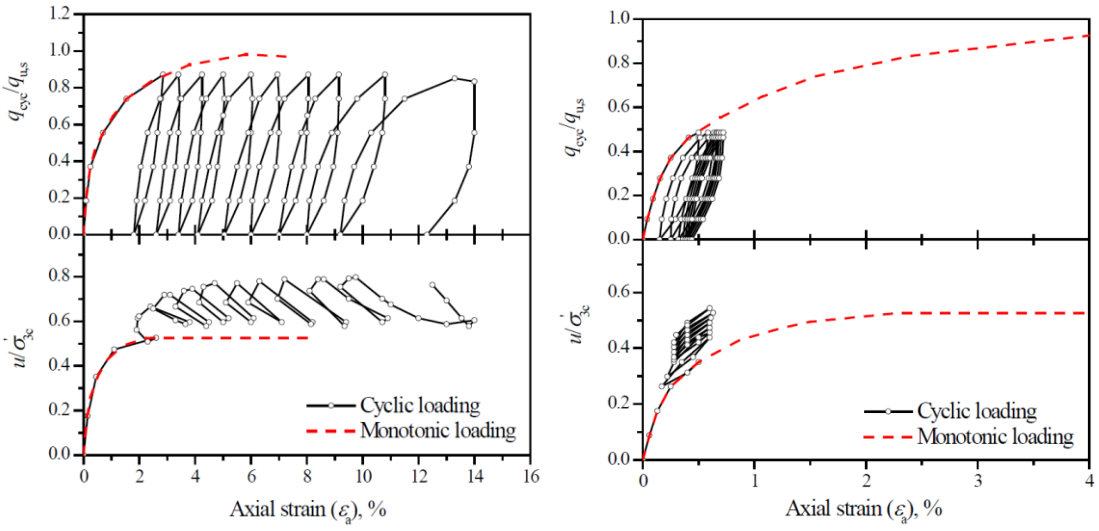

Figure 2.13 Cyclic triaxial tests of Sangrey et al. (1969): (a) CSR=0.8; (b) CSR=0.5 (redrawn by Ni (2012))

In order to compare the results of different tests, the cyclic stress ratio, CSR, is introduced to normalise the cyclic stress. The definitions are shown in Eq 2.16 and Eq 2.17. The cyclic stress ratio is defined as a ratio of the amplitude of cyclic stress to the deviator stress at failure in static test (Ansal and Erken, 1989, Zhou and Gong, 2001, Indraratna et al., 2009), or to the 2 times effective confining pressure (Brown et al., 1975, Miller et al., 2000, ASTM, 2004).

$$CSR = \frac{q_{cyc}}{q_{u,s}} = \frac{\sigma_{cyc}}{\sigma'_{1u,s} - \sigma'_{3u,s}} \quad \text{Eq 2.16}$$

$$CSR = \frac{q_{cyc}}{2\sigma'_3} = \frac{\sigma_{cyc}}{2\sigma'_3} \quad \text{Eq 2.17}$$

where q_{cyc} is the cyclic deviator stress, $q_{u,s}$ is the deviator stress of static test at failure, σ_{cyc} is the amplitude of cyclic stress, $\sigma'_{1u,s}$ and $\sigma'_{3u,s}$ are the effective axial and confining pressure at static failure, respectively, and σ'_3 is the effective confining pressure in the cyclic test.

It was explained that there would be a sudden change in the curve of excess pore pressure versus the number of cycles if cyclic stress ratio reaches a threshold value (Ni, 2012); and this very value is termed as the critical cyclic stress ratio. The critical cyclic stress ratio will be in the range of 0.5-0.8 if it is normalised by the deviator stress at failure in static test (Sangrey et al., 1969, Ansal and Erken, 1989, Zhou and Gong, 2001, Pillai et al., 2011).

2.5.3 Strain rate

Both the stress-strain curves and the ultimate undrained strength of saturated soils are affected dramatically by the loading rate (Casacrande and Wilson, 1951, Graham et al., 1983, Lefebvre and Leboeuf, 1987, Sheahan et al., 1996, Zhu and Yin, 2000, Torisu et al., 2012). The general conclusions are that the undrained shear strength increases with the strain rate and that the overall stress-strain curves depend on the loading/strain rate.

Graham et al. (1983) and Sheahan et al. (1996) suggested a method of describing the sensitivity of soil strength to the loading rate, which made comparison possible between various loading rate from test to test. A special parameter, $\rho_{\dot{\varepsilon}}$, which embodies the change in undrained shear strength with variations of loading/strain rate has a formation as shown below:

$$\rho_{\dot{\varepsilon}_{a0}}(\%) = \frac{\frac{\Delta S_u}{S_{u0}}}{\Delta(log\dot{\varepsilon}_a)} \times 100 \qquad \text{Eq 2.18}$$

where S_{u0} is the undrained shear strength at the reference load/strain rate, $\dot{\varepsilon}_0$, and ΔS_u is the increase in undrained shear strength for an increase in load/strain rate in logarithmic scale, $\Delta(log\dot{\varepsilon}_a)$.

Moreover, the sensitivity to the strain rate is related to the reference strain rate, and this rate dependence is a function of the strain range in tests (Sheahan et al., 1996).

The effect of strain rate was explained by Ni (2012) in two ways: the first one indicates that the increase in undrained shear strength is caused by a decrease in shear-induced excess pore pressure without changing the failure stress envelope; the second one suggests that an increase in strain rate causes less shear-induced excess pore pressure and mobilises more internal friction angle which in turn lifts the failure stress envelope.

In stress-control cyclic loading tests, the strain rate is related to the loading frequency. The frequency of cyclic tests in the laboratory was quite low in the early days because of limitations on the loading activator and pore pressure transducers; both of which needed a relatively long response time. However, with new measurement techniques, cyclic loading tests with high frequency are now possible. There are two test frames used now to study the strain rate dependence: one frame changes the frequency in a series of cyclic tests while the other one compares the performances of specimens between high frequency (high strain rate) and monotonic loading (low strain rate).

In the range of 0.1Hz to 1Hz, the cyclic undrained strength and the specimen modulus are almost independent of the loading frequency and the duration of repeated loading (Yasuhara et al., 1982). The limiting stress ratio was defined as a value below which cyclic loading has almost no weakening effect. The relationship between limiting stress ratio and loading frequency was found to depend on the methods of data processing, based on a series of stress and displacement controlled cyclic tests with frequencies ranging from 1/120-5Hz (Procter and Khaffaf, 1984). Specifically, if the limiting stress ratio is calculated using the modified strength, it will be independent of loading frequency, while if it is calculated by the static failure stress, it will increase with the

increase in loading frequency. Moreover, the performance of soft soil was significantly affected by the level of cyclic stress when the loading frequency was in a range of 0.1-5 Hz (Ni, 2012).

2.5.4 Overconsolidation ratio

The behaviour of soft clay is significantly influenced by the overconsolidation ratio, OCR, which is defined as the ratio of the maximum pressure in history to the present effective consolidation stress. Unfortunately, studies on the effect of OCR on the cyclic performance of soft soil are quite limited.

For the specimen under the same consolidation stress but with different OCRs, the development of excess pore pressure shows different paths (Takahashi et al., 1980). At a low OCR, the excess pore pressure increased slowly with the number of cycles and the effective stress path kept moving towards the failure envelope. For a high OCR, the effective stress path was already close to the envelope of failure stress in the early cycles.

Zhou and Gong (2001) suggested that the undrained secant shear modulus of soil clay decreased with an increase in the OCR, and that clay with a high OCR does not soften easily. This finding agreed with the tests of Vucetic and Dobry (1988), who stated that the OCR had a significant influence on the soil modulus.

With regards to the post-cyclic behaviour, the reduction in undrained shear strength after cyclic loading was only found for normally consolidated or slightly overconsolidated clay specimens. It was unlikely that the clay would generate a notable excess pore pressure with a high OCR value, so there were no substantial changes in the post-cyclic strength (Hyde and Ward, 1986). If the excess pore pressure dissipates

completely after cyclic loading, the undrained shear strength will increase because the dissipation of positive pore pressure means further consolidation for normally consolidated and slightly overconsolidated clay, but it will decrease for heavily overconsolidated clay due to the softening effect induced by the dissipation of negative pore pressure (Yasuhara, 1995).

2.6 Summary

This chapter presents a thorough review of previous research about performance of stone column, as well as some general understanding of behaviour of soft soil under cyclic loading. After reviewing the history of stone column, there appears a possibility of using stone column as ground improving method for transportation structures which has not been studied yet. During the construction of stone column, there is inevitably disturbance to surrounding soil, but this phenomenon has not been quantified in past research. Several important design parameters such as L/d ratio, area replacement ratio and stress concentration ratio are studied under static loading conditions. Previously, simple consolidation models are used to determine the consolidation rate of ground improved by stone columns, but some special features have not been included yet, therefore some changes must be made to the previous models. The basic knowledge of behaviour of soft soil under cyclic loading is introduced, because the research about the performance of ground improved with stone column under cyclic loading is missing. In conclusion, several important problems about stone column, such as installation effect, cyclic performance, more practical consolidation model, has not clearly solved yet, the following chapters will try to find some answers for these questions revealed in literature review.

Chapter-3 is related to the following publication: Tai, P., Indraratna, B., and Rujikiatkamjorn, C. (2017). "Experimental Simulation and Mathematical Modelling of Clogging in Stone Column". Canadian Geotechnical Journal, Published on the web 25 August 2017.

Chapter 3 Experimental Simulation and Mathematical Modelling of Clogging in Stone Column

3.1 Overview

Clogging of stone columns is derived from a mixture of column material and peripheral clay; it is a physical process rather than a biological or chemical cause. Physical clogging is a process whereby fine particles accumulate in the pore space of porous media by infiltration (Yong et al., 2013). Clogging related issues can generally be divided into two categories: the stability or erosion of base soil structures which provides fine base particles (Indraratna and Vafai, 1997), and the serviceability of the drainage layer such as filters or pavements which are in contact with the base soil (Siriwardene et al., 2007). Clogging of stone columns should fall into the second category. Clogging induced by the installation of stone columns has also been confirmed by centrifuge tests (Weber et al., 2010). Indraratna et al. (2013) stated that the consolidation of the surrounding soil would be reduced by initial clogging of column based on a numerical simulation, and subsequently, Basack et al. (2015) extended this model to capture time-dependent clogging. Deb and Shiyamalaa (2015) also proposed to include time-dependent clogging by considering reduced permeability with time.

Even though past research studies highlighted the importance of incorporating clogging in the analysis of consolidation, to the best of the author's knowledge, studies have rarely been reported where clogging is quantified accurately. One of the key objectives

of this chapter is to provide a detailed model test where clogging of stone column is assessed quantitatively. To deliver it, a single model column and its surrounding clay were compressed one-dimensionally (unit cell analysis), and after consolidation, a core sample was extracted and scanned using the computed-tomography (CT) technique. Subsequently, the extent of the clogging zone was evaluated, and the porosity of the granular mass could be calculated. The load-settlement response of this model test together with a past study (Basack et al. 2015) was then used to verify the newly proposed consolidation model. This consolidation model was solved numerically, and comparisons were then made with those solutions found in the literature.

3.2 Categorisation of clogging

The mechanisms of clogging in stone columns are different at various stages. Compaction or vibration is the main reason why clogging initiates during installation as the force applied to densify stone columns pushes the column material into the surrounding clay and thereby squeezes the fine soil grains into the gravel voids. It means that clogging already exists in the column to start with before consolidation begins. However, clogging can also develop during soil consolidation where the clay particles are forced to move laterally, and then become trapped at pore constrictions and continue to accumulate with time. Although the pores in stone column are larger than the clay particles, clogging can still occur due to bridges formed at the pore constrictions (Valdes and Santamarina, 2006) or initiating self-filtration (Reddi et al., 2000).

During installation, some initial clogging is inevitable, as the clay and granular material mix over a short period, compared to the time needed for soil consolidation. The properties of a clogged column depend on the amount of clay that intrudes into the

column skeleton. Permeability will decrease in this area of the column if the clay particles reduce the void ratio and obstruct the moisture movement. However, the compressibility of the clogged zone will increase if the retained clay is sufficient to reduce the inter-particle contact (friction). Previous studies state that time-dependent clogging is influenced by the diameter ratio of large particles to fine particles, the porosity of coarse material, the flow rate, fluid viscosity, suspended particle concentration and so on (Reddi et al., 2000, Valdes and Santamarina, 2006, Huston and Fox, 2015). A reduction in permeability due to clogging is understood based on the Kozeny-Carman theory which is widely used to predict the hydro-mechanical behaviour of a porous medium (Carrier III, 2003). Albeit variations of this original mathematical formulations, the intrinsic relationship that makes permeability to diminish as the porosity of the medium decreases is always valid (DeLeo, 1995). While the amount of retained base soil particles increases over time, the accumulated mass of trapped soil tends to decrease with distance from the inflow boundary (Alem et al., 2015). For the case of clogging in stone column, these findings mean that the extent of clogging would develop over time while the maximum reduction in permeability of the column is expected at the proximity to the soil/column boundary.

3.3 Model test and clogging identification

3.3.1 Selection of materials

The material for the model column was crushed from basalt collected from Boral quarry near Wollongong (NSW, Australia). Unlike the column material reported in previous model tests (Cimentada et al., 2011, Black et al., 2011), the maximum particle size of the material here is larger (gradation is shown in Figure 3.1) so that the angularity of

field column material could be reproduced to some extent. The maximum and minimum void ratios are obtained using the vibration table test and funnel pouring method, respectively. Constant head permeability tests are also carried out to determine its permeability at different densities. Several triaxial tests of this material are conducted to evaluate the internal friction angle and shear modulus, from which it appears that the compression modulus of the aggregates decreases with the increasing void ratio while the permeability remains almost constant.

Table 3.1 Properties of materials in model test

Properties of soil used in model test	
Kaolin Clay (commercial kaolin)	
Specific Gravity	[a]2.7
Liquid limit	[a]55
Plastic limit	[a]27
Compression Index	[a]0.42
Swelling Index	[a]0.06
Void ratio	[b]1.3/1.2
Vertical Permeability($\times 10^{-9}$ m/s)	[c]1.3/1.1
Compression modulus (MPa)	[c]1/1.3
Aggregates (Crushed Basalt)	
LA abrasion value	[d]15%
Point load index (MPa)	[d]5.39
Specific Gravity	2.65
Void ratio	0.65-1.08
Permeability ($\times 10^{-5}$ m/s)	1.9-4
Drained friction angle (Degrees)	47-52
Compression modulus (MPa)	[e]30-50

a. Obtained from Ni (2012)

b. Measured after 1D consolidation with 65kPa/110kPa vertical stress
c. Measured after anisotropic consolidation, σ_1'=65kPa/110kPa, σ_3'=50kPa
d. Value of Latite basalt from Indraratna et al. (1998)
e. Measured after isotropic consolidation, σ_3'=50kPa

Commercial kaolin clay (gradation in Figure 3.1) was selected as plastic clay for the model test. The properties of kaolin clay from slurry are corresponding to 65kPa and 110kPa pre-consolidation pressure. The shear modulus of kaolin clay was evaluated from several triaxial tests while the falling head permeability tests provide the permeability of kaolin clay at different void ratio; the measurements of permeability obtained agree with the test results given by Al-Tabbaa and Wood (1987). All the properties of materials are summarised in Table 3.1.

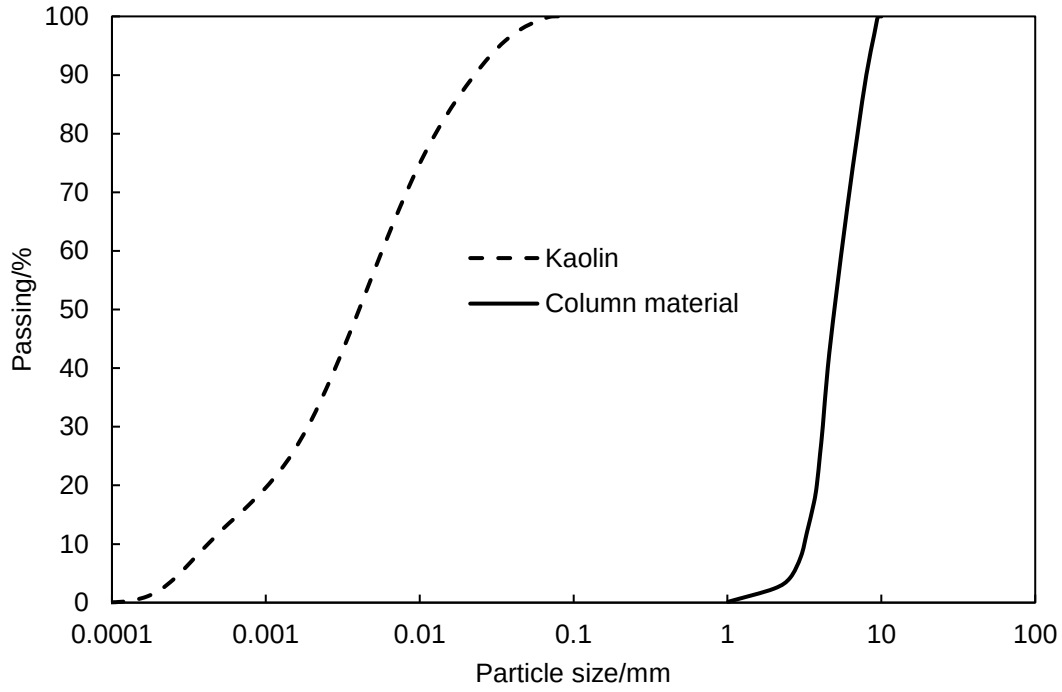

Figure 3.1 Gradations of material

3.3.2 Model test procedure

The kaolin clay slurry was prepared at 1.2 times liquid limit, corresponding to a water content of 67%, and then placed in a 760mm long cylindrical sample (300mm in

diameter) wrapped in a rubber membrane inside a 1-D loading rig as shown in Figure 3.2. A top load of 65kPa was then gradually applied to begin preliminary consolidation, after which the clay achieved an undrained shear strength of approximately 15kPa following the procedure adopted in (Mesri, 1975). At the end of this stage, the height of the sample was about 600mm.

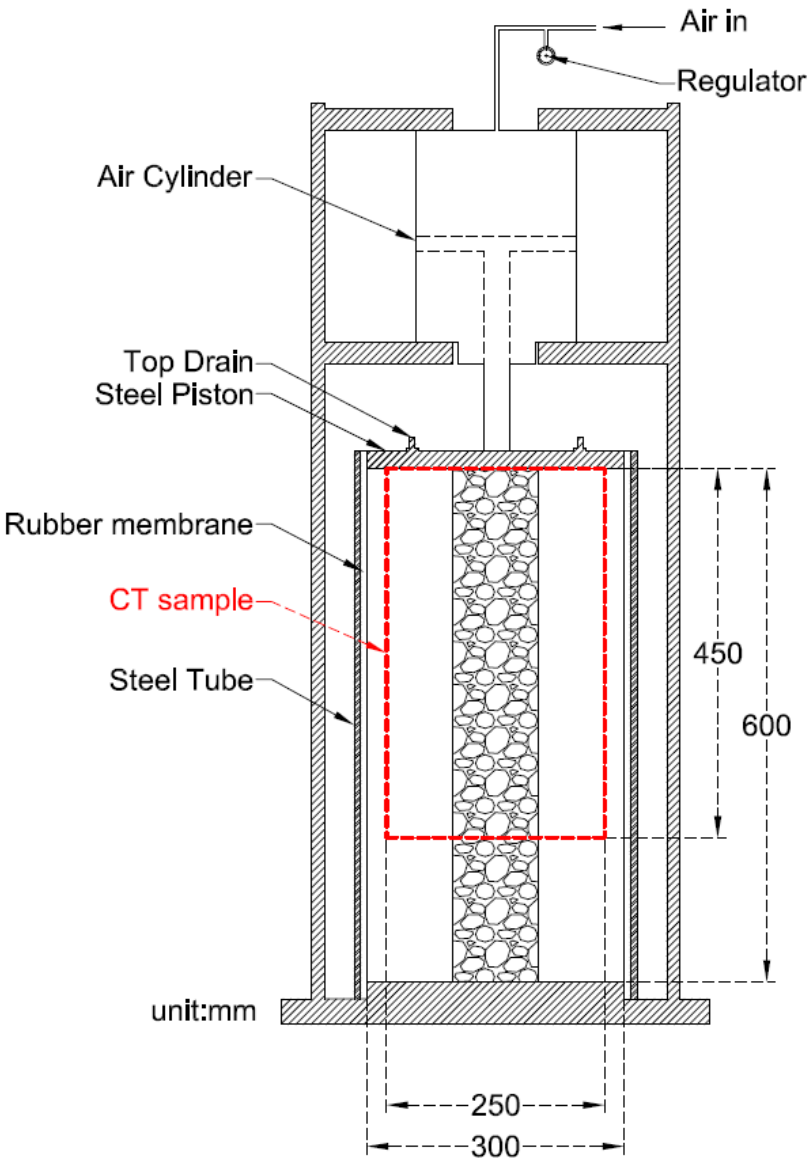

Figure 3.2 Setup of model test

Preliminary consolidation continued up to 30 days, and then a stone column consisting of crushed basalt particles was installed using a procedure described subsequently for simulating a replacement installation in the field. A tube of 100mm diameter was inserted into the middle of the clay sample to maintain a cylindrical cavity created when the clay in the tube was removed. Installation is a gradual process whereby the material is poured into the hole to a height of 110-120mm and then tamped down to a height of approximately 100mm, after the tube is pulled out another 100mm, and then a new layer of material is poured in. The total mass of aggregates was 7.75kg, and the cylindrically shaped column had a 50-55 mm radius, as measured on the top surface. It means that the average void ratio of the stone column only is approximately 0.9, which corresponds to a porosity of 0.49.

Then the specimen was placed under a vertical pressure which gradually increased from 65kPa to 210kPa. This top load was applied to the specimen through a rigid and permeable steel piston simulating “equal strain” consolidation (Barron, 1948). During consolidation, only top drainage was permitted, the loading force and associated settlement were recorded continuously.

3.3.3 CT scanning and image analysis

The core section of the post-consolidation test specimen (i.e. 250mm in diameter and 450mm high) was cut off with a sharpened PVC tube and scanned on an X-ray CT scanner (Toshiba Asteion S4 located at the CT Scanning Laboratory at the Centre for Geotechnical and Railway Research, University of Wollongong). The CT scanner can be classified as a high-resolution type (Ketcham and Carlson, 2001) with a resolution equivalent to 0.2mm which has an MTF (modulation transfer function) of 18 lp/cm at 0%.

The first test was conducted to evaluate the optimum scanning parameters and the best reconstructive function. The reconstructive function adopted possesses beam hardening that corrects the image artefacts which could result from the absence of lower energy x-rays. For this study, the scanning parameters were set at 135kV X-ray tube voltage and 200mA for the X-ray tube current. The X-ray beam was 3mm wide (i.e. slice thickness), the exposure time was 1second, and the field of view (FOV) was 21cm.

Although high energy X-rays (≥150kV) penetrate the objects more efficiently than lower energy X-rays, the latter shows any changes in density more distinctively (Ketcham and Carlson, 2001). The CT values that range from -1024Hu to +3071Hu, i.e. 4096 grey levels, cannot be viewed from a single view (Kalender, 2005). For that purpose, the complete grey scale is usually assigned a given interval of interest or window. Grey levels above the window are displayed in white whereas values below are displayed in black. The selection of an adequate window range is fundamental for isolating particular aspects the object imaged, particularly the width and centre of the window. The centre (C) represents the mean CT value displayed, while the window width (W) determines the contrast in which the image is viewed. The choice of C and W depends mainly on the range of densities that the object is expected to exhibit. In this study, different combinations of C and W were tried, and it was observed that a window having C of 900 and W of 2000 was the best for observing the unit stone column features.

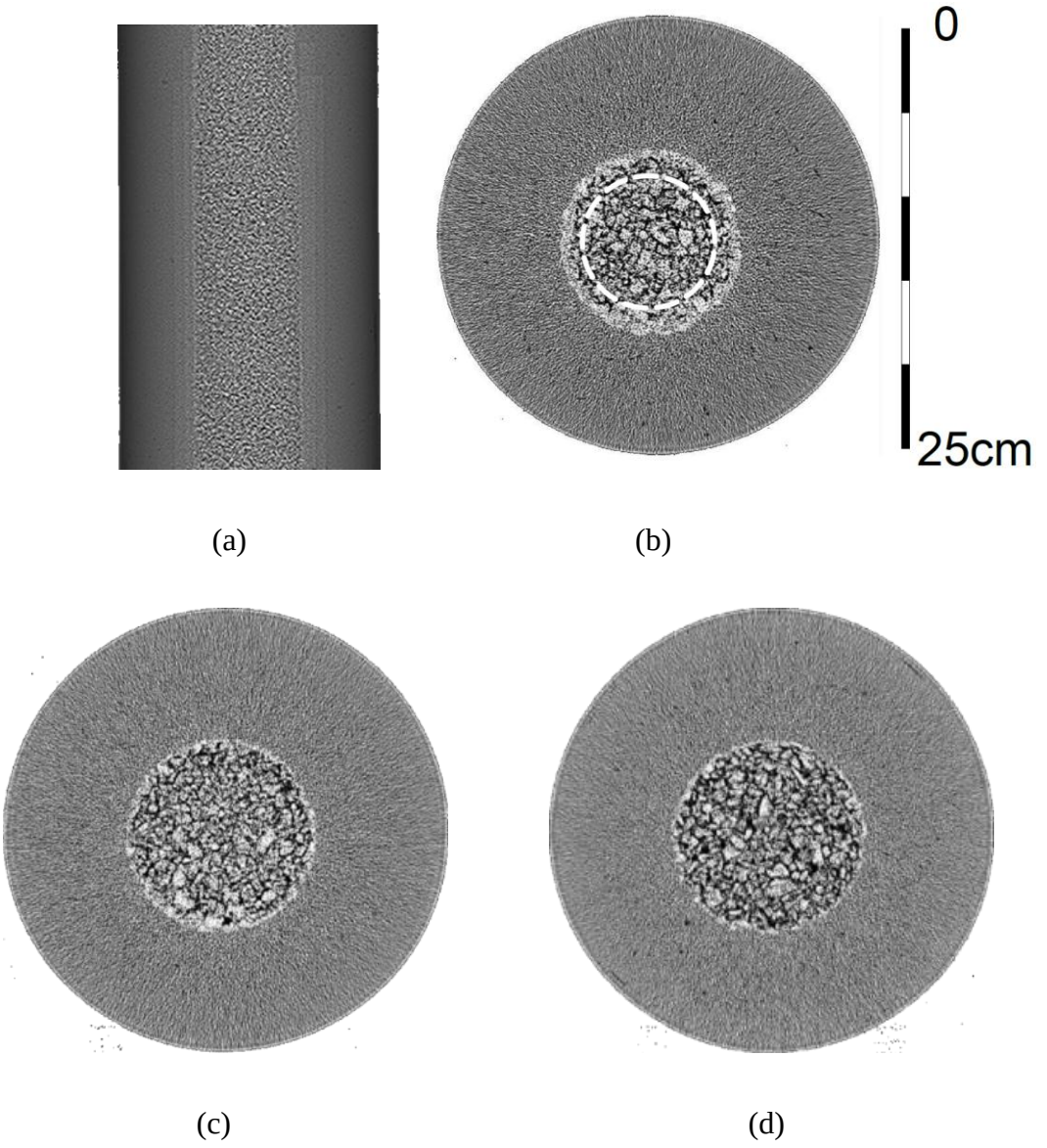

Figure 3.3 CT scan images: (a) longitudinal section; (b) cross-section (depth 15mm); (c) cross section (depth 130mm); (d) cross section (depth 395mm)

A longitudinal section was first obtained to examine the deformation of the entire column, and then 82 scans representing different cross-sections taken at different depths were conducted to expose the transition area between column and clay. An image of the longitudinal section displayed in Figure 3.3(a) shows that the model column retains its cylindrical shape after consolidation without any notable expansion. Three selected cross-sectional images are also given in Figure 3.3(b), (c) and (d), which correspond to the top, middle and bottom part of the CT sample respectively. It can be observed that

the clogging phenomenon is more severe in the top. Three main colour patterns were identified and correspond to the clean column zone, the clogged zone, and the clay zone, respectively. However, the resolution of scanner does not enable the pore sizes in clay to be observed, and thus the clay microstructure cannot be discerned in these tests, only the macrostructure and column aggregates can be easily distinguished.

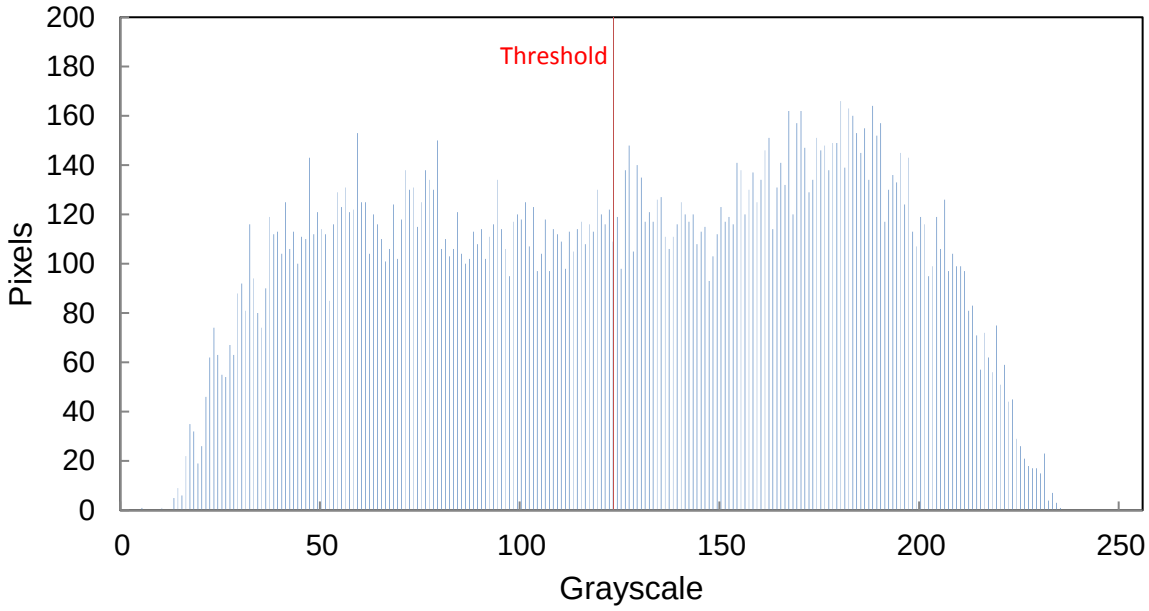

(a)

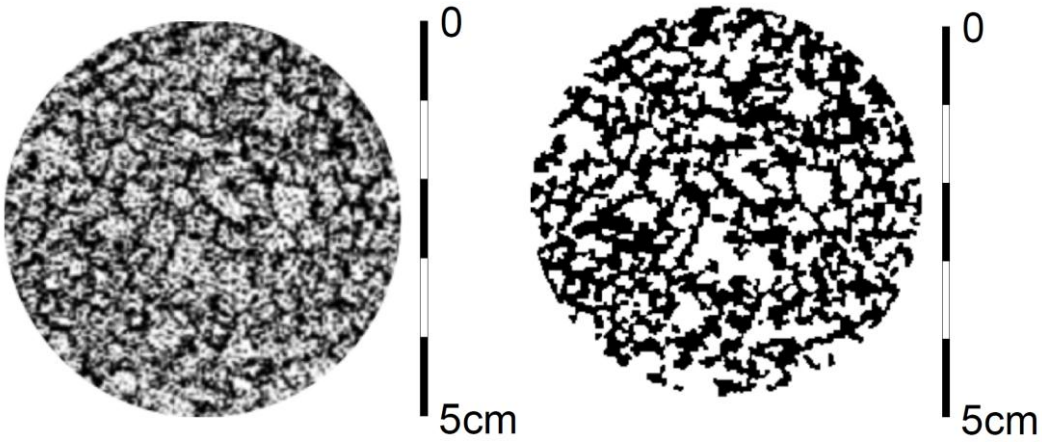

(b) (c)

Figure 3.4 (a) Histogram of cropped image; (b) clean column (depth-15mm); (c) image of clean column after binarization (depth-15mm)

Especially for the image corresponding to the depth of 15mm, a central circular part which represents the clean column was cropped and binarised after adopting a grayscale threshold (Otsu, 1975). The histogram of the cropped image is shown in Figure 3.4(a), while the images before and after binarization are displayed in Figure 3.4(b) and (c) respectively. Here the black pixels correspond to the pores and the white pixels the solid gravel particles. After binarization, the ratio of black pixels to all the pixels represents the porosity of the column. The mean value of porosity for all the images was slightly less than 0.5, which agreed with the void ratio of 0.96 that was determined earlier.

For a given volume of granular mass of this stone column, if the entire void space between coarse particles is entirely occupied by infiltrated clay, then the clay fraction in the clogged medium can be determined in the range of 0.32-0.34. The clay fraction is defined as the volume of fines in a unit volume of solids containing both fines and coarse grains (Simpson and Evans, 2016). It is also stated by Simpson and Evans (2016) that, when the clay fraction approaches a threshold of 0.2, it "demarcates a transition from a state where all coarse particles are touching each other". In other words, clay would begin displacing the coarse particles of the granular medium and break their contact beyond this threshold. The clay fraction in the current model test is well beyond this threshold.

The boundary of the clogged zone along the depth was determined as shown in Figure 3.5(a), and it quantitatively shows that clogging decreases in severity with depth. In terms of radius, the clogged zone occupies up to 20% of the outer ring of the entire column at the top 50mm, while it then decreases to around 10% at a depth of 50-100mm, and is even less than 5% for the remainder. The possible explanation is

presented as follow: The drainage is provided only at the top of the specimen setup. Also, the applied stress reaches a maximum at the top, and it diminishes with depth. It indicates that the soft soil (clay) at the top to become more affected by the generated hydraulic gradients in the shallow part of the column/soil compared to the deeper zone. As a result, a higher amount of soil is expected to be eroded into the column near the surface.

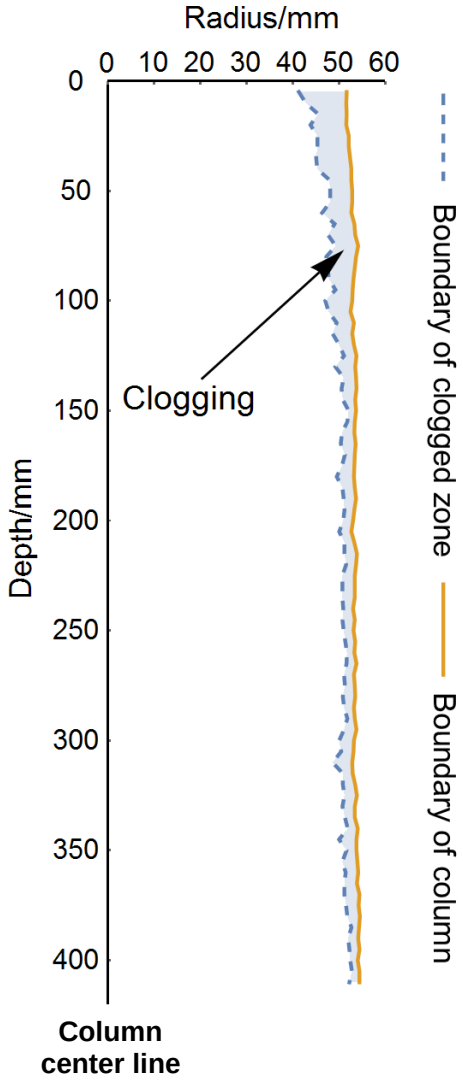

(a)

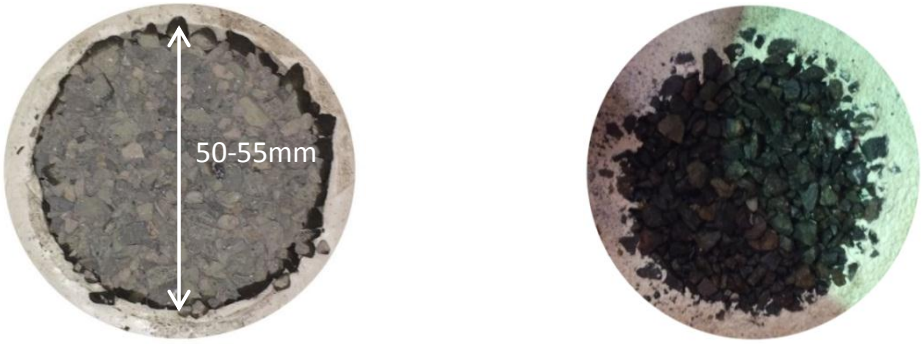

(b) (c)

Figure 3.5 (a) Extent of clogging in the CT sample; (b) surface view before test; (c) surface view after test

Moreover, the model column retains its cylindrical shape well after consolidation without any notable bulging. Photo images of the top surface of the column before and after the test are also shown in Figure 3.5(b) and (c) respectively. These images confirm that clogging is severe in the top column section while the internal part of the column remains relatively unaffected.

3.4 Properties of soil outside of the column

3.4.1 Soil in the clogged zone

The soil properties in the clogged zone are difficult to measure directly due to its small dimension. Therefore, an attempt was made to reproduce the soil mixture and examine how the properties of the mixture change with varying clay fractions. In this regard, different clay fractions were used to make several cylindrical samples and pre-loaded before conducting falling head permeability tests and compression tests to determine the corresponding permeability and compressibility properties. These properties were then compared to previous data (Watabe et al., 2011, Simpson and Evans, 2016) as shown in Figure 3.6. The current test results agree well with previous data. Due to

different size of coarse particles and loading paths used in various tests, two normalised parameters are defined to compare the results, hence,

$$\Delta m_v = \frac{m_{vm} - m_{vc}}{m_{vf} - m_{vc}} \quad \text{Eq 3.1}$$

$$\Delta k = \frac{\lg(k_c) - \lg(k_m)}{\lg(k_c) - \lg(k_f)} \quad \text{Eq 3.2}$$

where Δk and Δm_v are the normalised permeability and compressibility variation respectively; k_c and m_{vc} are the permeability and compressibility of coarse aggregates respectively; k_f and m_{vf} are the permeability and compressibility of the fines respectively; k_m and m_{vm} are the permeability and compressibility of the mixture, respectively.

The soil properties in the clogged zone were selected based on best-fit regression for a determined clay fraction of 0.32 (Figure 3.6).

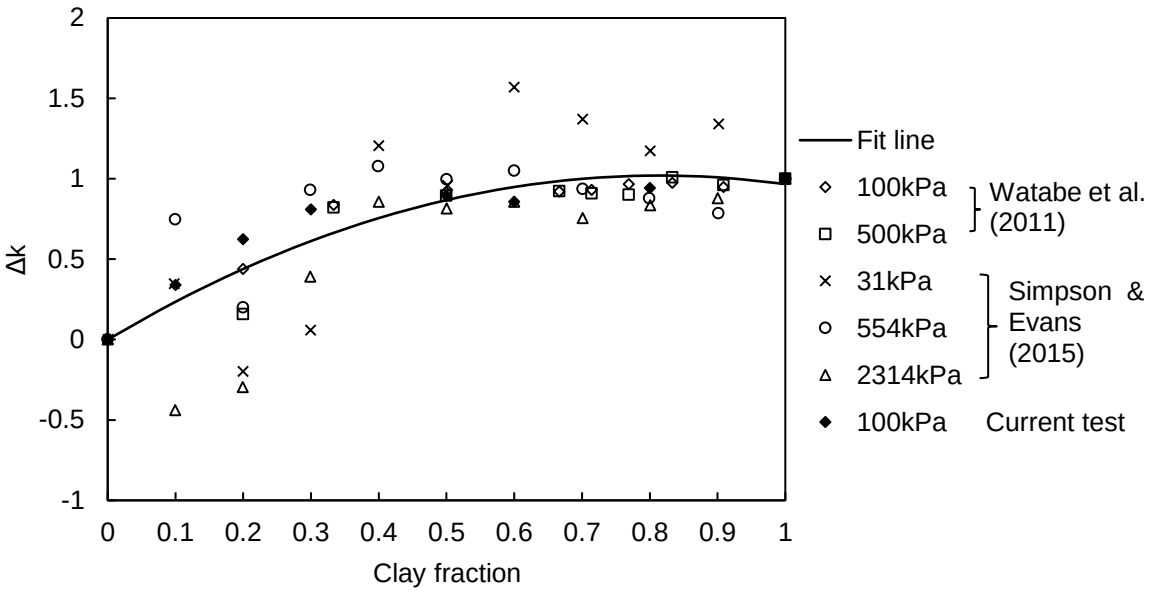

(a)

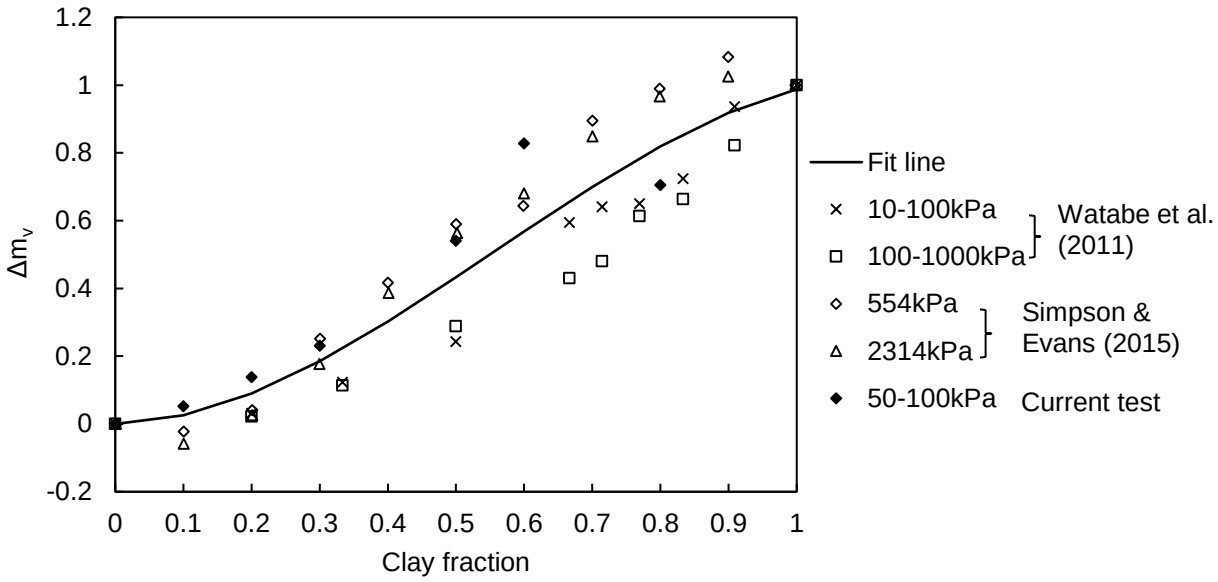

(b)

Figure 3.6 Change of mixture properties with clay fraction: (a) permeability; (b) compressibility

3.4.2 Pure clay

Several samples of pure clay were extracted from different depths and radii of the model test sample to detect any disturbance to the surrounding clay resulting from column installation. The samples were cut and trimmed carefully with 28mm diameter by 30mm high cutting rings, immersed in a tank of de-aired water tank two weeks for saturation, after which their water content was measured and the void ratio of each sample calculated. The varying void ratios with radius and depth are shown in Figure 3.7. It should be noted that the cutting ring walls are thin (i.e. 1mm) and thus it is assumed that the disturbance caused by inserting the ring can be negligible.

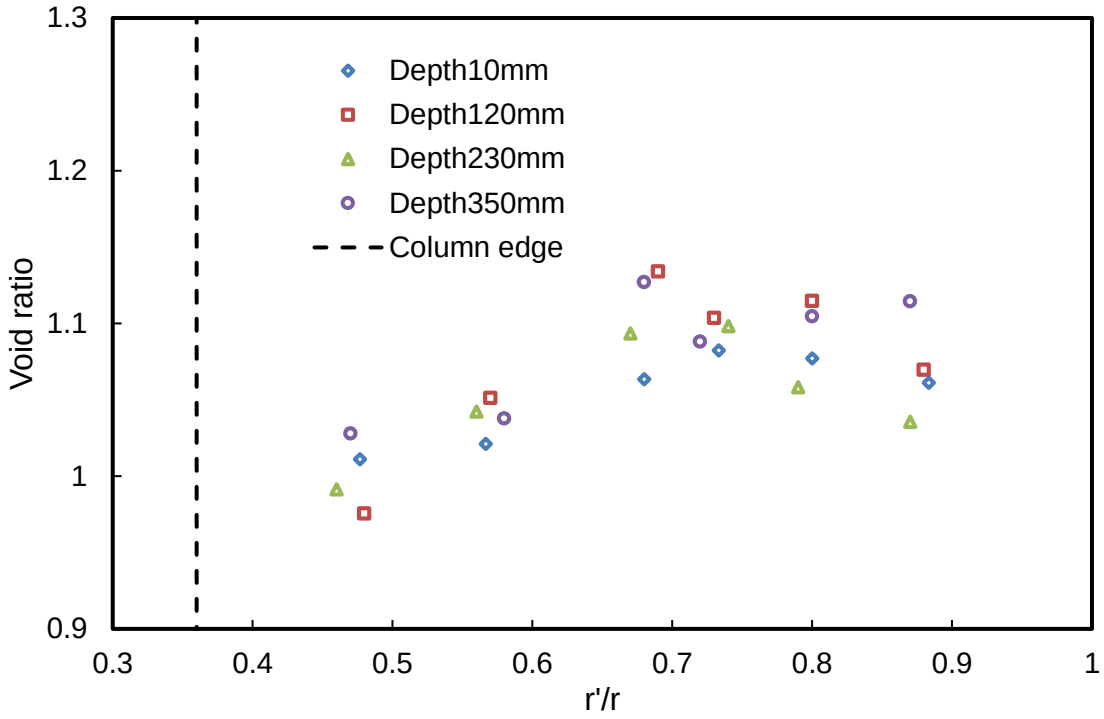

Figure 3.7 Void ratio of clay in different radius and depth

The average water content of clay was 40.2%, and the average bulk density of clay was 18.1 kN/m^3. All the void ratios are between 0.96-1.14, which is slightly lower than those under vertical stress of 65 kPa. It indicates that the surrounding soil has been consolidated. The corresponding horizontal permeability values were computed based on the empirical formulae proposed by Al-Tabbaa and Wood (1987), and the maximum and minimum horizontal permeability were calculated to be 1.94×10^{-9} m/s and 1.37×10^{-9} m/s respectively.

Moreover, the void ratio of the clay near the column is lower than the ratio further away, which agrees with the findings of Weber et al. (2010), but there is no particular sign of the void ratio changing with depth. It seems likely that installation slightly densified the clay near the column, but the effect regarding permeability was negligible. Therefore, the pure clay outside the column is treated as undisturbed.

3.5 Consolidation model considering time-dependent clogging

A mathematical expression was deemed necessary to describe the effect of clogging in stone column on the soil consolidation. Besides the dependence on time, the property of a clogged column also alters with the radius and depth, so for simplicity, the average properties of different zones of the column are used. As shown in Figure 3.8(a), this schematic illustration of the model column consists of a clean section and a clogged zone, and the clay area is divided into disturbed and undisturbed zones. The clogged zone is subdivided into two portions which correspond to initial clogging during installation and time-dependent clogging during consolidation, respectively. The average soil properties are assigned to each zone, and the extent of clogging is then simulated by moving the boundary between the clean section of the column and the clogged zone, as shown in Figure 3.8(b).

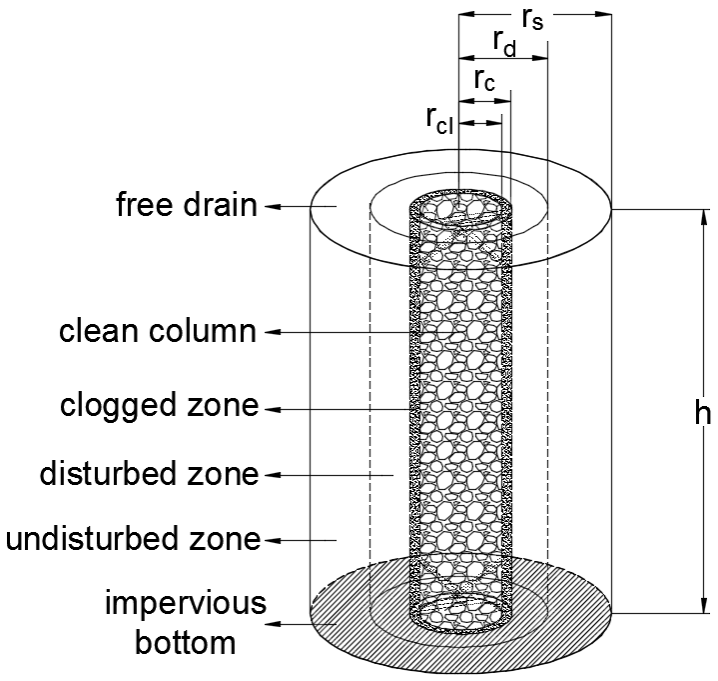

(a)

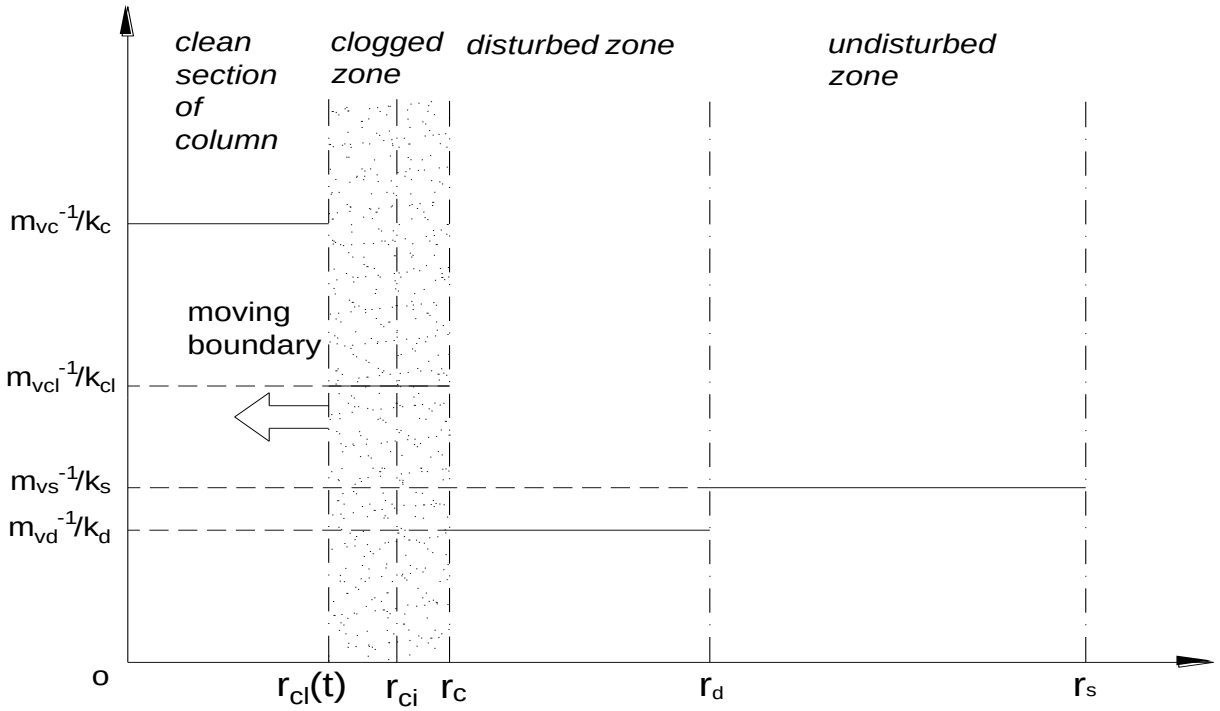

(b)

Figure 3.8 (a) Sketch of unit cell; (b) distribution of properties in unit cell

The principle exploited to obtain the mean permeability of the whole column is such that the water flows out of the column at a given time is assumed to remain constant at any depth. The mean compressibility is then determined by assuming that the vertical strain is the same for the clogged zone and the clean column (i.e. equal strain). The average permeability and compressibility can then be computed as:

$$\bar{k}_c(t) = \frac{k_c r_{cl}^2(t) + k_{cl}(r_c^2 - r_{cl}^2(t))}{r_c^2} \qquad \text{Eq 3.3}$$

$$\bar{m}_{vc}(t) = \frac{r_c^2}{\frac{r_{cl}^2(t)}{m_{vc}} + \frac{r_c^2 - r_{cl}^2(t)}{m_{vcl}}} \qquad \text{Eq 3.4}$$

where $\bar{k}_c(t)$ and $\bar{m}_{vc}(t)$ are functions of time which are used to define column permeability and compressibility respectively, k_c and k_{cl} are the permeability of soil in

the clean column and in the clogged zone respectively, m_{vc} and m_{vcl} are the coefficients of volume compressibility of soil in the clean column and clogged zone respectively, $r_{cl}(t)$ is a mathematical function to define the time-dependent boundary between the clean column and clogged zone, , and r_c is the radius of the column.

Two modes of clogging are hypothesised here; the first mode, as noted by "I" in Figure 3.9, shows that the clogging area extends linearly with time until a critical time, whereas in type "II" the radius of the clean column decreases exponentially until it is stable. The progress of clogging can then be described as follows:

$$\text{I:}\quad r_{cl}(t) = \begin{cases} r_{ci} - t\frac{r_{ci}-r_{cl}}{t_c} & (0 \le t < t_c) \\ r_{cl} & (t \ge t_c) \end{cases} \qquad \text{Eq 3.5}$$

$$\text{II:}\quad r_{cl}(t) = r_{cl} + (r_{ci} - r_{cl})e^{-4.6t/t_c} \qquad \text{Eq 3.6}$$

where r_{ci} represents the boundary of the clean column, and the clogged zone after initial clogging and r_{cl} is the final radius of the clean section of the column; t_c is the time when clogging is complete for pattern I, and when the time-dependent clogging area expands to 99% of its final value for pattern II. For pattern II, due to the exponential function used, 100% can only be reached when the time approaches infinity, so the constant, -4.6, in Eq 3.6 corresponds to 99% when the time reaches a critical value.

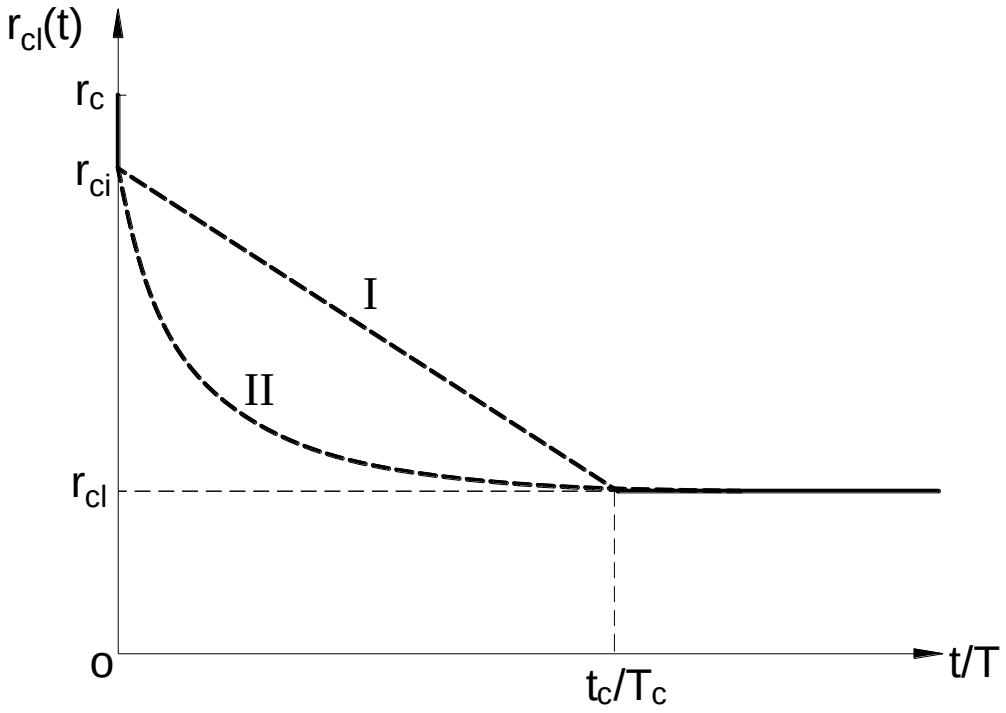

Figure 3.9 Patterns of clogging development

3.5.1 Governing equations

Several basic assumptions are made herein:

i. Due to the adoption of equal strain hypothesis for this unit cell, only the vertical strain is considered, and it is assumed to be uniform regardless of the radius at any depth;

ii. Traditional linear Darcy's law is assumed to be valid;

iii. Only vertical flow is considered in the column, while only radial flow is considered in the surrounding clay. Pore pressure in the clay varies with the radius and depth;

iv. The load on top of the unit cell is applied instantaneously and then held constant.

The stress distributions on the unit cell can then be determined through the effective stress principle as,

$$\pi(r_s^2 - r_c^2)\bar{\sigma}_s + \pi r_c^2 \bar{\sigma}_c = \pi r_s^2 \sigma \quad \text{Eq 3.7}$$

$$\bar{m}_{vs}(\bar{\sigma}_s - \bar{u}_s) = \bar{m}_{vc}(t)(\bar{\sigma}_c - u_c) = \varepsilon_v \quad \text{Eq 3.8}$$

$$\bar{m}_{vs} = \frac{r_s^2 - r_c^2}{\int_{r_c}^{r_s} \frac{2\pi r}{m_{vs}(r)} dr} \quad \text{Eq 3.9}$$

where $\bar{\sigma}_s$ and $\bar{\sigma}_c$ are the average total vertical stresses on the surrounding soil and the column at any depth respectively; $\bar{u}_s$ is the average excess pore pressure in the surrounding soil at any depth; u_c is the excess pore pressure in the column at any depth; $\bar{m}_{vs}$ is the average coefficient of volume compressibility of the surrounding soil; $m_{vs}(r)$ is a function of the radius for defining the variation of coefficient of volume compressibility in the surrounding soil; r_s is the radius of the influence zone, and ε_v is the vertical strain of both the column and the surrounding soil.

The compressibility of column varies with time due to clogging; not only it would affect the vertical strain directly according to Eq 3.8, but also the changing stiffness ratio of the column to clay would influence the build-up of excess pore water pressure. In this way, the 'equal strain' analysis is expected to give different pore pressure and consolidation results compared to the previous 'free strain' analysis of a unit cell (e.g. Indraratna et al. 2013; Basack et al. 2015).

For equal strain condition, the average excess pore water pressure at a given depth of the unit cell $\bar{u}$ and the corresponding rate of vertical strain at the same depth can be expressed by:

$$\bar{u} = \frac{1}{\pi r_s^2}(\bar{u}_s \int_{r_c}^{r_s} 2\pi r dr + u_c \int_0^{r_c} 2\pi r dr) \quad \text{Eq 3.10}$$

$$\frac{\partial \varepsilon_v}{\partial t} = \frac{\partial[\bar{m}_v(t) \cdot (\sigma - \bar{u})]}{\partial t} \quad \text{Eq 3.11}$$

$$\bar{m}_v(t) = \frac{r_s^2}{\frac{r_c^2}{\bar{m}_{vc}(t)} + \frac{r_s^2 - r_c^2}{\bar{m}_{vs}}} \quad \text{Eq 3.12}$$

where $\bar{m}_v(t)$ is the coefficient of volume compressibility of the unit cell.

If the column compressibility is made equal to that of the surrounding clay, then the current problem will become the same as radial consolidation of a vertical drain system. On the contrary, if the compressibility ratio of the column to clay is made to decrease to a sufficiently low value, then the vertical strain of the unit cell will diminish considerably to an extent that the soil consolidation will become negligible; thereby approaching a single pile foundation system.

If the volume change of the surrounding soil equals the change in flow volume, the following equation can describe the consolidation of surrounding clay:

$$\frac{1}{\gamma_w r}\frac{\partial}{\partial r}\left(k_s \cdot f(r) \cdot r \cdot \frac{\partial u_s}{\partial r}\right) = -\frac{\partial \varepsilon_v}{\partial t} \quad \text{Eq 3.13}$$

where k_s is the permeability of undisturbed clay, *f(r)* is a function used to describe the varying permeability of surrounding clay with radius, γ_w is the unit weight of water, and u_s is the excess pore pressure at a certain point in the surrounding clay.

The governing equation for the column can then be derived by assuming the column deformation to be equal to the net water flow, thus,

$$\frac{2k_s}{\gamma_w r_c}\frac{\partial u_s}{\partial r}\Big|_{r=r_c} + \frac{\bar{k}_c(t)}{\gamma_w}\frac{\partial^2 u_c}{\partial z^2} = -\frac{\partial \varepsilon_v}{\partial t} \quad \text{Eq 3.14}$$

Based on the unit cell hypothesis and strain compatibility requirement, the following boundary conditions are applied:

i. No water flow at the cylindrical surface and the bottom of unit cell;

ii. The pore pressure is continuous at the column-clay interface;

iii. Zero excess pore water pressure at the top surface (free-draining);

iv. The initial pore water pressure is assumed to be the same as the initial loading intensity.

Given the unit cell height as "h", these boundary conditions can be expressed as:

$$\left.\frac{\partial u_s}{\partial r}\right|_{r=r_s} = 0 \qquad \text{Eq 3.15}$$

$$\frac{\partial \bar{u}_s(h,t)}{\partial z} = \frac{\partial u_c(h,t)}{\partial z} = 0 \qquad \text{Eq 3.16}$$

$$u_s = u_c(r = r_c) \qquad \text{Eq 3.17}$$

$$\bar{u}_s(0,t) = u_c(0,t) = 0 \qquad \text{Eq 3.18}$$

$$\bar{u}_s(z,0) = u_c(z,0) = \sigma \ \ (z > 0) \qquad \text{Eq 3.19}$$

By combining the consolidation of the column and surrounding clay, several mathematical manipulations are made to obtain a unified governing equation.

Integrating Eq 3.13 regards to radius and using boundary condition Eq 3.15 would yield

$$\frac{\partial u_s}{\partial r} = \frac{\gamma_w (r_s^2 - r^2)}{2k_s f(r) r} \frac{\partial \varepsilon_v}{\partial t} \qquad \text{Eq 3.20}$$

Then substitute Eq 3.20 into Eq 3.14 will obtain:

$$\frac{r_s^2}{r_c^2}\frac{\partial \varepsilon_v}{\partial t} + \frac{\bar{k}_c(t)}{\gamma_w}\frac{\partial^2 u_c}{\partial z^2} = 0 \qquad \text{Eq 3.21}$$

If combining the integral of equation Eq 3.20 with boundary condition Eq 3.16, the equations below can be deduced

$$u_s - u_c = \frac{\gamma_w}{2k_s}\frac{\partial \varepsilon_v}{\partial t}\int_{r_c}^{r} \frac{r_s^2 - r^2}{f(r) r}\, dr \qquad \text{Eq 3.22}$$

Then the average pore pressure in the surrounding clay can be calculated

$$\bar{u}_s = \frac{1}{\pi(r_s^2 - r_c^2)} \int_{r_c}^{r_s} 2\pi r u_s dr = u_c + \frac{\gamma_w A}{k_s(r_s^2 - r_c^2)} \frac{\partial \varepsilon_v}{\partial t} \qquad \text{Eq 3.23}$$

Eq 3.23 can be manipulated further to obtain the second derivative of u_s regarding depth.

$$\frac{\partial^2 \bar{u}_s}{\partial z^2} = \frac{\partial^2 u_c}{\partial z^2} + \frac{\gamma_w A}{k_s(r_s^2 - r_c^2)} \frac{\partial^3 \varepsilon_v}{\partial t \partial z^2} \qquad \text{Eq 3.24}$$

Finally, a unified governing equation Eq 3.25 can be obtained by combining Eq 3.10, Eq 3.21 and Eq 3.24.

$$\bar{m}_v(t) \frac{\partial^3 \bar{u}}{\partial z^2 \partial t} + [\bar{m}_v{}'(t) + B] \frac{\partial^2 \bar{u}}{\partial z^2} + C \frac{\bar{m}_v(t)}{\bar{k}_c(t)} \frac{\partial \bar{u}}{\partial t} + C \frac{\bar{m}_v{}'(t)}{\bar{k}_c(t)} \bar{u} = C\sigma \frac{\bar{m}_v{}'(t)}{\bar{k}_c(t)} \qquad \text{Eq 3.25}$$

$$A = \int_{r_c}^{r_s} r \int_{r_c}^{r} \frac{r_s^2 - r^2}{f(r) r} dr\, dr$$

$$B = \frac{k_s r_s^2}{A \gamma_w}$$

$$C = -\frac{k_s r_s^4}{A r_c^2}$$

A collation of the mathematical consolidation models for soil improved by stone columns is enumerated in Table 3.2, in comparison with the current model.

Table 3.2 Comparison of consolidation models for stone column improved soil

Models	Clogging		Column deformation	Well resistance	Basic hypothesis
	Initial	Time-dependent			
Han & Ye (2001, 2002)	N/A	N/A	N/A	Yes	Equal strain
Wang (2009)	N/A	N/A	N/A	Yes	Equal strain
Xie et al. (2009)	N/A	N/A	Yes	Yes	Equal strain
Lu et al. (2010)	N/A	N/A	Yes	Yes	Equal strain
Indraratna et al. (2013)	Yes	No	N/A	N/A	Free strain
Basack et al. (2015)	No	Yes	N/A	N/A	Free strain
Deb & Shiyamalaa (2015)	No	Yes	N/A	N/A	Equal strain
Current model	Yes	Yes	Yes	Yes	Equal strain

3.5.2 Mathematical solution for 'no clogging' and 'clogging'

Eq 3.25 is a high-order non-homogeneous linear partial differential equation, so no existing method can be used directly to solve it. However, as suggested by various studies (Tang and Onitsuka, 1998, Leo, 2004, Lu et al., 2010, Lei et al., 2015), the mean excess pore water pressure at a given depth of unit cell can be expressed using a Fourier series, such as

$$\bar{u} = \sum_{n=1}^{\infty} T_n(t) \cdot sin(\alpha_n z) \qquad \text{Eq 3.26}$$

$$\alpha_n = \frac{2n-1}{2h}\pi$$

The item on the right-hand side of Eq 3.25 can also be expanded to a sinusoidal series, hence,

$$C\sigma \frac{\bar{m}_v{}'(t)}{\bar{k}_c(t)} = \frac{2C\sigma}{\alpha_n h}\frac{\bar{m}_v{}'(t)}{\bar{k}_c(t)} \sum_{n=1}^{\infty} sin(\alpha_n z) \qquad \text{Eq 3.27}$$

Substituting Eq 3.26 and Eq 3.27 into Eq 3.25, the following non-homogeneous ordinary differential equation is obtained,

$$T_n{}'(t)\bar{m}_v(t)\left(\frac{C}{\bar{k}_c(t)} - \alpha_n^2\right) + T_n(t)[C\frac{\bar{m}_v{}'(t)}{\bar{k}_c(t)} - \alpha_n^2(\bar{m}_v{}'(t) + B)] = \frac{2C\sigma}{\alpha_n h}\frac{\bar{m}_v{}'(t)}{\bar{k}_c(t)} \qquad \text{Eq 3.28}$$

The solution to Eq 3.28 cannot be derived by explicit integrals, but the function $T_n(t)$ could be solved numerically using the Runge-Kutta method. The average degree of consolidation in terms of excess pore water pressure for the unit cell $\bar{U}$, which changes with dimensionless time factor T, is then given by the following:

$$\bar{U} = 1 - \frac{\int_0^h \bar{u}dz}{\sigma h} = 1 - \sum_{n=1}^{\infty} \frac{T_n(T)}{\sigma h \alpha_n} \qquad \text{Eq 3.29}$$

$$T = \frac{k_s}{4m_{vs}\gamma_w r_s^2}t$$

3.5.3 Case of 'no clogging'

In the absence of clogging, Eq 3.25 simplifies to the form below,

$$\bar{m}_v \left(\frac{C}{k_c} - \alpha_n^2\right) T_n'(t) - B\alpha_n^2 T_n(t) = 0 \quad \text{Eq 3.30}$$

$$\bar{m}_v = \frac{r_s^2}{\frac{r_c^2}{m_{vc}} + \frac{r_s^2 - r_c^2}{\bar{m}_{vs}}}$$

An analytical solution for the average pore water pressure and the corresponding degree of consolidation can now be readily obtained for the case of no clogging, thus:

$$\bar{u} = \sum_{n=1}^{\infty} \frac{2\sigma}{\alpha_n h} \cdot e^{\frac{-B\alpha_n^2 k_c t}{\bar{m}_v(\alpha_n^2 k_c - C)}} \cdot sin(\alpha_n z) \quad \text{Eq 3.31}$$

$$\bar{U} = 1 - \sum_{n=1}^{\infty} \frac{2}{\alpha_n^2 h^2} e^{\frac{-B\alpha_n^2 k_c t}{\bar{m}_v(\alpha_n^2 k_c - C)}} \quad \text{Eq 3.32}$$

Table 3.3 Parameters for comparison of different consolidation models

Case of 'no clogging' (Indraratna et al. 2013)				
k_c(m/s)	k_s(m/s)	k_d(m/s)	r_c(m)	r_s/r_c
[a]1.6×10^{-6}	1.6×10^{-9}	1.6×10^{-10}	0.5	3
r_d/r_c	m_{vs}/m_{vc}	m_{vs}(MPa^{-1})	h(m)	
1.15	7	0.5	16	

Case of clogging				
Indraratna et al. (2013)	$\alpha = 0.5$		$\alpha_k = 0.5$	
Deb & Shiyamalaa (2015)	$\alpha_0 = 4\times10^{-5}s^{-1}$		$\beta = 10^{-12}s^{-1}$	
Current model	m_{vcl}/m_{vc}	k_{cl}/k_c	r_{cl}/r_c	T_c (when $r_{ci} = r_c$)
	[b]2	[b]0.1	[b]0.7	[b]1

a. obtained from Han & Ye (2002)
b. assumed for the present analysis

The case of ‘no clogging’ is now considered with parameters obtained from Indraratna et al. (2013), although the permeability of column is chosen according to Han and Ye (2002). The parameters for this case of ‘no clogging’ are listed in Table 3.3.

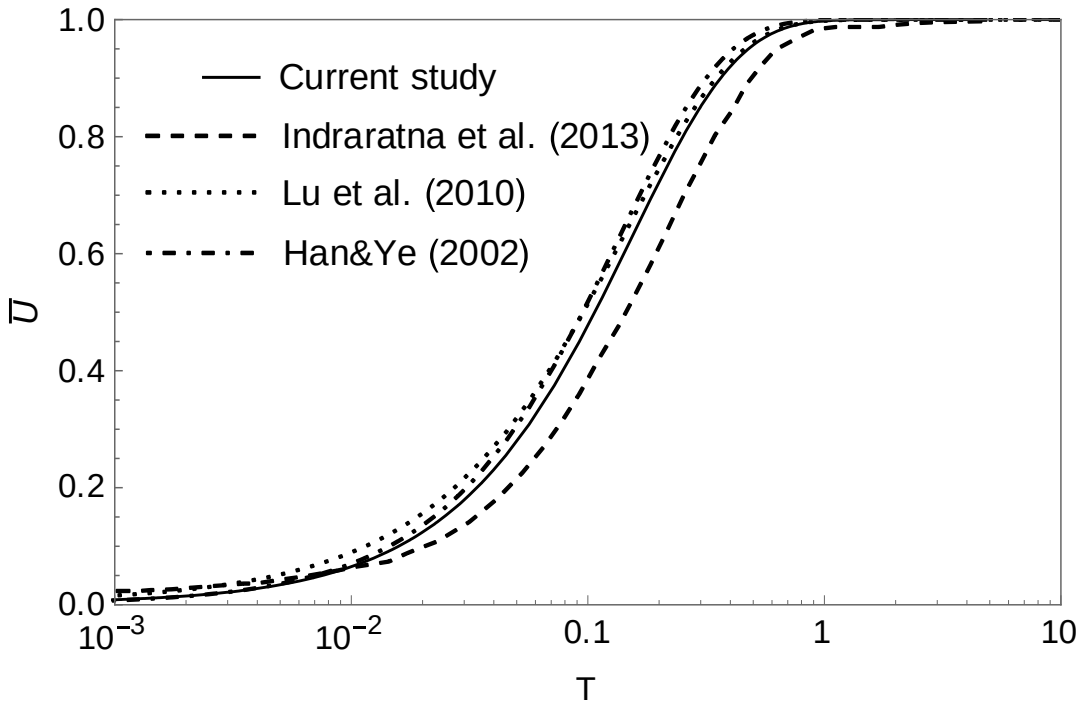

Figure 3.10 Comparison of consolidation rate with previous studies (no clogging)

The consolidation curves of different models are computed and plotted in Figure 3.10. The estimation of the average degree of consolidation given by the current model is almost identical to the previous solutions of ‘equal strain’ models (Han and Ye, 2002, Lu et al., 2010). The prediction by the model of Indraratna et al. (2013) underestimates consolidation, possibly because of its ‘free strain’ hypothesis.

3.5.4 Case of clogging

The effect of clogging has also been studied using the same case above but with additional clogging related parameters incorporated in the analysis. Indraratna et al. (2013) introduced two parameters to describe and support the concept of initial clogging: (i) the radius ratio of the clogged zone to the column, α; (ii) the ratio of clogged permeability to clean column permeability, α_k. In contrast, time-dependent clogging has been described based on release coefficient α_0 and capture coefficient β (Deb and Shiyamalaa, 2015). The clogged zone was evaluated to be as much as 20% in the current study, while the "penetration zone" was reported elsewhere to be about 30% (Weber et al. 2010). Based on these findings, a more conservative situation is assumed where a clogging zone over time is assumed to occupy the outer 30% of the column in terms of radius and any initial clogging is ignored. The clogging related parameters are also given in Table 3.3.

The current model prediction in comparison with above mentioned two models (i.e. initial clogging and time-dependent clogging) is plotted in Figure 3.11. The results show that the model proposed by Deb and Shiyamalaa (2015) predicts a faster consolidation rate, while the model by Indraratna et al. (2013) gives a lower degree of consolidation ($\bar{U}$) for the same time factor (T). The effect of omitting the change of column compressibility by Deb and Shiyamalaa (2015) could be the reason of a faster consolidation prediction. Moreover, in the model proposed by Indraratna et al. (2013), the 'worst-case scenario' was considered where maximum clogging would occur at the initial stage, therefore, the subsequent consolidation rate is significantly impeded as expected.

Using the current model, different scenarios of clogging could be considered and simulated: (i) no time-dependent clogging ($r_{ci} = r_{cl}$), i.e. clogging is assumed to have finished initially before any consolidation; and (ii) linear and exponential patterns of clogging over time in lieu of initial clogging ($r_{ci} = r_c$).

Through comparison of these scenarios, it is also observed (Figure 3.11) that the assumption of maximum clogging at the initial stage can delay the consolidation process further compared to the time-dependent clogging models, and that there will be further delay in consolidation if the clogging process follows pattern II (exponential) instead of pattern I (linear).

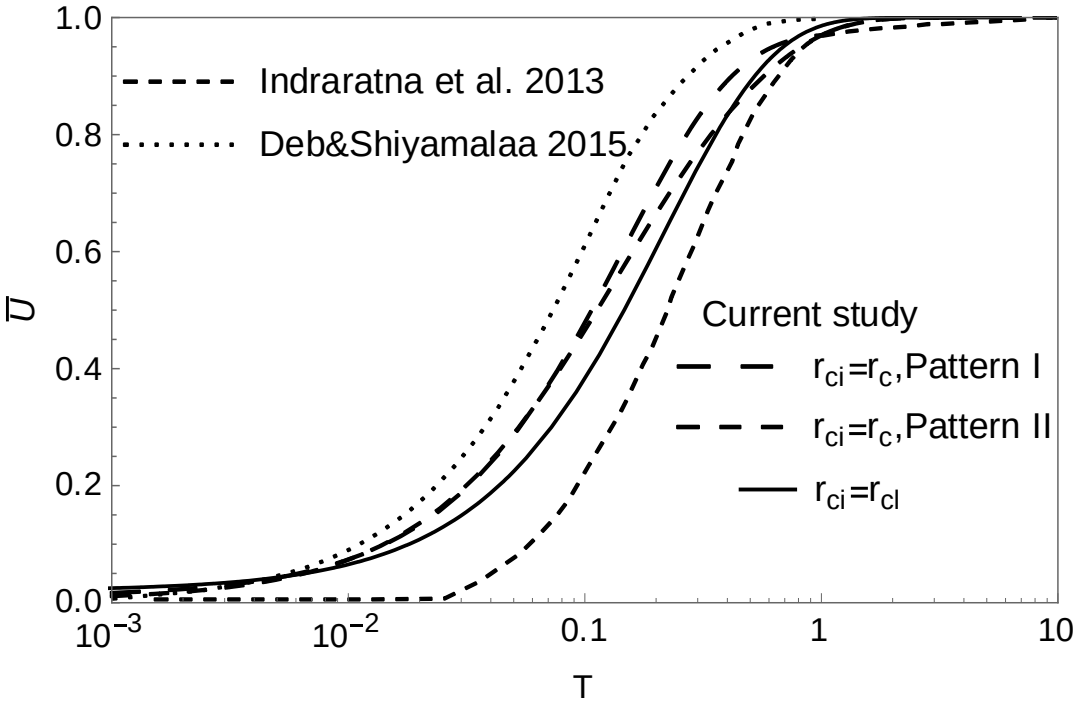

Figure 3.11 Comparison of consolidation rate with previous studies (including clogging)

3.6 Theoretical model validation by physical modelling

In this section, the proposed consolidation model formulated and described earlier will be validated using two laboratory physical model tests. One of them was elaborated given earlier in the 'Model Test' section. The other one was reported by Basack et al. (2015).

Table 3.4 Parameters for predicting model tests

	Current model test	Model test by Basack et al. (2015)
k_c(m/s)	*a* 3×10^{-5}	–
k_s(m/s)	*a* 1.3×10^{-9}	10^{-9}
k_{cl}/k_c	*b* 10^{-3}	–
r_c(m)	*c* 0.055	0.05
r_s(m)	*c* 0.15	0.15
r_{cl}/r_c	0.9	0.92
h(m)	*c* 0.6	0.6
m_{vs}(MPa^{-1})	*a* 1	2
m_{vs}/m_{vc}	*a* 30	–
m_{vs}/m_{vcl}	*b* 3.9	–

a. chosen based on material tests
b. determined through the fit line in Figure 3.6
c. measured directly

The parameters used to predict model tests are listed in Table 3.4. The properties of the clean column and surrounding clay were obtained in the laboratory as discussed earlier. Because of the smaller particle size, the stiffness of model column was lower than the value of 48-120 MPa as mentioned in previous studies (Ambily and Gandhi, 2007, Arulrajah et al., 2009, Fatahi et al., 2012). There was no disturbance to pure clay outside the column as indicated by the measurement of the void ratio of the surrounding clay after testing. The soil properties in the clogged zone were selected based on best-fit regression for a determined clay fraction of 0.32.

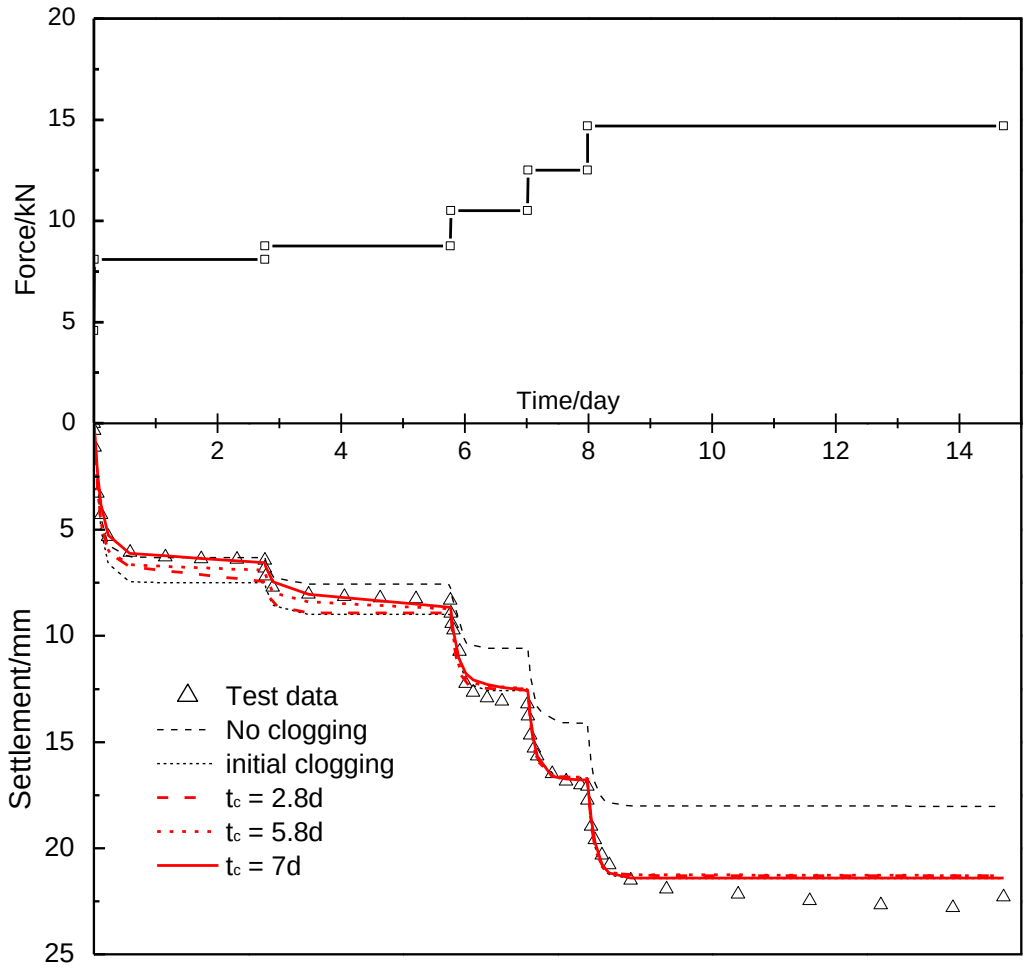

(a)

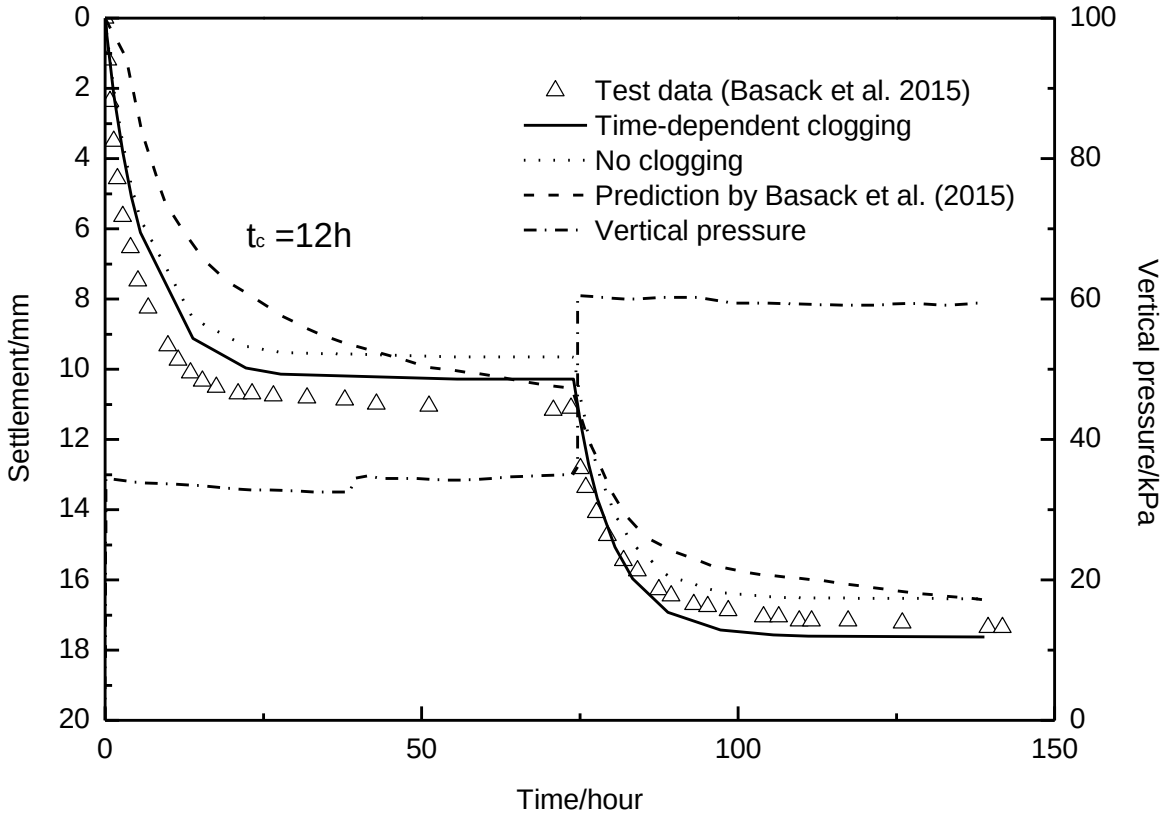

(b)

Figure 3.12 Comparison of settlement between test data and predictions: (a) current model test; (b) model test by Basack et al. (2015)

A comparison between the current model test and corresponding theoretical predictions is shown in Figure 3.12(a). If clogging is neglected, the settlement prediction is accurate only at the beginning, i.e. after the first stage of loading there is a notable discrepancy, and the overall settlement is underestimated by about 15%. If clogging occurs initially, the calculated settlement is higher than the observed data during the first stage of loading, but then converges to the actual settlement curve. The calculations corresponding to the cases of 'no clogging' and 'initial clogging' provide upper and lower limits, respectively. Time-dependent clogging is more apparent compared to initial clogging, according to the examination of photo images of the column surface before and after testing. Unfortunately clogging process (rate and extent) could not be quantified to define a critical time accurately at which the soil consolidation is

significantly influenced by the clogging of the column. Both the reduction in permeability and the increase in compressibility were assumed to follow an exponential pattern (pattern II). It is observed that the calculated settlements will agree with the laboratory measurements if time-dependent clogging is considered with the appropriate choice of a critical time.

Figure 3.12(b) shows the comparisons using the current model based on time-dependent clogging with the model proposed by Basack et al. (2015) together with the measured data. It is noted that the initial part of the load-settlement response of the test was not suitable for the application of current consolidation model due to the effect of unloading and recompression. Therefore, only the data after recompression was selected to verify the proposed model. The radius ratio of the clean column to the whole column was reported to be 0.92 which is slightly lower than the current model test, but the relevant soil properties are not found, so they were chosen as the same value as the current model test. The results demonstrate that improved predictions can be made using the current unit cell model where clogging of the column can increase the overall compressibility of the unit cell under equal strain condition.

It is interesting to see that the corresponding settlement prediction with time-dependent clogging becomes higher than the case of 'no clogging'. The reasons for this can be explained as follows: clay intrusion into the granular assembly can increase the column compressibility (i.e. reduction of inter-particle friction) hence the settlement at a given applied load under equal strain condition. Moreover, the stress distribution on top of the unit cell also varies (less load taken by the column) which could then lead to a higher stress transfer to the surrounding soil, hence an increased consolidation settlement of the clay. If the applied load is independent of time, the settlement would depend on

both the degree of soil consolidation and the compressibility of the unit cell. The extent of clogging can increase the compressibility of the whole unit cell thus the associated settlement. Slight clogging of stone column barely retards the rate of surrounding soil consolidation, while substantially increased clogging can impede drainage through the granular pile, requiring more time to attain the ultimate settlement. In this respect, it is perceived that a critical situation may exist below which the settlement can be adversely affected due to clogging. However, such an analysis that requires coupling of clay infiltration to the column with the soil consolidation theory is beyond the scope of this paper and will be discussed in the future.

3.7 Summary

A detailed physical model test of a unit cell (i.e. single stone column) was conducted to study clogging, together with loading and settlement data. After consolidation, a core part of the model test sample was exhumed, and an image analysis using computed tomography (CT scan) was employed to quantify the extent of clogging. It could be seen that the clogged zone progressed with consolidation and occupied almost 20% of the outer ring of the model column towards the top; the extent of clogging decreased rapidly with depth until it eventually vanished. The porosity of the column was also obtained through weight-volume calculations and from image analysis; the results from both methods showed a good agreement. These clogging parameters were then used to predict the consolidation behaviour, and compare with the laboratory measurements.

A consolidation model capturing both initial clogging and time-dependent clogging in a stone column unit cell was proposed, where the changes of properties of the stone column due to clogging were considered by different clogging patterns. The proposed model predictions were also compared with those of previous studies (with and without

clogging); it is found that notable discrepancies exist between models which involve clogging. The results under ‘no clogging’ and ‘initial clogging’ situations represented the upper and lower boundaries of the predictions. In particular, the current model with equal strain condition indicated that the clogging in stone column could lead to increased compression because the intrusion of fines to the granular assembly at the column top can increase its compressibility, and thereby the overall settlement of the unit cell under the equal strain condition. This observation may conflict with the ‘free strain’ condition, where the clogging of the column and the corresponding reduction in excess pore pressure dissipation can lead to a decreased rate of soil consolidation.

Chapter 4 A Consolidation Model for ground improved with stone column between 'Equal Strain' and 'Free Strain'

4.1 General

Traditional consolidation theory which combined vertical and radial flow to study vertical drains started with Barron (1948), where two different fundamental assumptions were proposed, which are "equal strain" and "free strain". For a unit cell which consists of homogeneous soil, "equal strain" generally assumes that the vertical strain is always uniform at a given depth as consolidation progresses and therefore the vertical stress on top of the unit cell is uneven, whereas "free strain" results from a uniform vertical stress at the top surface, and differential settlement has no influence on the distribution of vertical stress throughout the consolidation process. Various solutions for radial consolidation have been developed based on these two assumptions (Hansbo et al., 1981, Tang and Onitsuka, 1998, Zhu and Yin, 2001, Leo, 2004, Walker and Indraratna, 2006, Rujikiatkamjorn and Indraratna, 2015, Lei et al., 2015). The average degrees of consolidation were calculated based on "equal strain" and "free strain" solutions respectively, but the difference is small and normally within 5% (Richart, 1959, Zhu and Yin, 2004b). Therefore, vertical drains can be designed where either "equal strain" or "free strain" can be assumed.

The consolidation theory of stone column is usually modified based on traditional theories of vertical drain. A simplified method to estimate the average degree of consolidation of stone column reinforced foundation was proposed by Han and Ye (2001) with consideration of well resistance and soil disturbance. Consolidation under time-dependent loadings was studied using an analytical solution proposed by Wang

(2009). Solutions that combined vertical and radial flow, as well as incorporated column deformation, were proposed by Xie et al. (2009) and Lu et al. (2010). Apart from these studies where "equal strain" assumption was adopted, Indraratna et al. (2013) gave a numerical solution for soft soil improved with stone column based on "free strain" by considering the arching effect. However, there is still a large disparity in the results of those solutions presented above. The choice between "equal strain" and "free strain" in stone column system seems to be more vital than for vertical drains.

Flexible vertical drains have a negligible effect on the stiffness of the entire ground, so the soft soil with vertical drains can be treated as a single material; this may be the reason why the results for flexible drains between "equal strain" and "free strain" solutions are similar. Unlike flexible drains, the stiffness of stone column cannot be ignored so there is the inevitable redistribution of stress at the top surface of a unit cell; hence the "free strain" assumption is not realistic. However, since the foundation from which uploads are transferred is not perfectly rigid (i.e., highway or railway embankments are recognised as flexible foundations), a differential settlement between a column and the surrounding soil can always be expected, as a result, "equal strain" is not reasonable for stone column either.

In this chapter, a consolidation model is presented where a situation between "equal strain" and "free strain" is assumed, and the foundation stiffness is included in the governing equation. An analytical solution is found to predict the average degree of consolidation, the redistribution of vertical stress, and the development of differential settlement in a unit cell. Through varying the stiffness of foundation, this model can also be converted to solutions of "equal strain" and "free strain"; these solutions agree

well with the existing solutions. Finally, this model is used to discuss the effect of foundation stiffness on the consolidation of soft ground improved by stone column.

4.2 Model establishment

In order to consider the effect of the foundation, a layer is added to the top of the original unit cell to represent the foundation (Figure 4.1).

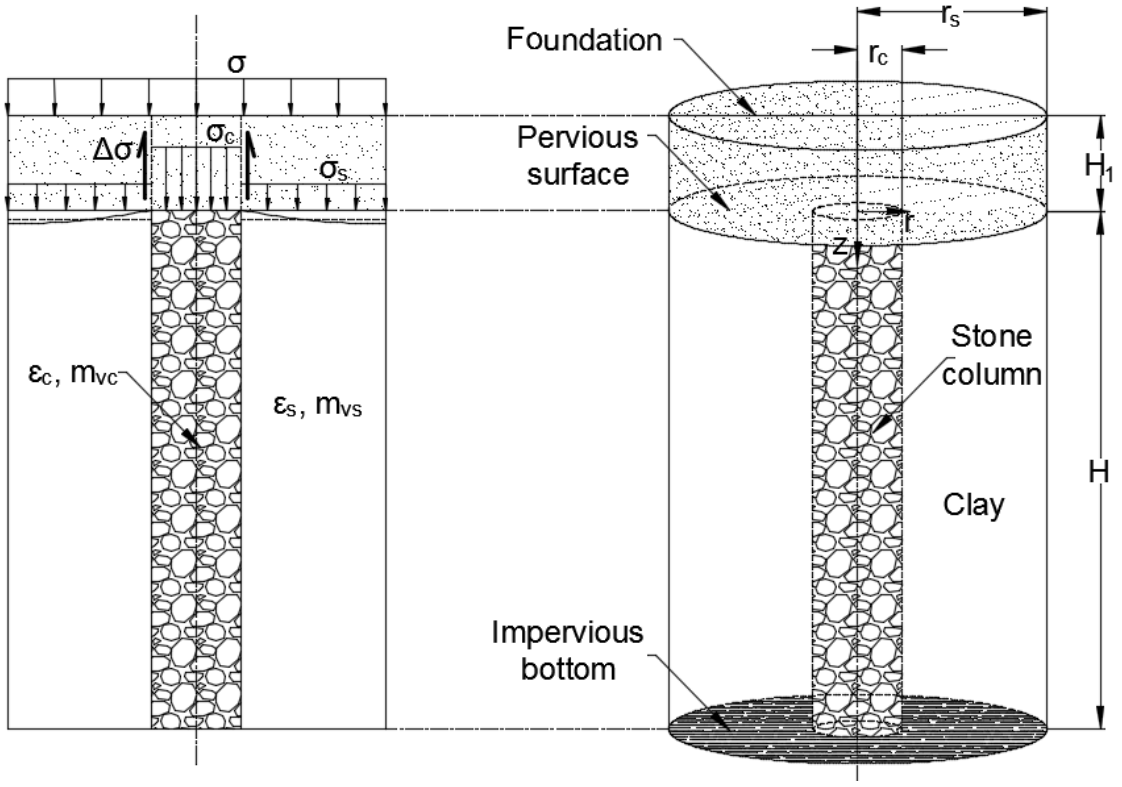

Figure 4.1 Sketch of model to be analysed

Several basic assumptions are made as follows:

1. Inside the stone column, only vertical flow is considered and only radial flow is considered in the surrounding clay.
2. Darcy's law is assumed to be valid.
3. The load on top of the foundation is uniform and constant, and the vertical stress induced by this load is uniform regardless of depth.

4. The unit weight of the foundation layer is ignored, and the amount of compression in the foundation layer is not included.
5. Any possible shear stress at the column-soil interface is not considered.
6. Vertical strain of stone column, ε_c, is independent of the radius, but the vertical strain of surrounding soil is related to the radius, and the closer it is to the column the less it is. For simplicity, the average vertical drain of surrounding soil, ε_s, is used.

The vertical strain of stone column and surrounding soil can be calculated using the equation below:

$$m_{vs}(\sigma_s(t) - \bar{u}_s(z,t)) = \varepsilon_s(z,t) \quad \text{Eq 4.1}$$

$$m_{vc}(\sigma_c(t) - \bar{u}_c(z,t)) = \varepsilon_c(z,t) \quad \text{Eq 4.2}$$

where σ_c and σ_s are the vertical stress on top of the stone column and surrounding soil respectively, $\bar{u}_c$ and $\bar{u}_s$ are the average excess pore pressure of stone column and surrounding soil respectively, and m_{vc} and m_{vs} are the coefficients of compressibility of stone column and surrounding soil respectively.

By considering the force equilibrium in the foundation layer, the loads on top of the embankment should be equal to the supporting force on the top surface of the unit cell.

The redistribution of vertical stress can be calculated by including the shear stress in the foundation, while the shear stress in the foundation can be calculated based on differential settlement (Eq 4.3, Eq 4.4, and Eq 4.5):

$$\pi(r_s^2 - r_c^2)\sigma_s(t) = \pi(r_s^2 - r_c^2)\sigma - \Delta\sigma \cdot H_1 \cdot \pi r_c \quad \text{Eq 4.3}$$

$$\pi r_c^2 \sigma_c(t) = \pi r_c^2 \sigma + \Delta\sigma \cdot H_1 \cdot \pi r_c \quad \text{Eq 4.4}$$

$$\frac{\int_0^H \varepsilon_s(z,t)dz - \int_0^H \varepsilon_c(z,t)dz}{H_1} K = \Delta\sigma \quad \text{Eq 4.5}$$

where r_c and r_s are the radius of the stone column and unit cell respectively, H_1 is the thickness of the foundation layer, K is the stiffness of the foundation, and $\Delta\sigma$ is the shear stress in the foundation layer.

The mechanism whereby shear stress is generated in the foundation may differ depending on the type of foundation materials (i.e. concrete, sandy soil, asphalt). Using soil as an example, this kind of redistribution of vertical stress is also known as the arching phenomenon, which is a complex problem and a consensus on its solution has not yet been achieved. The shear stress is calculated using a method which is similar to "trapdoor theory" proposed by Terzaghi (1943) to simplify this problem.

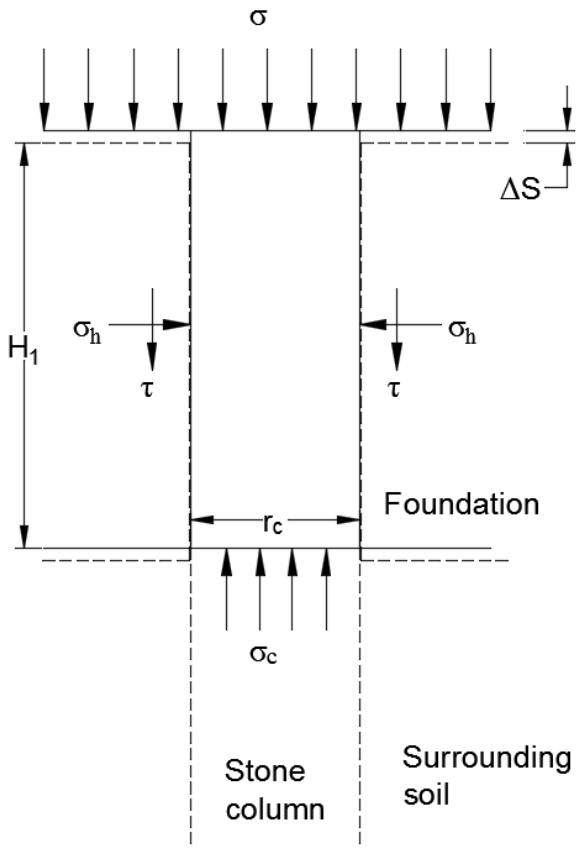

(a)

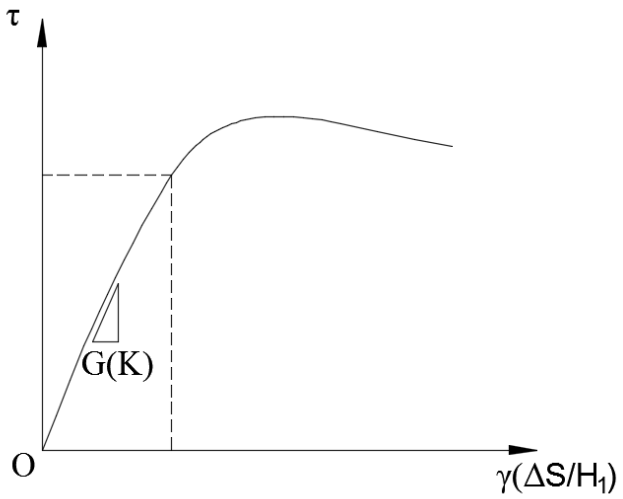

(b)

Figure 4.2 (a) Shear stress in foundation; (b) typical stress-strain relationship in direct shear test

In this study, it is assumed that when differential settlement occurs, a cylindrical sliding surface with the same diameter as the stone column appears in the foundation (Figure 4.2(a)). The shear stress, τ, at this sliding surface is related to the normal stress, σ_h. An analogy can be drawn between the generation of shear stress in the foundation and direct shear tests (Taylor, 1948, Schofield and Wroth, 1968, Ishibashi and Hazarika, 2010); a typical stress-strain curve in direct shear test is shown in Figure 4.2(b). The differential settlement allowed in a foundation is limited, so it is reasonable to consider that its stress-strain curve is still in the linear stage, and therefore, the shear stress in the foundation layer is assumed to be proportional to its shear strain in this chapter (Eq 4.5). The slope of the stress-strain curve in a direct shear test defines the shear modulus, *G*, whereas in this model the slope of shear stress versus normalised differential settlement, $\Delta S/H_1$, is termed as the stiffness of foundation, *K*.

By integrating Eq 4.1 and Eq 4.2 regarding the depth and then substituting Eq 4.3, Eq 4.4 and Eq 4.5 into those two equations, the relationship between vertical strain and

excess pore pressure can be found. Through those two equations shown below, the calculation of vertical strains is independent of the foundation thickness:

$$\frac{\partial \varepsilon_s}{\partial t} = \frac{m_{vc}m_{vs}KHr_c^2\frac{\partial \bar{u}_c}{\partial t} - (m_{vs}r_c + KH)(r_c^2 - r_s^2)\frac{\partial \bar{u}_s}{\partial t}}{r_c^2(KHm_{vc} + r_c - m_{vc}m_{vs}HK) - r_s^2(r_c + m_{vc}m_{vs}KH)} \quad \text{Eq 4.6}$$

$$\frac{\partial \varepsilon_c}{\partial t} = \frac{m_{vc}r_c[m_{vs}KHr_c + r_s^2 - r_c^2]\frac{\partial \bar{u}_c}{\partial t} + m_{vc}m_{vs}KH(r_s^2 - r_c^2)\frac{\partial \bar{u}_s}{\partial t}}{r_c^2(KHm_{vc} + r_c - m_{vc}m_{vs}HK) - r_s^2(r_c + m_{vc}m_{vs}KH)} \quad \text{Eq 4.7}$$

where H is the thickness of the unit cell.

Deformation of both the stone column and surrounding clay should be equal to the net flow entering the system. Based on this equilibrium, the governing equation can be established regarding the consolidation of clay and column respectively, as equations Eq 4.8 and Eq 4.9 shows.

$$\frac{1}{\gamma_w r}\frac{\partial}{\partial r}\left(k_s(r)r\frac{\partial u_s}{\partial r}\right) = -\frac{\partial \varepsilon_s}{\partial t} \quad \text{Eq 4.8}$$

$$\frac{2k_s}{\gamma_w r_c}\frac{\partial u_s}{\partial r}\Big|_{r=r_c} + \frac{k_c}{\gamma_w}\frac{\partial^2 \bar{u}_c}{\partial z^2} = -\frac{\partial \varepsilon_c}{\partial t} \quad \text{Eq 4.9}$$

where u_s is a function of radius and depth to represent the pore water pressure in surrounding soil, $k_s(r)$ is a function of radius to describe variations in permeability in the surrounding soil, k_c is the permeability of the stone column, and γ_w is the unit weight of water.

Several boundary conditions are clarified to solve this problem:

1. At the external boundary of the unit cell, there is no flow.
2. The pore water pressure is a continuum at the interface between the stone column and surrounding soil.
3. The top surface of the unit cell is a free drain plane.

4. The bottom of the unit cell is impermeable.

$$\left.\frac{\partial u_s}{\partial r}\right|_{r=r_s} = 0 \qquad \text{Eq 4.10}$$

$$u_s = \bar{u}_c(r = r_c) \qquad \text{Eq 4.11}$$

$$\bar{u}_s(0,t) = \bar{u}_c(0,t) = 0 \ \ (t > 0) \qquad \text{Eq 4.12}$$

$$\frac{\partial \bar{u}_s(h,t)}{\partial z} = \frac{\partial \bar{u}_c(h,t)}{\partial z} = 0 \qquad \text{Eq 4.13}$$

There is a controversy for the determination of initial pore pressure at the top surface of unit cell: it should always be zero due to free drainage condition, but on the other hand, it should be equal to the magnitude of the vertical load because the unit cell is in undrained condition at the moment of loading. To justify this condition, the excess pore water pressure at the top surface of the unit cell is prescribed as follows: when vertical loads are applied, the induced excess pore water pressure is uniform in the unit cell and equal to the vertical loads, in another words, the unit cell is in an undrained condition; when consolidation begins, the excess pore pressure is immediately dissipated to zero at the surface of the unit cell.

The initial condition can be expressed as Eq 4.14.

$$\bar{u}_s(z,0) = \bar{u}_c(z,0) = \sigma \qquad \text{Eq 4.14}$$

Integrating Eq 4.8 concerning the radius from r to r_s, and then combining Eq 4.10 would yield:

$$\frac{\partial u_s}{\partial r} = \frac{\gamma_w(r_s^2 - r^2)}{2k_s(r)r}\frac{\partial \varepsilon_s}{\partial t} \qquad \text{Eq 4.15}$$

Substituting Eq 4.15 into Eq 4.9 would yield:

$$\frac{r_s^2 - r_c^2}{r_c^2}\frac{\partial \varepsilon_s}{\partial t} + \frac{k_c}{\gamma_w}\frac{\partial^2 \bar{u}_c}{\partial z^2} = -\frac{\partial \varepsilon_c}{\partial t} \quad \text{Eq 4.16}$$

Integrating Eq 4.15 regarding the radius again from r_c to r, the following equation can be deduced by considering boundary condition stipulated in Eq 4.11.

$$u_s - \bar{u}_c = \frac{\gamma_w}{2k_s}\frac{\partial \varepsilon_s}{\partial t}\int_{r_c}^{r} \frac{r_s^2 - r^2}{f(r)r}dr \quad \text{Eq 4.17}$$

A relationship can also be established between the average pore pressure in surrounding clay and the pore pressure in the stone column.

$$\bar{u}_s = \frac{1}{\pi(r_s^2 - r_c^2)}\int_{r_c}^{r_s} 2\pi r u_s dr = \bar{u}_c + \frac{\gamma_w A}{k_s(r_s^2 - r_c^2)}\frac{\partial \varepsilon_s}{\partial t} \quad \text{Eq 4.18}$$

$$A = \int_{r_c}^{r_s} r \int_{r_c}^{r} \frac{r_s^2 - r^2}{f(r)r}dr\,dr \quad \text{Eq 4.19}$$

Combining Eq 4.6 with Eq 4.18 gives:

$$\bar{u}_s = \bar{u}_c + B\frac{\partial \bar{u}_c}{\partial t} + C\frac{\partial \bar{u}_s}{\partial t} \quad \text{Eq 4.20}$$

$$B = -\frac{m_{vc}m_{vs}AKHr_c^2\gamma_w}{k_s(r_c^2 - r_s^2)[Km_{vc}H(r_c^2 - r_s^2) + r_c(r_c^2 - r_s^2) - KHr_c m_{vs}]} \quad \text{Eq 4.21}$$

$$C = -\frac{A(KHm_{vc}m_{vs} + m_{vs}r_c)\gamma_w}{k_s[Km_{vc}H(r_s^2 - r_c^2) + m_{vs}KHr_c^2 + r_c(r_s^2 - r_c^2)]} \quad \text{Eq 4.22}$$

Then substituting Eq 4.6 and Eq 4.7 into Eq 4.16 would yield:

$$\frac{\partial \bar{u}_s}{\partial t} = D\frac{\partial \bar{u}_c}{\partial t} + E\frac{\partial^2 \bar{u}_c}{\partial z^2} \quad \text{Eq 4.23}$$

$$D = \frac{r_c^2[m_{vc}r_c(r_c^2 - r_s^2) - m_{vc}m_{vs}KHr_s^2]}{(r_c^2 - r_s^2)[m_{vs}r_c(r_c^2 - r_s^2) - m_{vc}m_{vs}KHr_s^2]} \quad \text{Eq 4.24}$$

$$E = -\frac{k_c r_c^2 [K m_{vc} H (r_c^2 - r_s^2) + r_c (r_s^2 - r_c^2) - m_{vs} K H r_c^2]}{\gamma_w (r_c^2 - r_s^2)[m_{vs} r_c (r_c^2 - r_s^2) - m_{vc} m_{vs} K H r_s^2]} \quad \text{Eq 4.25}$$

Finally, a governing equation regarding variable, $\bar{u}_c$, can be obtained.

$$C \cdot E \frac{\partial^3 \bar{u}_c}{\partial z^2 \partial t} - E \frac{\partial^2 \bar{u}_c}{\partial z^2} + (B + C \cdot D) \frac{\partial^2 \bar{u}_c}{\partial t^2} + (1 - D) \frac{\partial \bar{u}_c}{\partial t} = 0 \quad \text{Eq 4.26}$$

4.3 Solutions

The variable separation method is used to solve this problem. It is assumed that excess pore water pressure in the stone column can be calculated based on two functions, each depending on only one variable.

$$\bar{u}_c = T(t) \cdot Z(z) \quad \text{Eq 4.27}$$

The governing equation can be transformed into two ordinary differential equations (ODE) below.

$$-\frac{(B + C \cdot D) T''(t) + (1 - D) T'}{C \cdot E \cdot T'(t) - E \cdot T(t)} = \frac{Z''}{Z} = -\alpha^2 \ (\alpha > 0) \quad \text{Eq 4.28}$$

where α is a positive constant to be determined.

4.3.1 General solution

Those two ODE equations in Eq 4.28 can be categorised as second order linear ODEs, their solution is readily given based on basic ODE theory.

$$Z_n(z) = a_n \cdot \sin(\alpha_n z) \quad \text{Eq 4.29}$$

$$T_n(t) = b_n e^{\beta_n \cdot t} + c_n e^{\theta_n \cdot t} \quad \text{Eq 4.30}$$

$$\alpha_n = \frac{(2n - 1)\pi}{2H} \quad (n = 1,2,3, \dots) \quad \text{Eq 4.31}$$

$$\beta_n = \frac{-1 + D + CE\alpha_n^2 - \sqrt{-4(B+CD)E\alpha_n^2 + (1 - D - CE\alpha_n^2)^2}}{2(B+CD)} \quad \text{Eq 4.32}$$

$$\theta_n = \frac{-1 + D + CE\alpha_n^2 + \sqrt{-4(B+CD)E\alpha_n^2 + (1 - D - CE\alpha_n^2)^2}}{2(B+CD)} \quad \text{Eq 4.33}$$

where the coefficients "a_n", "b_n", and "c_n" are integration constants.

After obtaining solutions for ODEs (Eq 4.29 and Eq 4.30) the pore pressure in the stone column and surrounding soil can be written as shown below.

$$\bar{u}_c = \sum_1^n (a_n b_n e^{\beta_n \cdot t} + a_n c_n e^{\theta_n \cdot t}) \sin(\alpha_n z) \quad \text{Eq 4.34}$$

$$\bar{u}_s = \sum_1^n [a_n b_n [1 + (CD + B)\beta_n - CE\alpha_n^2] e^{\beta_n \cdot t} + a_n c_n [1 + (CD + B)\theta_n - CE\alpha_n^2] e^{\theta_n \cdot t}] \sin(\alpha_n z) \quad \text{Eq 4.35}$$

In Eq 4.34 and Eq 4.35, only two integration constants need to be decided, which are "$a_n b_n$" and "$a_n c_n$" respectively. The initial condition (Eq 4.14) can be used to determine these two constants.

$$a_n b_n = \frac{\sigma(-1 + D - CE\alpha_n^2 + \sqrt{-4(B+CD)E\alpha_n^2 + (1 - D - CE\alpha_n^2)^2})}{\alpha_n H \sqrt{-4(B+CD)E\alpha_n^2 + (1 - D - CE\alpha_n^2)^2}} \quad \text{Eq 4.36}$$

$$a_n c_n = \frac{\sigma(1 - D + CE\alpha_n^2 + \sqrt{-4(B+CD)E\alpha_n^2 + (1 - D - CE\alpha_n^2)^2})}{\alpha_n H \sqrt{-4(B+CD)E\alpha_n^2 + (1 - D - CE\alpha_n^2)^2}} \quad \text{Eq 4.37}$$

The average degree of consolidation for the whole unit cell, $\bar{U}$, can be determined.

$$\bar{U} = 1 - \frac{\left(1 - \frac{r_c^2}{r_s^2}\right)\bar{u}_s + \frac{r_c^2}{r_s^2}\bar{u}_c}{\sum_1^n \alpha_n \sin(\alpha_n z)\, \sigma H} \quad \text{Eq 4.38}$$

The vertical strains of stone column and surrounding soil can be calculated according to Eq 4.6 and Eq 4.7 with a combination of the initial condition.

$$\varepsilon_s = \frac{m_{vc}m_{vs}KHr_c^2(\bar{u}_c - \sigma) - (m_{vs}r_c + KH)(r_c^2 - r_s^2)(\bar{u}_s - \sigma)}{r_c^2(KHm_{vc} + r_c - m_{vc}m_{vs}HK) - r_s^2(r_c + m_{vc}m_{vs}KH)} \quad \text{Eq 4.39}$$

$$\varepsilon_c = \frac{m_{vc}r_c[m_{vs}KHr_c + r_s^2 - r_c^2](\bar{u}_c - \sigma) + m_{vc}m_{vs}KH(r_s^2 - r_c^2)(\bar{u}_s - \sigma)}{r_c^2(KHm_{vc} + r_c - m_{vc}m_{vs}HK) - r_s^2(r_c + m_{vc}m_{vs}KH)} \quad \text{Eq 4.40}$$

The stress concentration ratio, n_s, can be calculated as:

$$n_s(t) = \frac{m_{vs}\int_0^H \varepsilon_c(z,t)dz + m_{vc}m_{vs}\int_0^H \bar{u}_c(z,t)dz}{m_{vc}\int_0^H \varepsilon_s(z,t)dz + m_{vc}m_{vs}\int_0^H \bar{u}_s(z,t)dz} \quad \text{Eq 4.41}$$

The differential settlement on top of the unit cell, ΔS, can be calculated using the equation below.

$$\Delta S(t) = \int_0^H \varepsilon_s(z,t)dz - \int_0^H \varepsilon_c(z,t)dz \quad \text{Eq 4.42}$$

4.3.2 Equal strain

The equal strain hypothesis is valid when the stiffness of the foundation approaches infinity (K→+∞), then there would be no differential settlement developed during the consolidation process.

Subsequently, the governing equation can degenerate into the form below.

$$CE\frac{\partial^3 \bar{u}_c}{\partial z^2 \partial t} - E\frac{\partial^2 \bar{u}_c}{\partial z^2} + (1 - D)\frac{\partial \bar{u}_c}{\partial t} = 0 \quad \text{Eq 4.43}$$

$$\bar{u}_s = \bar{u}_c + CE\frac{\partial^2 \bar{u}_c}{\partial z^2} \quad \text{Eq 4.44}$$

$$\frac{\partial \varepsilon_s}{\partial t} = \frac{\partial \varepsilon_c}{\partial t} = -\frac{r_c^2\frac{\partial \bar{u}_c}{\partial t} + (r_s^2 - r_c^2)\frac{\partial \bar{u}_s}{\partial t}}{(r_s^2 - r_c^2)/m_{vs} + r_c^2/m_{vc}} \quad \text{Eq 4.45}$$

Note that the secondary differential item about time has been cancelled, so the two ODEs after variable separation become the equations below.

$$\frac{(D-1)T'(t)}{C\cdot E\cdot T'(t)-E\cdot T(t)}=\frac{Z''}{Z}=-\alpha^2(\alpha>0) \quad \text{Eq 4.46}$$

Following a similar procedure as section 4.3.1, the solutions for the average excess pore pressure and vertical strain of a unit cell can be deduced.

$$\bar{u}_c=\sum_1^n \frac{2\sigma r_s^2}{H[CE\alpha_n^3(r_c^2-r_s^2)+\alpha_n r_s^2]} e^{\frac{E\alpha_n^2 t}{-1+D+CE\alpha_n^2}} \sin[\alpha_n z] \quad \text{Eq 4.47}$$

$$\bar{u}_s=(1-CE\alpha_n^2)\bar{u}_c \quad \text{Eq 4.48}$$

$$\varepsilon_s=\varepsilon_c=-\frac{r_c^2\bar{u}_c+(r_s^2-r_c^2)\bar{u}_s-\sigma r_s^2}{(r_s^2-r_c^2)/m_{vs}+r_c^2/m_{vc}} \quad \text{Eq 4.49}$$

There is no differential settlement for equal strain so the stress concentration ratio can be determined using Eq 4.41.

4.3.3 Free strain

The free strain hypothesis means that a foundation would not change the distribution of vertical stress on top of the unit cell, so the vertical stress is uniform, the stiffness of the foundation is negligible, and the differential settlement only depends on the compression modulus of stone column and surrounding soil.

$$m_{vs}(\sigma-\bar{u}_s)=\varepsilon_s \quad \text{Eq 4.50}$$

$$m_{vc}(\sigma-\bar{u}_c)=\varepsilon_c \quad \text{Eq 4.51}$$

The structure of the degenerated equation for free strain is the same as that given in Section 4.3.1, and therefore its solutions can be obtained using general solutions with updated parameters (B=0 & K=0).

$$C \cdot E \frac{\partial^3 \bar{u}_c}{\partial z^2 \partial t} - E \frac{\partial^2 \bar{u}_c}{\partial z^2} + C \cdot D \frac{\partial^2 \bar{u}_c}{\partial t^2} + (1 - D) \frac{\partial \bar{u}_c}{\partial t} = 0 \qquad \text{Eq 4.52}$$

$$\bar{u}_s = \bar{u}_c + C \cdot D \frac{\partial \bar{u}_c}{\partial t} + C \cdot E \frac{\partial^2 \bar{u}_c}{\partial z^2} \qquad \text{Eq 4.53}$$

4.4 Discussion

4.4.1 Comparison with previous studies

In order to verify the proposed model, comparisons are made with existing consolidation models under a hypothesis of equal strain (Han and Ye 2001, Lu et al. 2010) or free strain (Indraratna et al. 2013).

The general parameters used in the calculation are cited from Indraratna et al. (2013) and presented in Table 4.1.

Table 4.1 Parameters used for comparison with existing models

k_s(m/s)	k_c/k_s	r_c(m)	r_s(m)	r_d/r_c
1.6×10^{-9}	10^3	0.5	1.5	1.15
k_d/k_s	M	γ_w(kN/m^3)	H(m)	m_{vs}(MPa^{-1})
0.1	7	10	16	2

The ratio of the coefficient of compressibility of clay to the column, *M*, is assigned a value of 7. The smear effect is considered, and the radius ratio of smear zone, r_d, to the

stone column is about 1.15, and the permeability in the smear zone, k_d, decreases to one-tenth of undisturbed clay. The effect of clogging in the stone column is ignored.

The comparison in Figure 4.3 shows that the average degree of consolidation for a unit cell calculated using the proposed model agrees well with previous studies, no matter which hypothesis is used (equal strain or free strain). Moreover, the consolidation under free strain is slower than under equal strain conditions. The horizontal coordinate is the time factor, T, which can be defined by the equation below.

$$T = \frac{k_s t}{4 m_{vs} \gamma_w r_s^2} \qquad \text{Eq 4.54}$$

However, the proposed model has a special feature: for free strain, the degree of consolidation is higher than for equal strain at the beginning of consolidation, but then the degree of consolidation increases slowly, and as a result, the consolidation curve of free strain falls under that of equal strain.

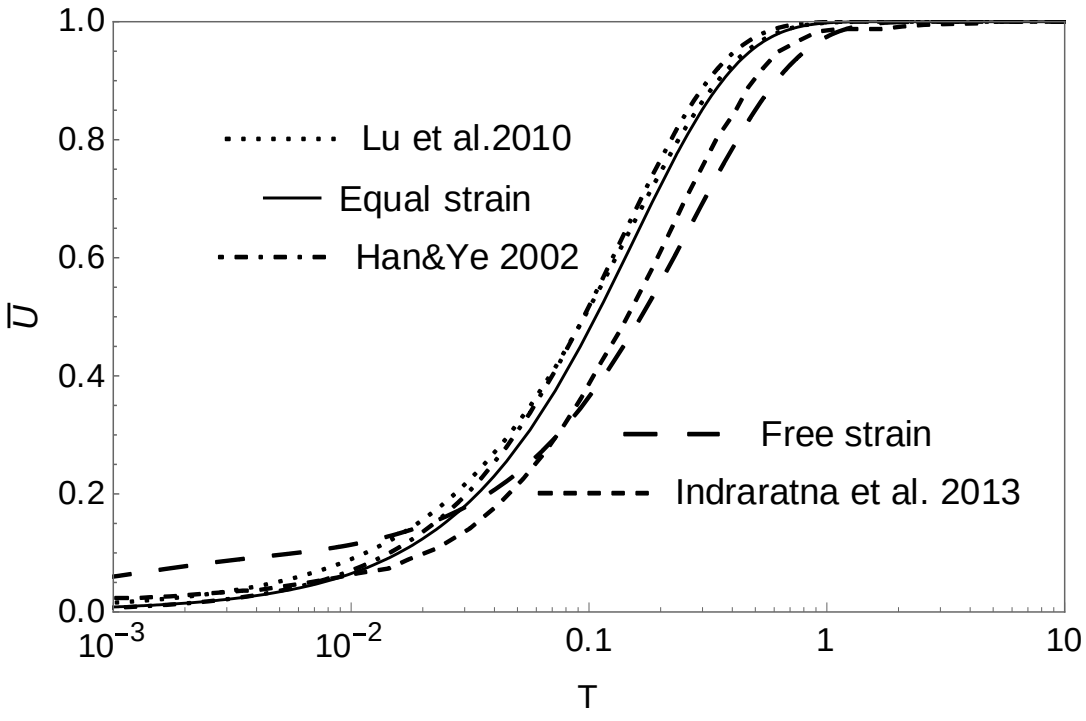

Figure 4.3 Comparison between proposed model and previous models

4.4.2 Differences between “equal strain” and “free strain”

There is no redistribution of vertical stresses on top of the column and surrounding soil under “free strain” conditions, so the stress concentration ratio is always equal to 1. However, the distribution of vertical stress for “equal strain” changes as consolidation processes, as shown in Figure 4.4.

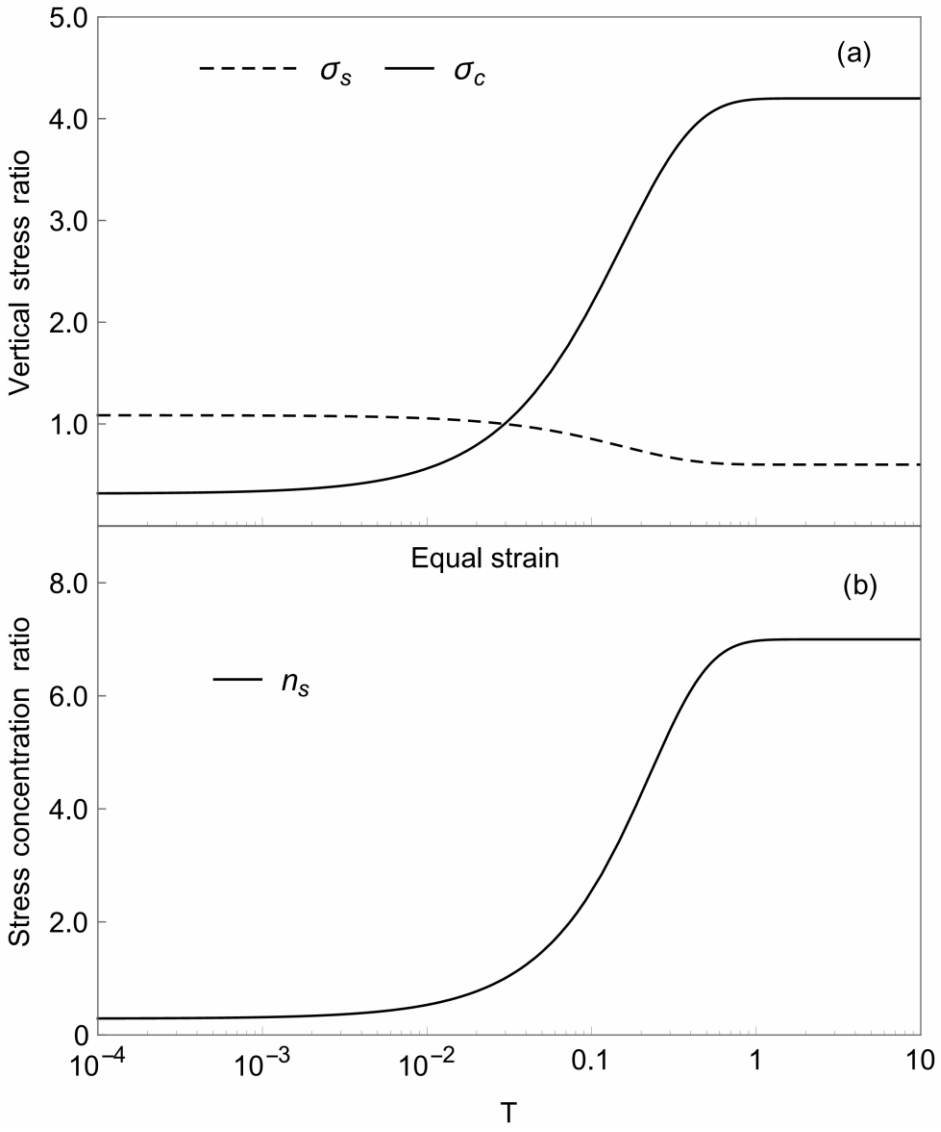

Figure 4.4 Distribution of vertical stress on top of the unit cell: (a) vertical stress ratio; (b) stress concentration ratio

In the beginning, most of the vertical loads are carried by the surrounding soil, and the vertical stress ratio on top of the stone column remains at a low level. Consequently, the

vertical stress ratio on the surrounding soil is larger than 1 to maintain the force equilibrium. However, as consolidation proceeds, the stress in surrounding clay decreases while the vertical stress on the stone column increases and this finding echoes the statement of Han and Ye (2001). As a result, the stress concentration ratio increases with time until it reaches the same value as the modulus ratio of column material to soil. The excess pore water pressures under both hypotheses were also calculated using the currently proposed model.

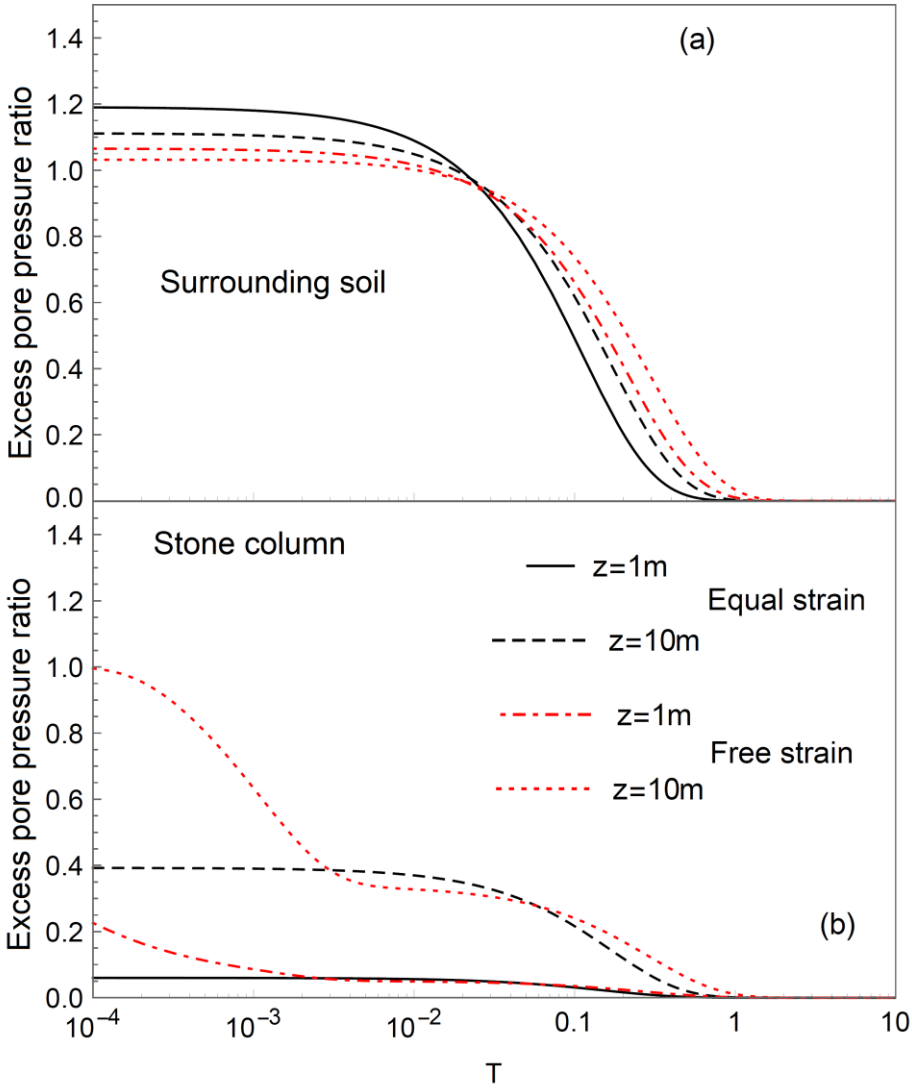

Figure 4.5 Development of excess pore pressure for equal strain and free strain (depth of 1m and 10m): (a) in surrounding soil; (b) in stone column

The evolution of excess pore pressure is presented in Figure 4.5 (a) and (b) for the surrounding soil and stone column. Generally, "equal strain" generates higher pore pressure in surrounding soil and lower pore pressure in the stone column. The dissipation rate of excess pore pressure in surrounding soil is faster for "equal strain", but it decreases with depth. When the excess pore pressure in stone column is considered, the differences between solutions under different assumptions become negligible after a short time.

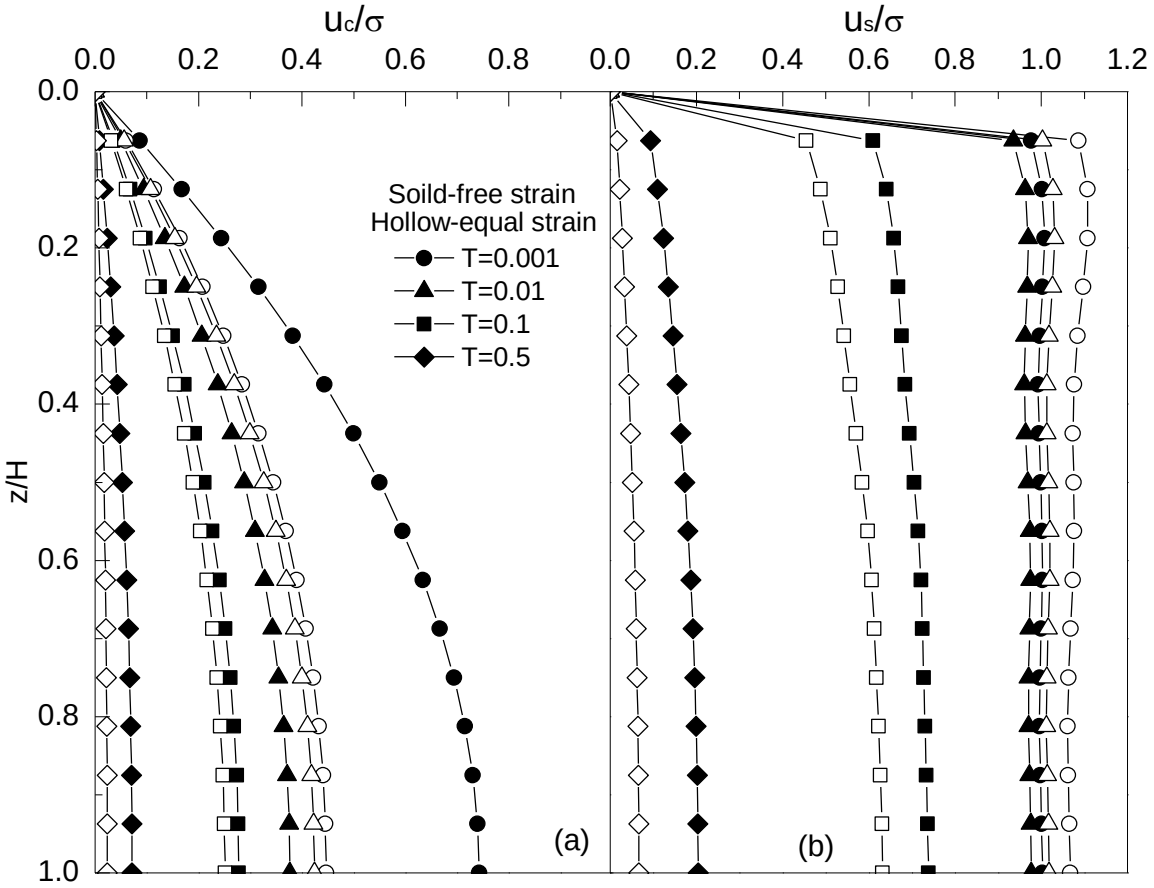

Figure 4.6 Excess pore pressure profiles: (a) in stone column; (b) in surrounding soil

The profiles of excess pore pressure at different times are given for stone column and surrounding soil in Figure 4.6 (a) and (b) respectively. When the time factor reaches 0.001, the excess pore pressure ratio in stone column is up to 0.8 for free strain and less than 0.4 for equal strain. After a short period (T= 0.1), the pore pressure ratio in the

stone column decreases to about 0.2 for both equal strain and free stain. Unlike equal strain, the amount of dissipated pore pressure in stone column is much higher for free strain at the beginning of consolidation, so the degree of consolidation under free strain is higher at the start. Figure 4.6 also shows that the excess pore pressure in stone column increases with depth while pore pressure in the surrounding soil is not sensitive to depth. These pore pressure profiles indicate that more time is needed to complete consolidation under free strain conditions.

4.4.3 Effect of foundation stiffness

In practice, the stiffness of a foundation is neither infinity nor zero, so the performance of stone column is between equal strain and free strain. The differences between foundations with varying stiffnesses are studied using the same basic parameters provided in Table 4.1.

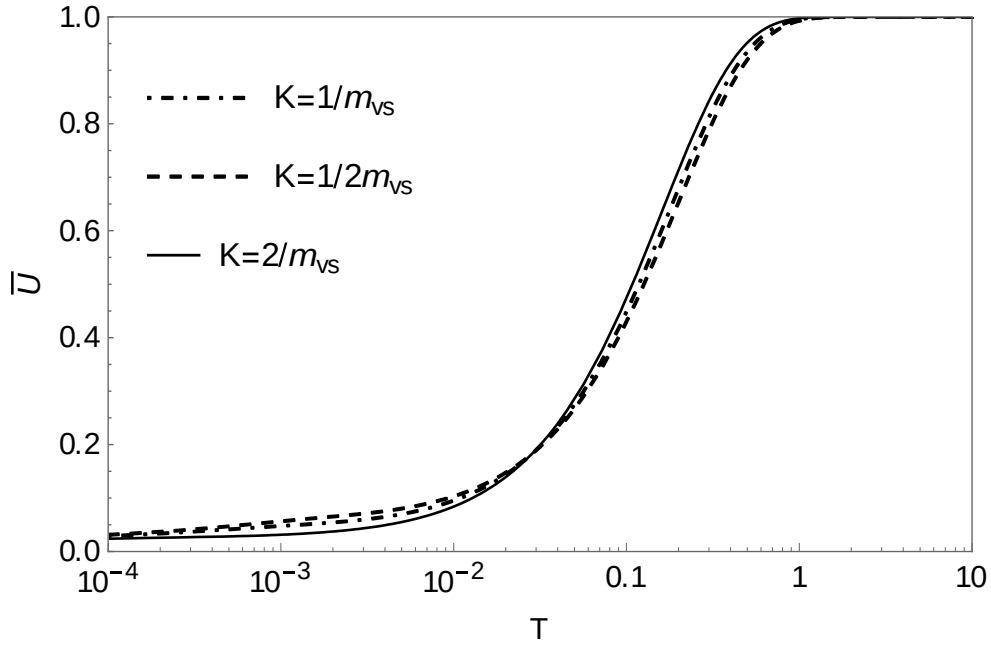

Figure 4.7 Effect of foundation stiffness on the average degree of consolidation

Figure 4.7 shows that the consolidation rate increases when foundation becomes stiffer, but the difference is relatively small when the stiffness ratio (K/m_{vs}) varies between 0.5 and 2.

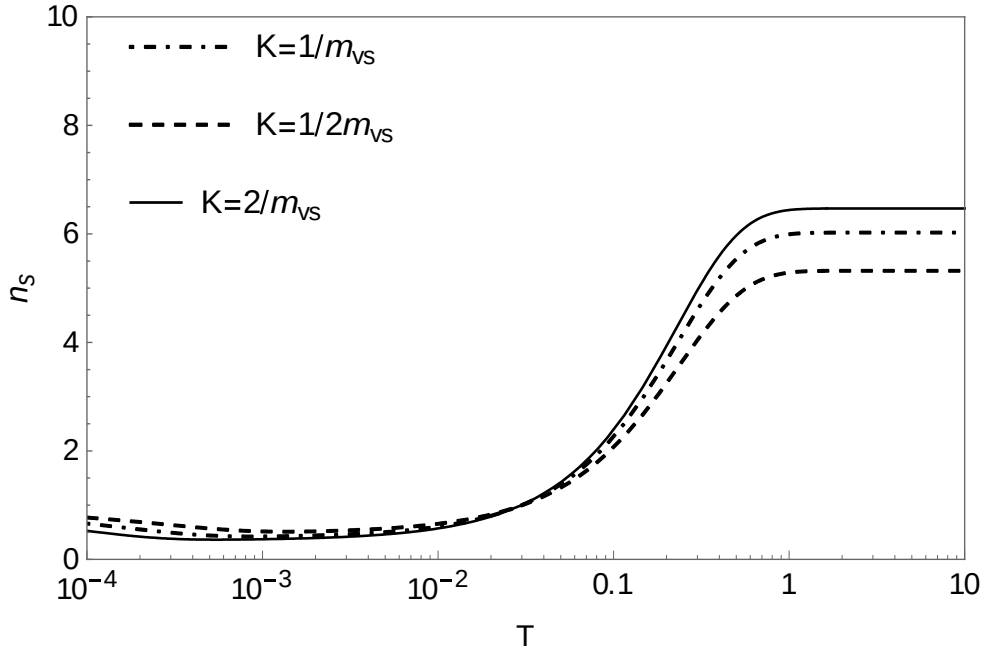

Figure 4.8 Effect of foundation stiffness on stress concentration ratio (n_s)

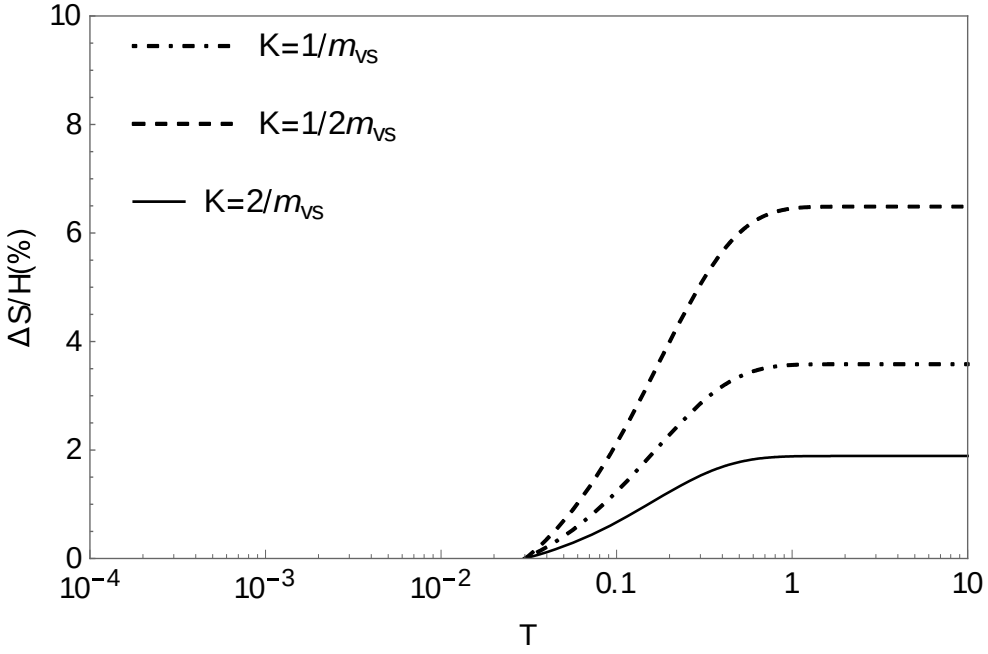

Figure 4.9 Effect of foundation stiffness on differential settlement

As Figure 4.8 shows, the stress concentration ratio on top of a unit cell rises as consolidation processes, and this ratio will increase if the foundation stiffness increases. However, in this case, the steady stress concentration ratio has an upper limit of 7 (corresponding to equal strain condition), which is the value of the modulus ratio of stone column to clay.

The differential settlement between stone column and the surrounding soil also develops over time. If the foundation becomes stiffer, there will be less differential settlement observed (Figure 4.9). The differential settlement ratio is defined as the ratio of different settlement at the top of the unit cell to the height of the unit cell, and it varies between 2% and 6%.

In practice, the modulus ratio of column to clay is in the range of 10-40 (Hu, 1995, Kelly, 2014). The influence of foundation stiffness under different modulus ratios is studied, and the results are shown in Figure 4.10. Based on elastic theory, the coefficient of compressibility can be calculated through a combination of Poisson's ratio, v, and Young's modulus, E_0 (Han and Ye, 2001).

$$m_v = \frac{(1+v)(1-2v)}{E_0(1-v)} \qquad \text{Eq 4.55}$$

Han and Ye (2001) suggested that Poisson's ratios for stone column and surrounding soil should be chosen as 0.15 and 0.45 respectively. By using these two parameters, the ratio of coefficient of compressibility of clay to column is determined to be in the range of 2 to 11 when the modulus ratio of column to clay varies between 8 and 40.

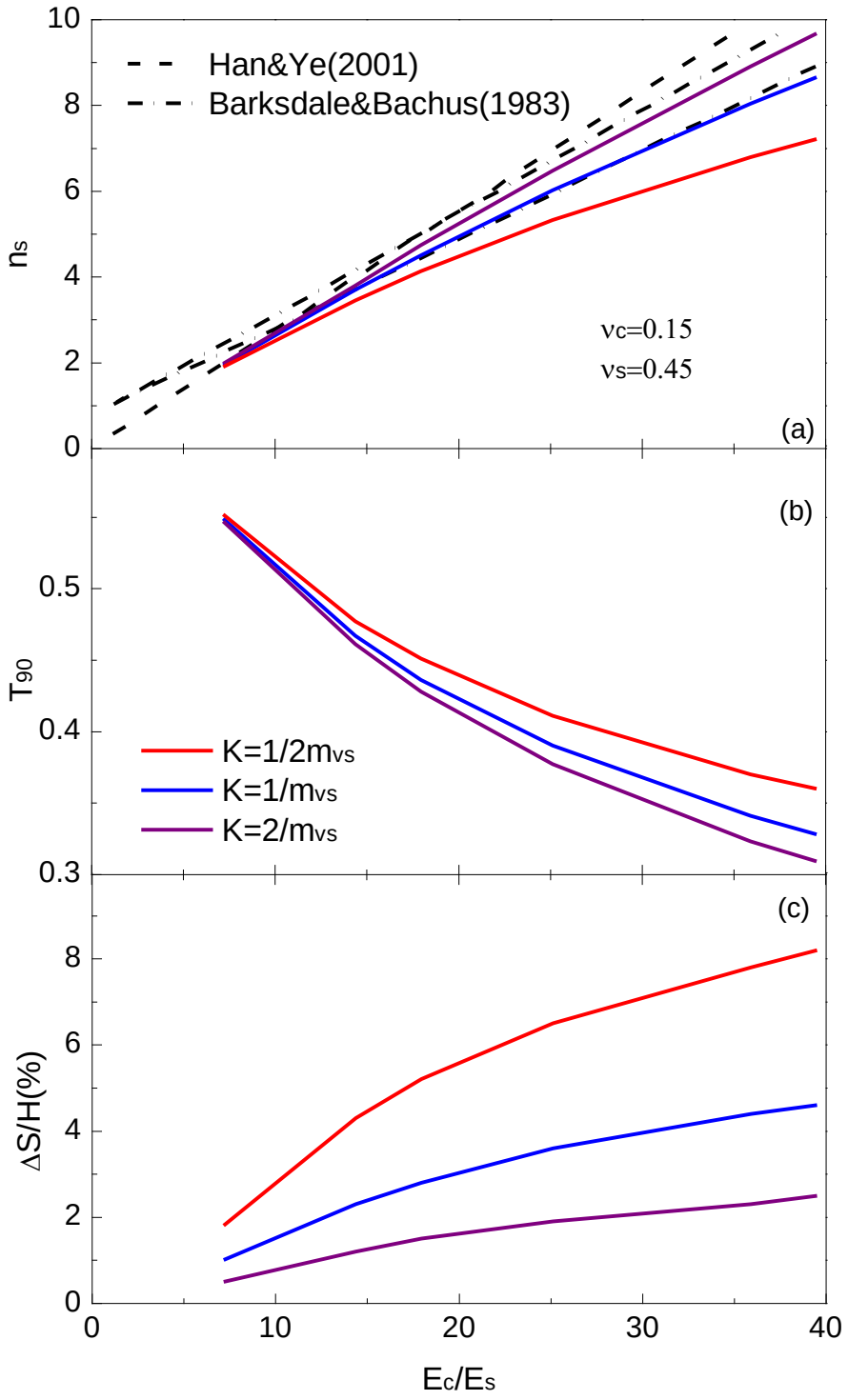

Figure 4.10 Effect of foundation stiffness with increasing modulus stone column: (a) steady stress concentration ratio; (b) time to achieve 90% of consolidation degree (T_{90}); (c) differential settlement at the top of unit cell ($\Delta S/H$)

The stress concentration ratio becomes steady when consolidation is complete. The steady stress concentration ratio under different modulus ratios was compared to previous predictions (Barksdale and Bachus, 1983, Han and Ye, 2001) in Figure 4.10(a), and these results agree with each other. The steady stress concentration ratio increases with an increase in both modulus ratio and foundation stiffness, but the effect of foundation stiffness becomes negligible when modulus ratio is small. According to Mitchell (1981), the steady stress concentration ratio was between 2 and 6 in the field; this statement can be explained by including the foundation stiffness.

The time factor corresponding to 90% of the degree of consolidation, T_{90}, was also calculated under different modulus ratios and different foundation stiffness. Figure 4.10(b) shows that the time needed to achieve 90% of consolidation degree increases as the foundation stiffness decreases, but this effect is not notable when the modulus ratio is small.

The differential settlement is also influenced by the modulus ratio. It shows in Figure 4.10(c) that the different settlement ratio increases with an increase in modulus ratio, but it decreases as the foundation stiffness increases.

The effect of foundation stiffness on consolidation rate was also studied by calculating the time factor needed to achieve 90% of consolidation degree under different radius ratios of the unit cell to column (r_s/r_c) and different permeability ratios of column to the surrounding soil (k_c/k_s). In situations where radius ratio varies in a typical range (1.5-3.5), and permeability ratio varies between 10^3 and 10^6, the conclusion is still valid that consolidation rate increases as the foundation becomes stiffer.

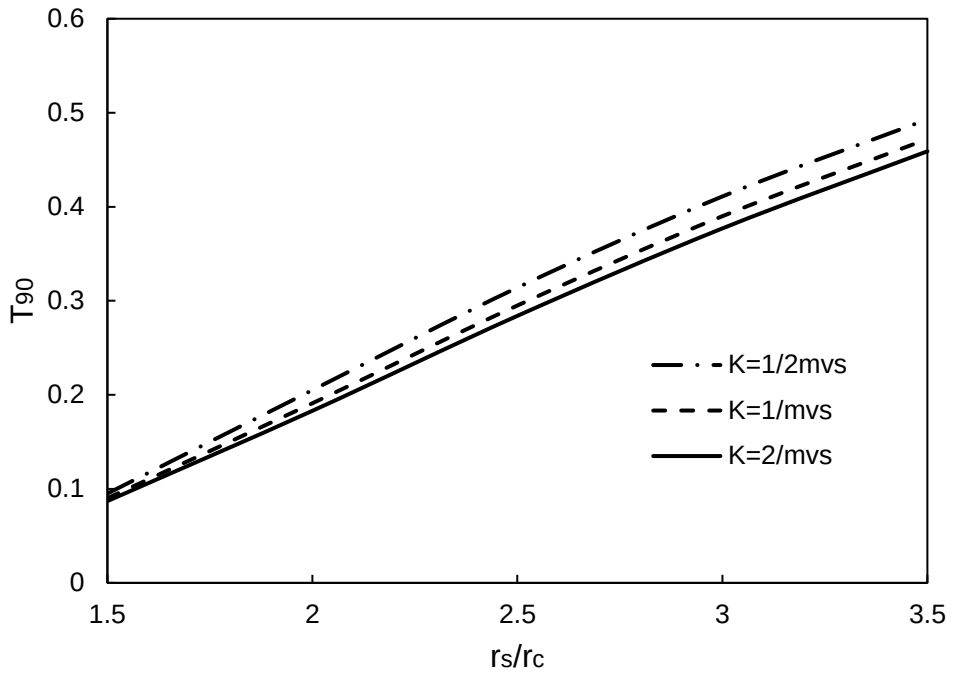

Figure 4.11 The effect of foundation stiffness on T_{90} under different radius ratio (r_s/r_c)

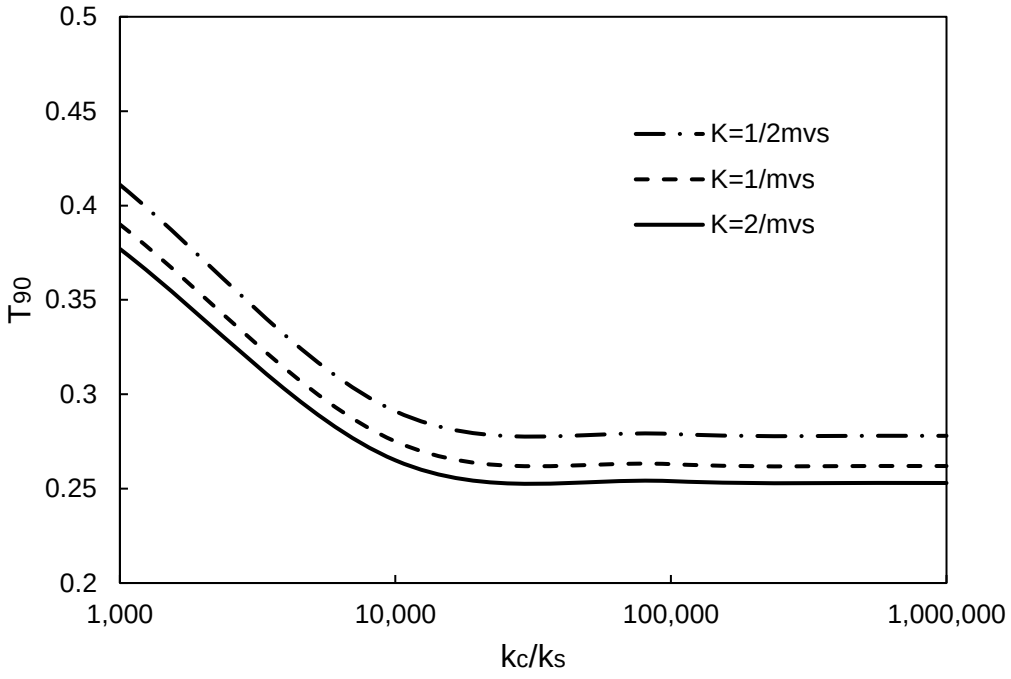

Figure 4.12 The effect of foundation stiffness on T_{90} under different permeability ratio (k_c/k_s)

4.5 Model limitation

Although the proposed model can provide solutions of ground improved with stone column for equal strain, free strain, and situations in between, by considering the foundation stiffness, there are also inevitable limitations that must be pointed out:

1. Shear resistance is assumed only from the foundation, but resistance can also be expected from the column-clay interface due to static friction, even if there is no relative sliding at the interface.
2. The vertical strain in the surrounding soil is not uniform; it is greater closer to the column.
3. The sliding surface in the foundation layer is not real, and the generated shear stress should have an upper limit which equals to the shear strength of the foundation material.

4.6 Summary

A consolidation model that considers the effect of foundation stiffness on a unit cell improved by stone column was presented in this chapter. A foundation layer was added to the top of the original unit cell. The stress distribution at the top of the ground was related to the shear resistance provided by the foundation due to differential settlement. The shear stress in the foundation layer was calculated using a method similar to "trapdoor" theory.

The consolidation of ground improved with stone column under equal strain, free strain, and situations in between can be analysed using this model. Closed-form solutions are found through the variable separation method and are given in the form of Fourier series. The solutions of "equal strain" and "free strain" agree well with previous

consolidation models. Consolidation under free strain condition developed faster than equal strain initially, but then the consolidation rate of equal strain was higher than that of free strain due to the development of excess pore water pressure and stress redistribution.

For situations between equal strain and free strain, parameter studies were also carried out to determine the influence of foundation stiffness. The time needed to achieve 90% of consolidation degree will reduce, the steady stress concentration ratio will increase, and the differential settlement at the ground surface will decrease if the stiffness of foundation increases. The effect of foundation stiffness on consolidation under different modulus ratios (E_c/E_s), radius ratios (r_s/r_c), and permeability ratios (k_c/k_s) were also studied.

Chapter 5 Laboratory Study of Performance of Stone Column under Cyclic Loading

5.1 General

Settlement control is a primary concern for modern infrastructures built on soft soil including high-speed rails and highways, due to the stringent settlement criteria. Pile foundation is a popular ground improvement method, but the construction cost is often higher than other methods such as vertical drains (combining with preloading), or stone columns, or chemical stabilisation. Since stone columns can shorten the drainage path and stiffen the ground, they have already been suggested as one of the suitable approaches for stabilising the potential liquefaction of soil.

Analysis and design application based on a simplified consolidation theory was therefore developed to evaluate the possibility of using stone column in liquefiable soil (Seed and Booker, 1977, MATSUBARA et al., 1988). Shaking table model tests were carried out to study the effectiveness of stone columns as a countermeasure against liquefaction during simulated earthquakes (Sasaki and Taniguchi, 1982, Adalier et al., 2003, Huang et al., 2016). The results of full-scale tests were also reported to reveal the response of deep foundations with and without stone columns to controlled blasting (Ashford et al., 2000). Moreover, the three-dimensional finite-element analysis was also conducted to evaluate the reinforcement of stone column treated ground in terms of reducing seismic stresses and lateral deformation (Rayamajhi et al., 2016a, Rayamajhi et al., 2016b). Adalier and Elgamal (2004) stated that the cases of utilising stone columns under seismic condition were somewhat limited, and the gravel drain systems perform well during earthquake events.

The build-up of excess pore water pressure and the accumulating of settlement are generally of concerned for transportation infrastructures. Installation of stone columns is likely to improve the foundation performance under repeated loading. Therefore a laboratory study is presented in this Chapter to investigate the use of stone columns to improve soft soil ground subjected to traffic loading. The performance of ground improved with stone column was studied through model tests and compared to tests where the ground was not improved or actively drained and stabilised by vertical drains. Furthermore, the effect of cyclic stress ratio (CSR), loading frequency and confining pressure were also investigated. Finally, a test including consecutive loading and rest periods was carried out to show a strengthening effect under traffic loading.

5.2 Description of laboratory test

5.2.1 Design of model tests

There are a number of parameters that may affect the load-settlement performance of foundations improved with stone columns; those non-dimensionalised factors included **L/D, L/d, d/d_g, A_r, ϕ', G_c/G_s (E_c/E_s), q_c/p_0', k_c/k_s** (Hu, 1995, Shahu and Reddy, 2011), where, L is the column length, D is the diameter of footing, d is the diameter of column, d_g is the mean particle size of column material, A_r is the area replacement ratio, ϕ' is the internal friction angle of column material, G_c is the shear modulus of column material, G_s is the shear modulus of soft clay, E_c is the Young's modulus of column material, E_s is the Young's modulus of soft clay, q_c is the vertical stress applied, p_0' is the initial mean soil stress, k_c is the permeability of column material, k_s is the permeability of soft clay.

Based on field applications, geometry of stone column, material modulus, bulk density and permeability were reported by several researchers (Hu, 1995, Ambily and Gandhi, 2007, Guetif et al., 2007, White et al., 2007, McCabe et al., 2009, Bouassida and Carter, 2014, Kelly, 2014). These typical parameters of field cases are given in Table 5.1.

Without a proper prototype, there are usually no exact values for these dimensionless parameters to follow in model tests. While they can be chosen freely within the range of typical field data, they must eventually be compatible with laboratory equipment.

For the current large-scale testing, the diameter and length of the model column were decided to be 100 mm and 600 mm, respectively. Therefore, the area replacement ratio for the model tests would be 11% if considering that the diameter of the whole sample is 300 mm. The material for the model column was crushed from basalt collected from Boral quarry near Wollongong (NSW, Australia). As a result, the size ratio of smallest dimension to maximum particle is 10.5. Commercial kaolin was used in model tests due to its low sensitivity, relatively high permeability, ease of saturation, and good uniformity.

Most laboratory-scale model tests of stone columns often used sand as column material due to the limitation of equipment size (Wood et al., 2000, Black et al., 2007, Weber et al., 2010, Cimentada et al., 2011). Based on the parallel gradation concept (Indraratna et al., 1993), a parallel particle distribution curve was adopted to obtain the gradation of model column material as shown in Figure 5.1(a). One of the advantages of employing gravel rather than sand is that the similarity of angularity between model and prototype can be maintained as shown in Figure 5.1(b). However, some sacrifices in the model tests are inevitable, such as a reduction of the internal friction angle if the size of the column material is scaled down.

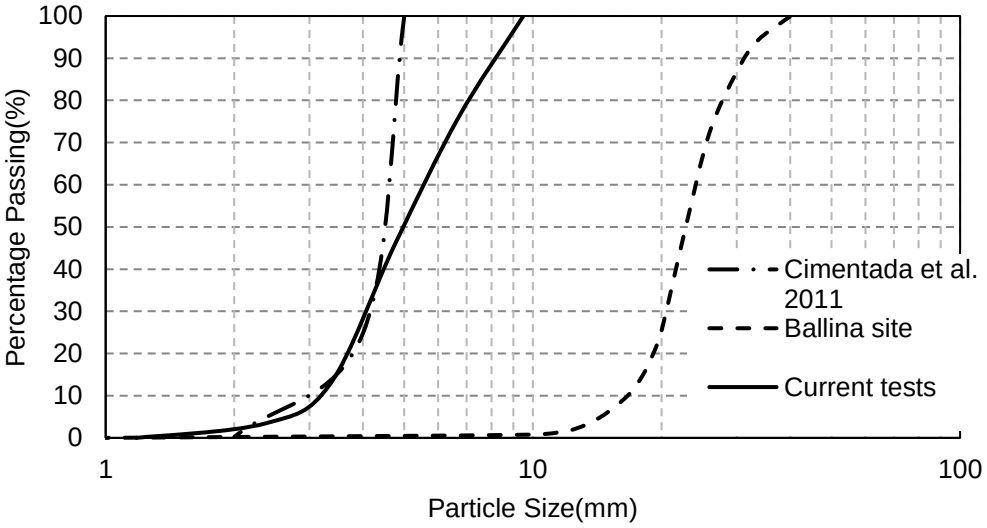

(a)

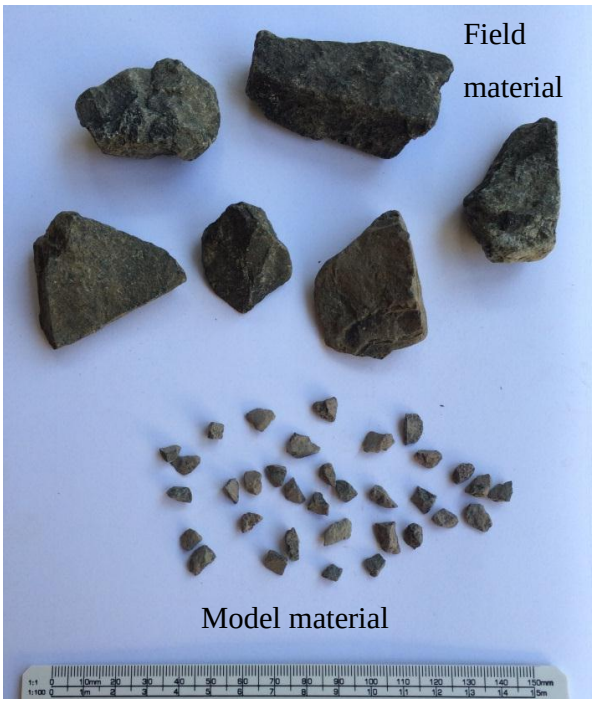

(b)

Figure 5.1 (a) Comparison of gradations of column aggregate; (b) material of field stone columns and model columns in laboratory

After determining the geometry of model column and the properties of the materials (details of test materials can be found in Table 3.1 of Chapter 3), the corresponding

dimensionless parameters between this model and typical prototype are listed in Table 5.1 below.

Table 5.1 Dimensionless parameters of stone columns in model tests and field

	L/D	L/d	d/d_g	A_r	ϕ'	E_c/E_s	q_c/p_0'	k_c/k_s
[b]Field	0.9-12	4-20	10-26	0.1-0.4	38-45	8-39.5	0.7-4.8	10^5-10^7
Model tests	2	6	20	0.11	45-51	25-50	[a]1.4	10^4-10^5

a. This value is corresponding to confining pressure of 50kPa
b. Collected from Hu (1995), Ambily and Gandhi (2007), Guetif et al. (2007), White et al. (2007), McCabe et al. (2009), Bouassida and Carter (2014), Kelly (2014).

While the controlling dimensionless parameters of model tests were set to be in the range of typical field values, the model could not wholly replicate field situations; it is still expected that the fundamental characteristics of field stone column can be simulated in the model test.

5.2.2 Test preparation

Kaolin clay was mixed to the liquid limit (67% water content) and then poured into a rubber membrane mould to form a cylindrical sample with diameter of 300 mm and length of 760 mm. During mixing, the clay slurry was stirred thoroughly and left to stand for two to three hours in order to make sure the clay was fully saturated. Vaseline was applied inside the rubber membrane to minimise the friction between rubber membrane and clay.

The membrane with thickness of 3 mm was chosen for model tests, which is enough to support the soft sample during preparation and transport, and meanwhile not too stiff to affect the test results significantly. The effect of membrane is complex, and no

consensus has been reached on a sophisticated membrane correction. Therefore, a simplified method from ASTM D4767-11 was adopted for membrane correction. The Young's modulus of the membrane material was determined to be roughly 2200 kPa. The difference of deviator stress needs to be subtracted from the measured value using the equation provided by ASTM D4767-11 below.

$$\Delta(\sigma_1 - \sigma_3) = \frac{4E_m t_m \varepsilon_a}{D_c} \qquad \text{Eq 5.1}$$

where, $\Delta(\sigma_1 - \sigma_3)$ is the correction of deviator stress, D_c is the diameter of specimen after consolidation, E_m is the Young's modulus for membrane material, t_m is the thickness of the membrane, ε_a is the axial strain.

To simulate in-situ clay, a one-dimensional pre-consolidation pressure of 65 kPa was applied to achieve an undrained shear strength of 15 kPa occurred within 30 days. The final sample height before transferring to large-scale-triaxial apparatus was almost 600 mm, as shown in Figure 5.2(a). Then the model stone column was installed using the replacement method.

The installation procedure is as follows:

1. A 100 mm-diameter PVC tube was gently inserted vertically into the centre of the clay sample to form and maintain a cylindrical cavity;
2. Another steel tube with a slightly smaller diameter was then inserted inside the PVC tube. Upon suction, the clay in the tube was removed, and the steel tube was pulled out;
3. The inner surface of the PVC tube was cleaned and then model column was shaped layer by layer: for each layer, material was poured in to a height of 110 mm and then tamped down to approximately 100 mm to achieve a dry density of

1.3 g/cm^3; the PVC tube was then pulled out by 100 mm, and a new layer of material was added to start the next layer.

After installation, the radius of the model column was about 50-55 mm on the top surface. Throughout all the tests, the average void ratio of the model column was approximately 0.9.

While preparing the sample, four small pore pressure gauges (size less than 10mm) which should experience the same settlement as clay, were placed at different positions inside the sample. After installation, two soil pressure gauges with size less than 50mm (also known as small pressure plate) were also installed on the top of the sample to measure the total stress. The positions of the sensors are given in Figure 5.2(b).

(a)

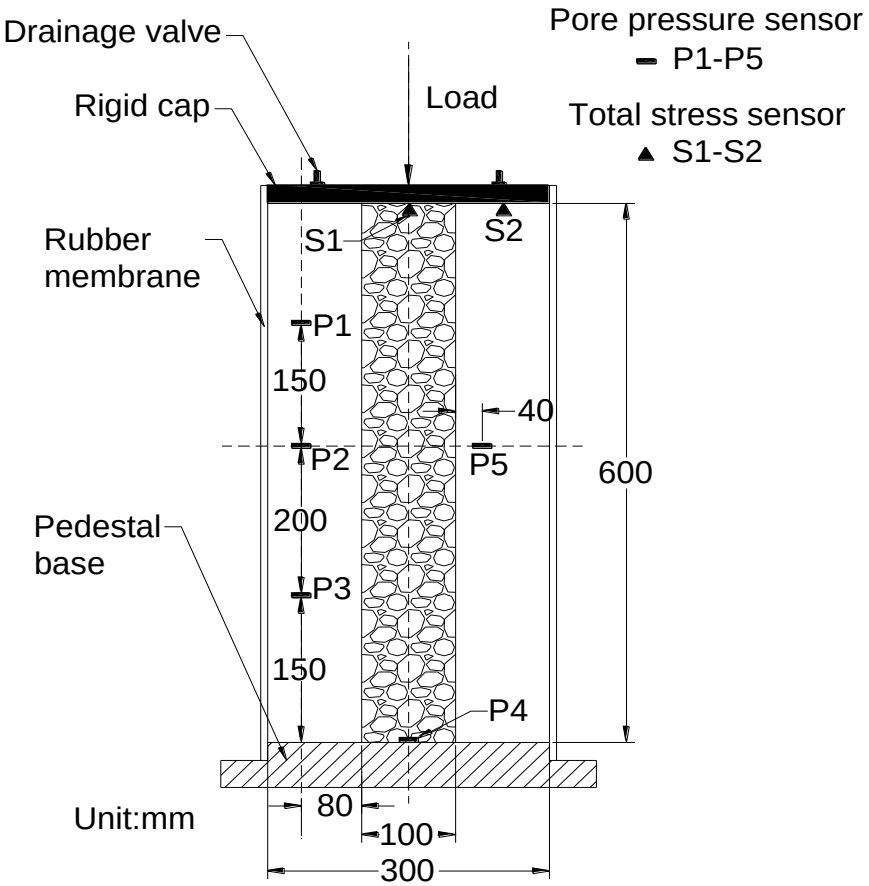

(b)

Figure 5.2 (a) Sample after pre-consolidation; (b) positions of sensors

Due to the insufficiency of both data logger and sensors at high reading frequency, the measured data cannot reflect changes during an individual loading cycle, but the trend could still be used to compare the performance of stone columns under cyclic loading. The measurements were assumed to be the mean values of a reading interval. This uncertainty poses no significant problems, especially when the specimens are subjected to a large number of cycles (Brown et al., 1975). Moreover, the measurements taken during and after cyclic loading showed acceptable continuity in terms of trend and magnitude, thus providing more confidence in the data obtained.

5.2.3 Test procedures

The cyclic tests were carried out via the large-scale triaxial apparatus designed and built at the University of Wollongong (Figure 5.3), detailed information of which can be found elsewhere (Indraratna et al., 1998, Lackenby et al., 2007, Indraratna et al., 2009). Note that the pre-consolidated samples might be disturbed due to unloading during column installation and transferring; therefore additional anisotropic consolidation stage was conducted before cyclic loading application to simulate field conditions.

Figure 5.3 Large-scale triaxial apparatus

While the lateral stress on the subgrade is usually low and between 15 to 60 kPa (Li and Selig, 1996, Miller et al., 2000, Liu and Xiao, 2010), the effective confining pressures in the model tests were chosen to be 20 kPa, or 50 kPa, or 80 kPa. Meanwhile, the axial force on the top surface of the sample was 2.8 kN, which is equivalent to the stress

induced by a 2m high embankment. A particular test was also carried out with a confining pressure of 24 kPa and an axial stress of 16 kPa, to be comparable with previous tests (Indraratna et al., 2009).

The change of stress of a soil element induced by a moving load within its longitudinal plane was described by Brown (1996): "There are pulses of vertical and horizontal stress accompanied by a double pulse of shear stress with a sign reversal on the vertical and horizontal planes", which means not only the magnitude of principal stress but also the rotation of the principal plane takes place. Despite using triaxial equipment, it is a model test rather than an element test, so the principal stress rotation is not considered in this research, and conventional one-way stress controlled triaxial tests are used to simulate traffic load; the focus was only on the magnitude of cyclic vertical stress.

There is a linear speed-stress-frequency relationship in the ballast layer given by Indraratna et al. (2010). Beneath the ballast layer, attenuation is occurring because of both geometry damping and material damping as the depth increases. If only geometry damping is considered and the trapezoidal approximation (2:1 method) is used to describe the dispersion of stress (Indraratna et al., 2011), the maximum vertical stress on top of the subgrade can decrease below 100 kPa, as shown in Figure 5.4. This calculation is consistent with the field measurements (Liu and Xiao, 2010), which are between 50 kPa to 110 kPa, and therefore in most of the tests, the cyclic deviator stress was chosen in this range.

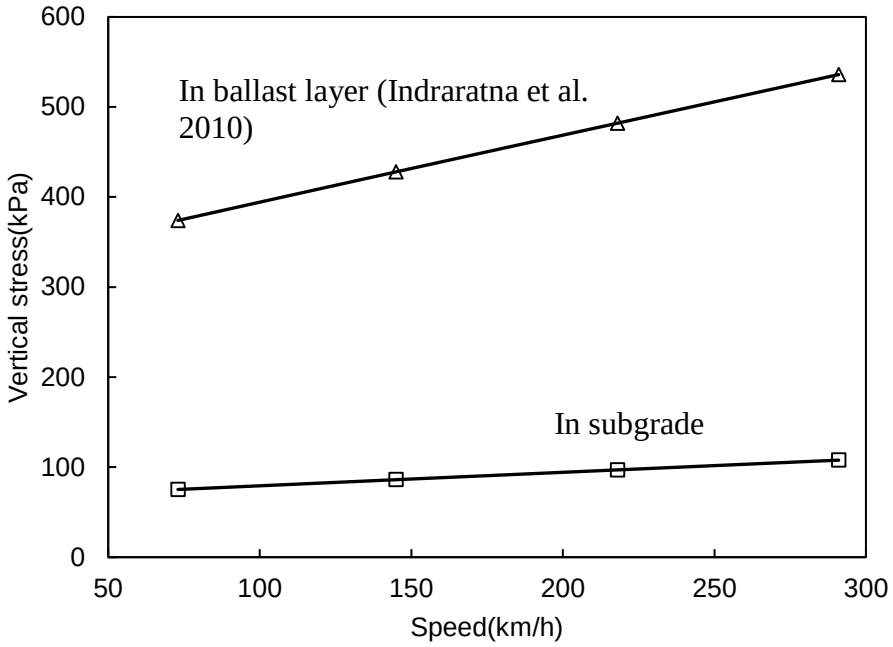

Figure 5.4 Vertical stress induced by moving train

Field measurements showed the loading frequency on subgrade is about 4-5Hz, which is much lower than the frequency in the ballast layer and less sensitive to the train speed (Liu and Xiao, 2010). Another field measurement reported by Indraratna et al. (2009) also indicates that "a cyclic deviatoric stress of 50-100 kPa and a load frequency of 5-10 Hz are typically obtained at the subgrade when a freight train approaches a speed of 100 km/h". Therefore the maximum loading frequency in the model tests was chosen to be 10 Hz.

For field conditions, it is not appropriate to classify ground improved with stone column under traffic loading as being in an undrained condition when the long-term behaviour is of concern. However, even if drainage is permitted, excess pore water pressure would probably still accumulate due to the low permeability of clay. Partially drained conditions were termed to describe this situation, which means that the drainage valves

are open during the triaxial test, while there is still a possibility of the pore pressure build-up.

5.2.4 Test programme

First, a test under the same conditions described by Indraratna et al. (2009) was carried out to study the effectiveness of stone column compared to cases with and without vertical drains, and then a series of tests were planned to investigate the influence of CSR, the loading frequency, and the confining pressure. Finally, a test with several loading stages and rest periods was carried out.

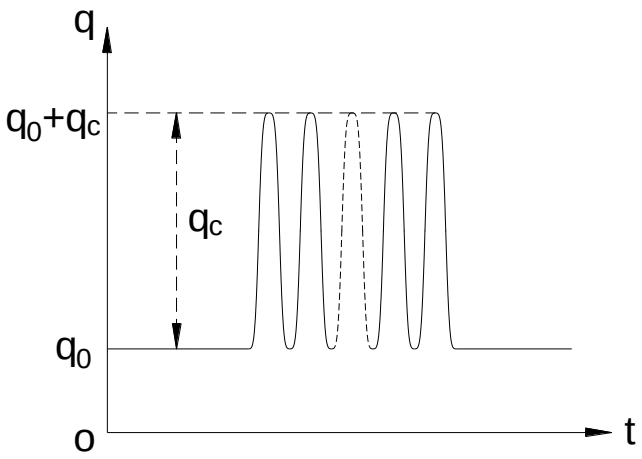

Figure 5.5 Loading characteristics

The loading procedure follows the pattern shown in Figure 5.5, where q_0 stands for the axial stress before cyclic loading, and q_c is the magnitude of cyclic stress.

The cyclic stress ratio is defined as the ratio of cyclic deviator stress to 2 times the confining pressure.

$$CSR=\frac{q_c}{2\sigma_3'} \qquad \text{Eq 5.2}$$

where σ_3' is the effective confining pressure.

Test programme is summarised in Table 5.2. During each test, vertical strain, pore water pressure, and total stress was monitored. After cyclic loading, the model stone column was removed, and then the cavity was refilled with concrete, to obtain the deformation of the model column.

Table 5.2 List of cyclic model tests

Test No.	Loading Frequency(Hz)	q_c(kPa)	Confining pressure(kPa)	p_0'(kPa)	Number of cycles
C1	5	22	24	29.3	10^5
C2	5	30	50	63.3	10^5
C3	5	60	50	63.3	10^5
C4	5	70	50	63.3	10^5
C5	5	80	50	63.3	<1000
C6	0.1	30	50	63.3	2000
C7	1	30	50	63.3	20000
C8	1	60	50	63.3	20000
C9	1	80	50	63.3	<1000
C10	10	30	50	63.3	10^5
C11	10	60	50	63.3	10^5
C12	10	90	50	63.3	<1000
C13	5	30	20	33.3	<1000
C14	5	30	80	93.3	10^5
C15	5	60	80	93.3	10^5
C16	5	90	80	93.3	10^5
C17	5	120	80	93.3	<1000
C18	5	30/60/90/120	50	63.3	10^5(each q_c)

5.3 Repeatability of model tests

To verify the repeatability, two tests carried out under some conditions are presented here; denoted as C2 and C18 (the first stage) respectively.

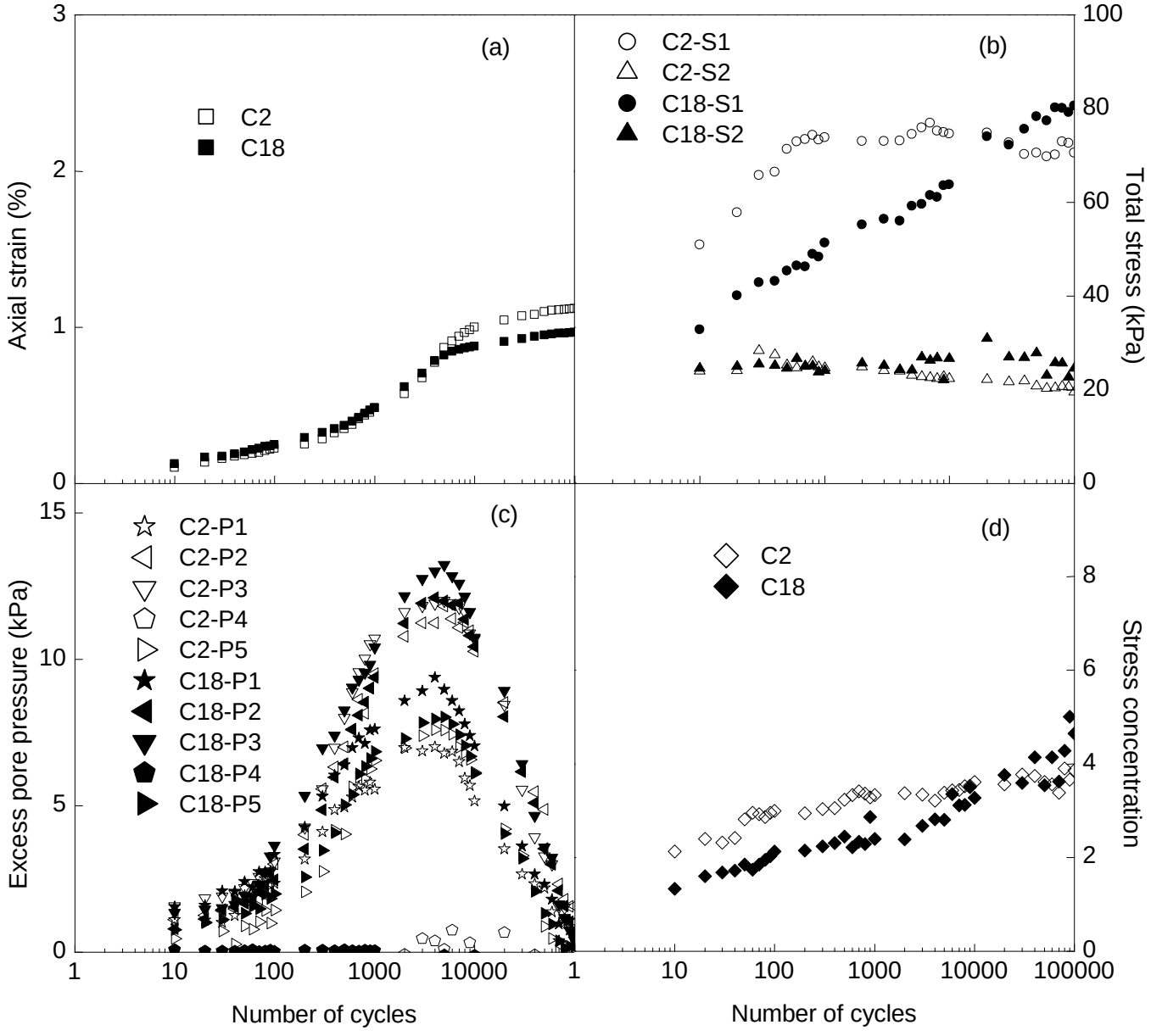

Figure 5.6 Comparison of test C2 and C18 (the first stage): (a) axial strain; (b) total pressure; (c) stress concentration ratio; (d) pore pressure P1-P5

Figure 5.6 shows all the measurements from those two model tests, including total stresses on the top surface of the column and the surrounding clay, vertical strain and

pore water pressure. The final vertical strains of those two tests are similar (Figure 5.6(a)). Moreover, the stresses on top of the column and the clay, and the resulting stress concentration ratio are also at the same level, as displayed in Figure 5.6(b) and (d). The measured pore pressures agreed from test to test with negligible differences (Figure 5.6(c)). Overall, the test results are consistent in both tests, so the repeatability of model tests is confirmed.

5.4 Performance of unit cell with a single stone column

The performance of soft soil under cyclic loading with and without prefabricated vertical drains was presented by Indraratna et al. (2009) using the same test apparatus described in this Chapter. It was stated that PVD could prevent the build-up of excess pore water pressure during cyclic loading. In order to compare the performance of different methods of improvement, a model test C1 was conducted under the same conditions, except that the inclusion was replaced by a stone column.

The ratio of excess pore water pressure is defined here as the ratio of excess pore pressure generated by cyclic loading, u_g, to the initial effective mean principle stress, σ_0'.

$$r_u = \frac{u_g}{\sigma_0'} \qquad \text{Eq 5.3}$$

Figure 5.7 shows that the sample without improvement failed quickly under cyclic loading; the axial strain would come to 4% within 3000 cycles if a vertical drain was installed, but the long-term safety was unknown; if a stone column is installed the axial strain would be decreased to less than 3% after 100,000 cycles (see next section Figure 5.8).

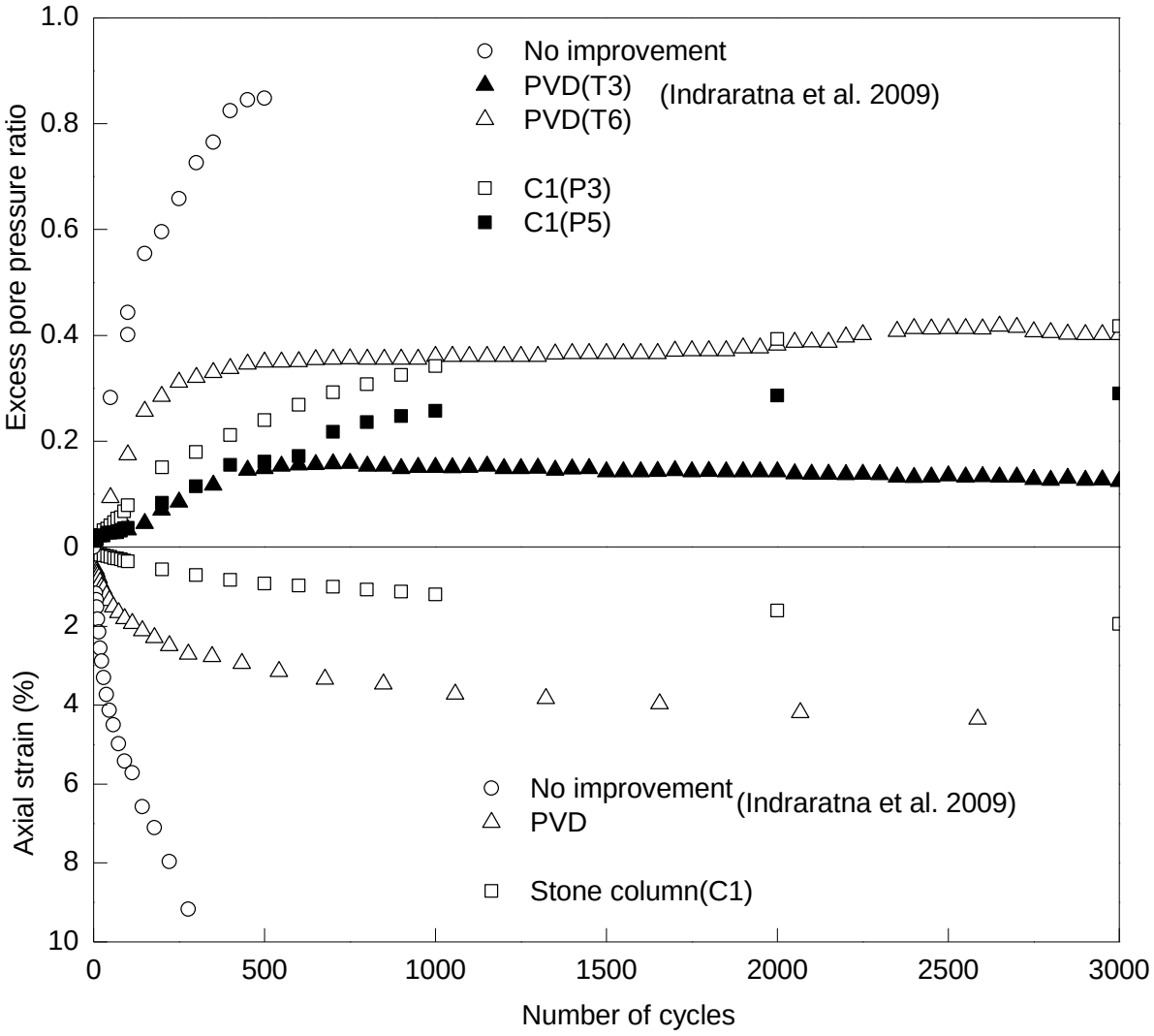

Figure 5.7 Performance of stone column and PVD under cyclic loading

The excess pore pressure ratio was more than 0.8 for the unimproved sample leading to rapid failure. Further dissipation through the vertical drain and stone column was efficient, and the excess pore water pressure remained below 0.4 after 3000 cycles. Installing a stone column would largely reduce the axial strain and prevent the accumulation of excess pore water pressure.

5.5 Typical sensor responses

The typical sensor readings corresponding to Test C1 are given below in Figure 5.8. Note that the excess water pressure induced by cyclic loading increases with depth and

distance to the column, but the difference between the bottom and middle measurement point (P2 and P3) is negligible, and there is no excess water pressure observed inside the column (P4).

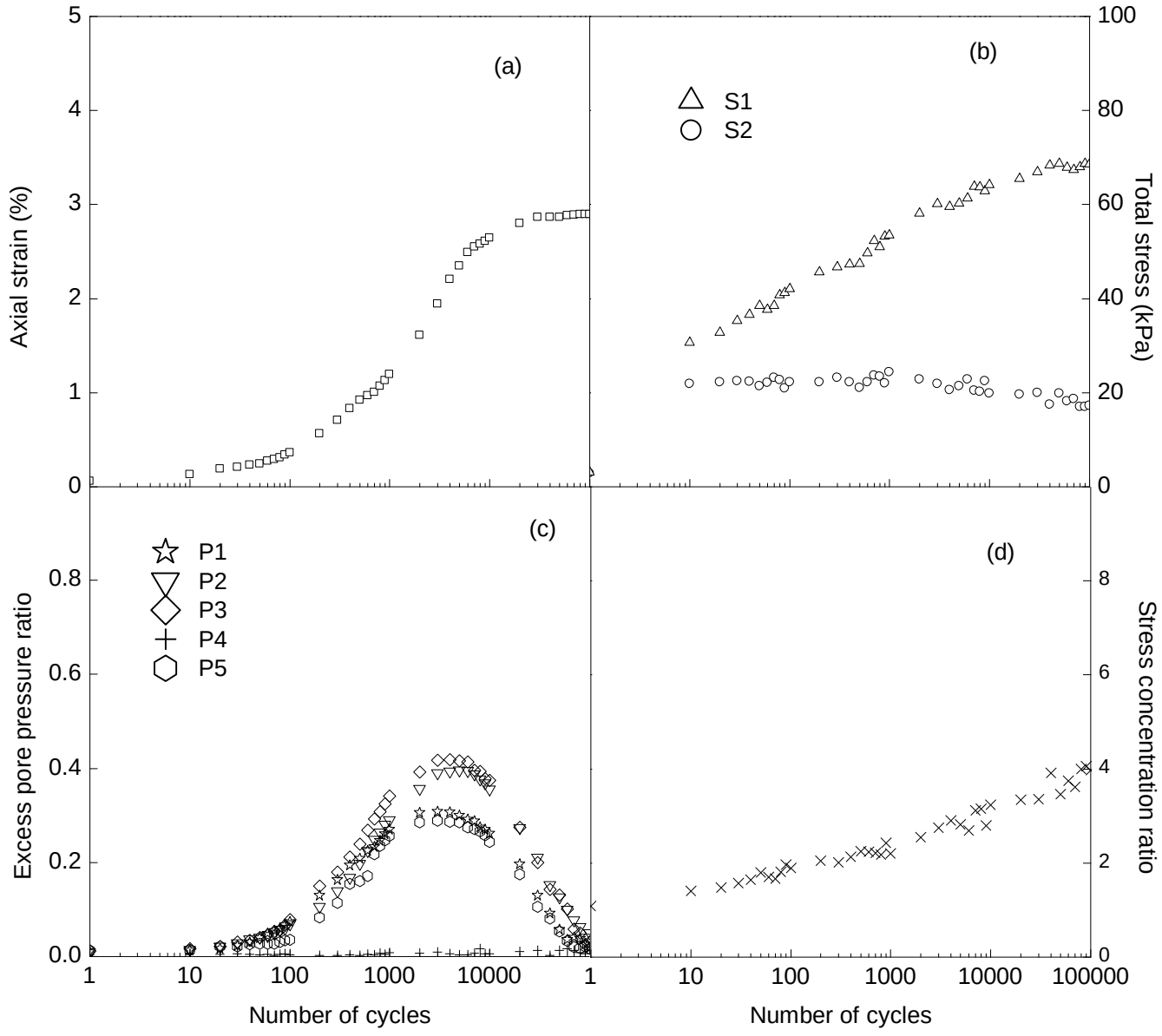

Figure 5.8 Typical response of sensors (C1): (a) axial strain; (b) total stress; (c) pore pressure; (d) stress concentration ratio

According to the measurement from pressure plates, the stress on top of the column increases with the number of cycles while the stress on the surrounding clay decreases slightly; this finding agrees with the proposal of Han & Ye (2001) that the vertical load

tends to concentrate on the column during consolidation. The resulting stress concentration ratio also increases with time and lies between 2 and 6. These behaviours are consistent in all the partially drained cyclic tests, except for the failed samples.

5.6 Factors affecting performance of stone column under cyclic loading

5.6.1 Effect of CSR

The effect of CSR (0.3, 0.6, 0.7 and 0.8) was studied by applying different cyclic stresses (30 kPa, 60 kPa, 70 kPa and 80 kPa) onto the entire top surface of the sample with an effective confining pressure of 50 kPa and a loading frequency of 5 Hz.

As shown in Figure 5.9(a), the critical cyclic stress ratio (CCSR) lies between 0.7 and 0.8 based on vertical strain measurement. When the CSR is relatively low (e.g. 0.3), the vertical strain after 100,000 cycles is within 2%, but when the CSR becomes higher (e.g. 0.6-0.7), the final vertical strain could be up to 4% approaching a stable phase. The axial strain would develop significantly within 100 cycles until failure if the CSR is too high (e.g. 0.8). This finding agrees with previous research of soil under cyclic loading which suggests that a CCSR value exists (Sangrey et al., 1969, Ansal and Erken, 1989, Zhou and Gong, 2001, Pillai et al., 2011).

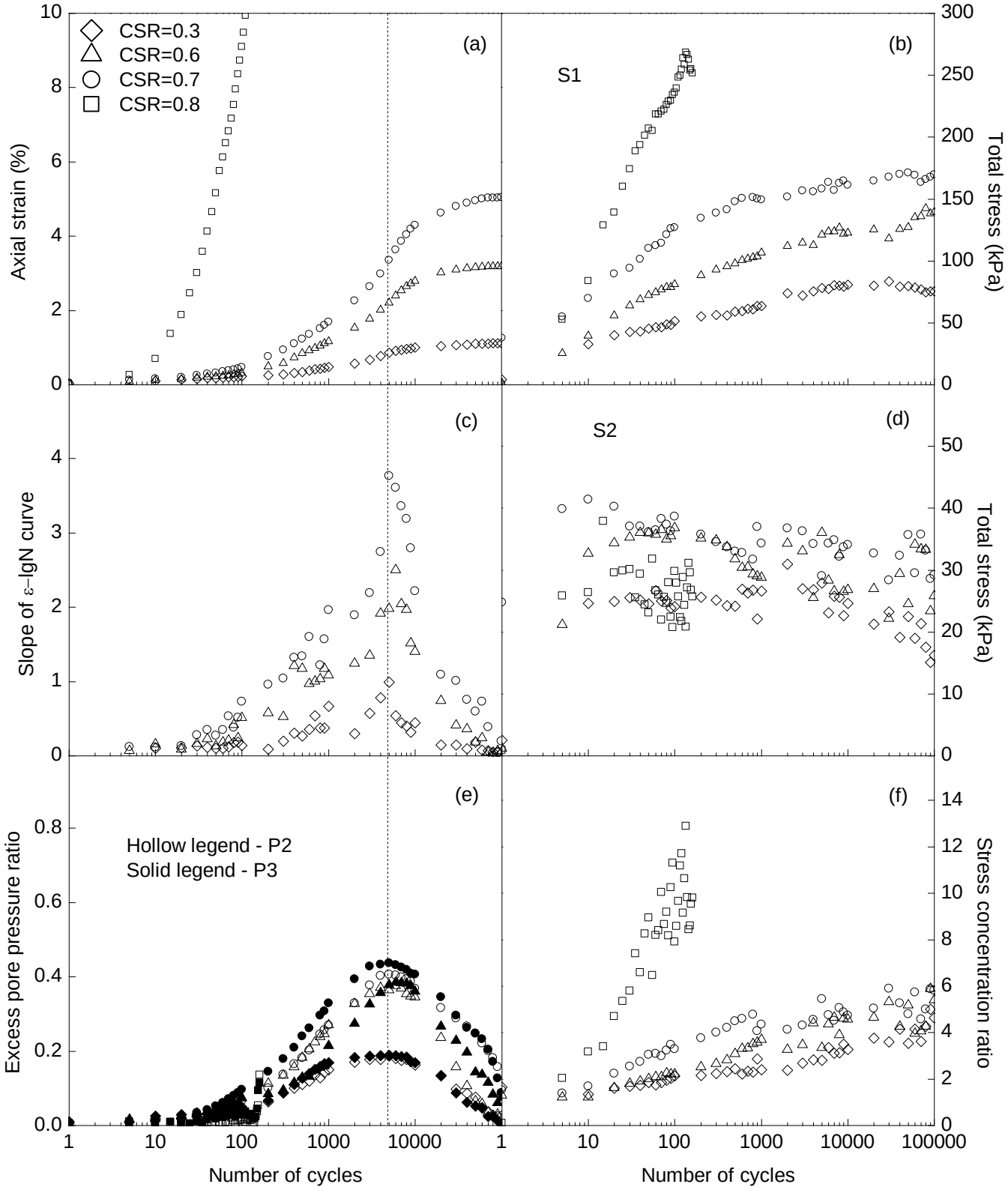

Figure 5.9 Cyclic performance of stone column with different CSRs: (a) axial strain; (b) total stress S1; (c) slope of ε_a–logN curve; (d) total stress S2; (e) pore pressure P2 and P3; (f) stress concentration ratio

The total stress on top of the sample shows that the stress on the column increases as the cyclic deviator stress increases while the stress on the soil decreases slightly (Figure 5.9(b) and (d)). For stable samples, an application of 30 kPa cyclic stress can result in a 50 kPa rise in the total stress on the column; the stress concentration ratio is in the range of 2 to 6 (Figure 5.9(f)). If the cyclic stress is too high, no difference in stress on the surrounding clay will be observed, but the stress on the column and the stress concentration will rapidly increase to a much higher value.

Due to unexpected sensor failures, only three pore pressure sensors were available for comparison, i.e. P2, P3, and P4. The reading of Sensor P4 which was located at the bottom of column suggests that there is no excess pressure built up in the column due to its high permeability. There is not much difference between P2 and P3, as shown in Figure 5.9(e) which indicates that the pore pressure between the middle and bottom part of clay was similar; it can also be observed that the ratio of peak pore pressure increases as CSR increases.

For the case where the sample fails (e.g. CSR-0.8), the excess pore water pressure only starts to increase after a substantial deformation appears (vertical strain>10%), and it would not exceed 0.2 even after vertical strain reaches 20%. This observation shows that an abrupt increase in excess pore water pressure is not always accompanied by failure. When the sample fails the stress on the column increases but the stress on the soft soil remains the same, so there may be no build-up of excess pore water pressure in the surrounding soil.

If the slope of the axial strain curves (against the number of cycles in a logarithm scale) is determined, the number of cycles corresponding to the peak slope will always match

the number of cycles when the peak excess pore water pressure appears, as shown in Figure 5.9(c) and (e).

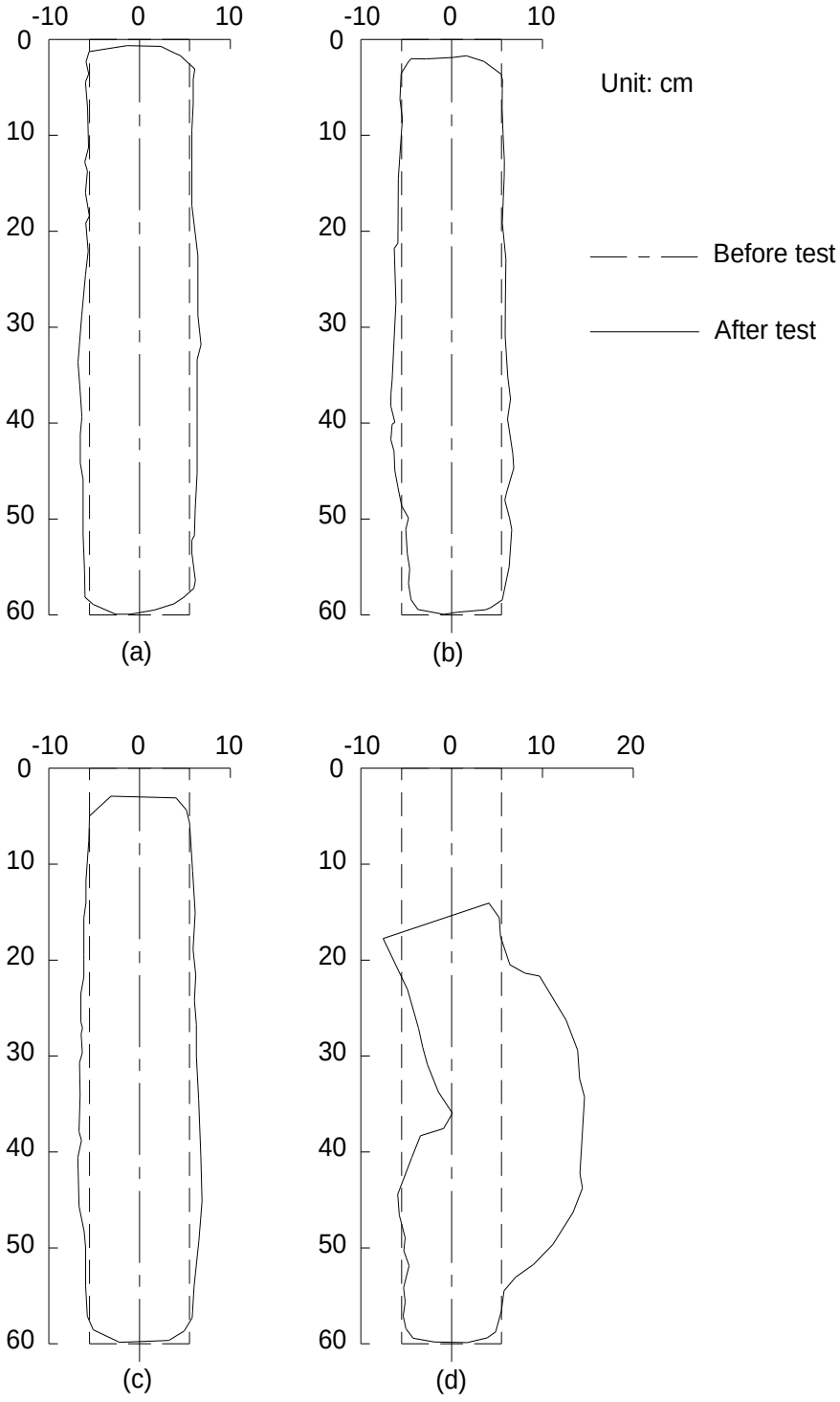

Figure 5.10 Profiles of exhumed stone columns after cyclic loading: (a) CSR=0.3; (b) CSR=0.6; (c) CSR=0.7; (d) CSR=0.8

After the tests, the samples were removed from the triaxial chamber, the model column material was vacuumed out, and the void was immediately filled with quick forming concrete. Then the concrete columns were exhumed after 24 hours and the profiles of these columns are shown in Figure 5.10. The sample under a CSR of 0.8 shows bulging and shearing failure, as shown in Figure 5.10(d), whereas other samples still retained the cylindrical shape after the tests, even though the diameter of the column has increased slightly, as displayed in Figure 5.10(a), (b) and (c).

5.6.2 Effect of loading frequency

The effect of the frequency of cyclic loading was studied by applying four different loading frequencies in each test, 0.1 Hz, 1 Hz, 5 Hz, and 10 Hz with a CSR of 0.3 and an effective confining pressure of 50 kPa. Unlike other sections, the measurements are plotted in time domain hereby to enable comparison among various frequencies.

Since the CSR is relatively small, the final vertical strain is within 3%, despite the loading frequency, as shown in Figure 5.11(a). When the loading frequency is below 5 Hz, the final vertical strain appears to be independent of it, but if the frequency rises to 10 Hz, there is an apparent increase in the final settlement.

Regarding the stress on the column during the cyclic tests, it is highest for the case of 10 Hz and lowest for the case of 5 Hz. This observation agrees with the measurement of vertical strain (Figure 5.11(b)). The readings of total stress sensors on top of the clay showed consistency regardless of the frequency (Figure 5.11(d)). The stress concentration ratio was within 7 for all frequencies (Figure 5.11(f)).

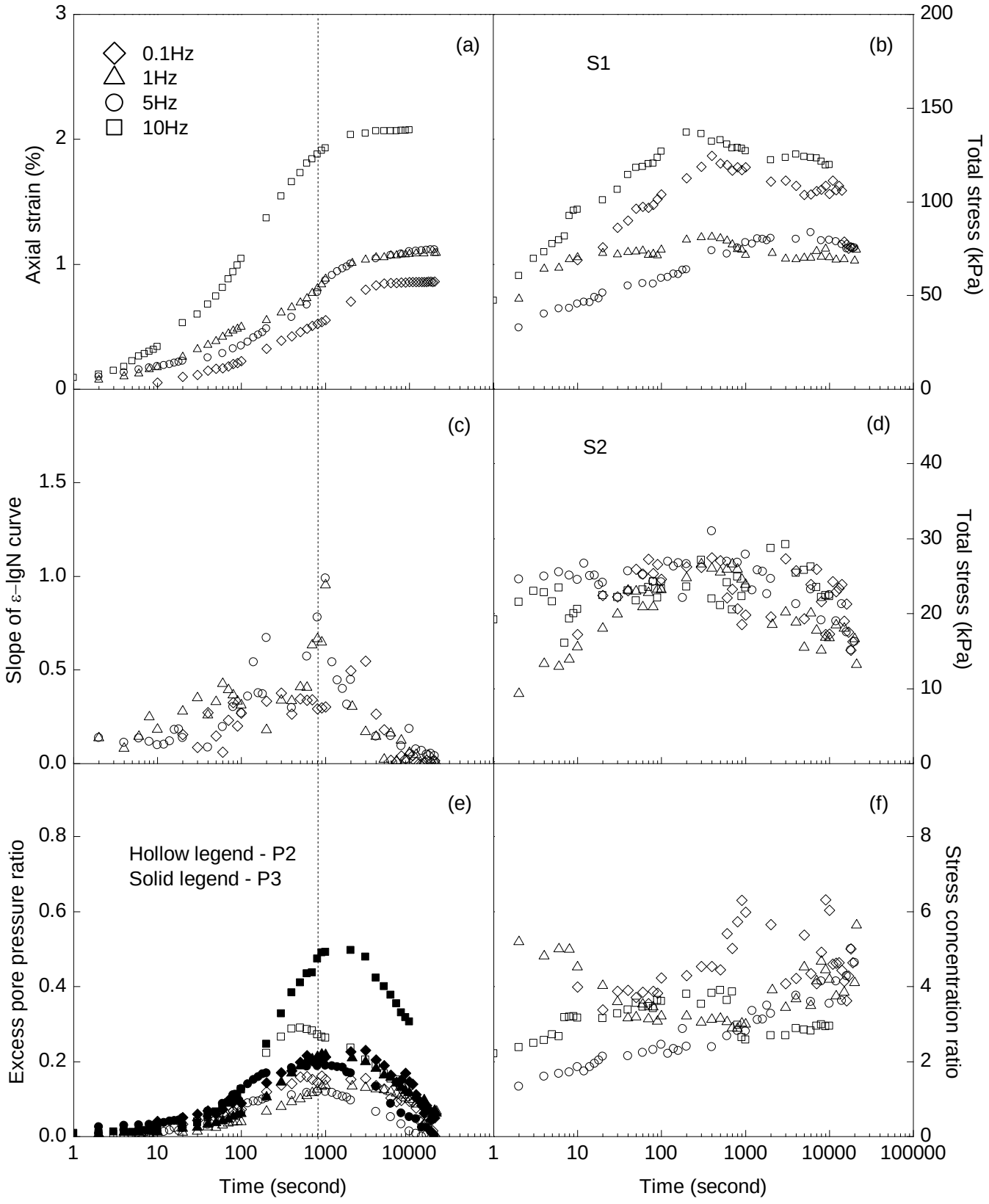

Figure 5.11 Cyclic performance of stone column with different loading frequency: (a) axial strain; (b) total stress S1; (c) slope of ε_a-log t curve; (d) total stress S2; (e) pore pressure P2 and P3; (f) stress concentration ratio

The responses of pore pressure sensor suggest the same conclusion as above, so when the loading frequency increased to 10 Hz, the sample behaves differently. As Figure 5.11(e) shows, the peak pore pressure ratios are similar in those cases where the frequency is below 10 Hz, while the same ratio climbs to a much higher value for the case of 10 Hz. Another conclusion to be drawn is that the higher the loading frequency, the later the peak pore pressure appears in terms of loading cycles.

Previous studies (Jiang et al., 2010, Mortezaie and Vucetic, 2013) show that the loading frequency has minor influence on the performance of soft soil samples under cyclic loading. The tests with frequencies below 5 Hz in the current study agree well with other past studies, but when the frequency reaches 10 Hz, the sample with stone column performed differently. Despite that the stress concentration ratio remains the same, the axial strain and excess pore water pressure increase compared to the cases with low frequency. A threshold loading frequency may exist (between 5 Hz and 10 Hz) beyond which the effect of increasing frequency becomes no longer marginal, and the samples become more vulnerable to cyclic loading.

5.6.3 Effect of confining pressure

The confining pressure around the stone column in the field varies with depth; hence, investigating the effect of confining pressure on the performance of stone column under cyclic loading is necessary. With the same CSR and loading frequency, several tests were carried out under different confining pressures of 20 kPa, 50 kPa, and 80 kPa representing lateral earth pressure at depths of roughly 2m, 4m, and 7m respectively.

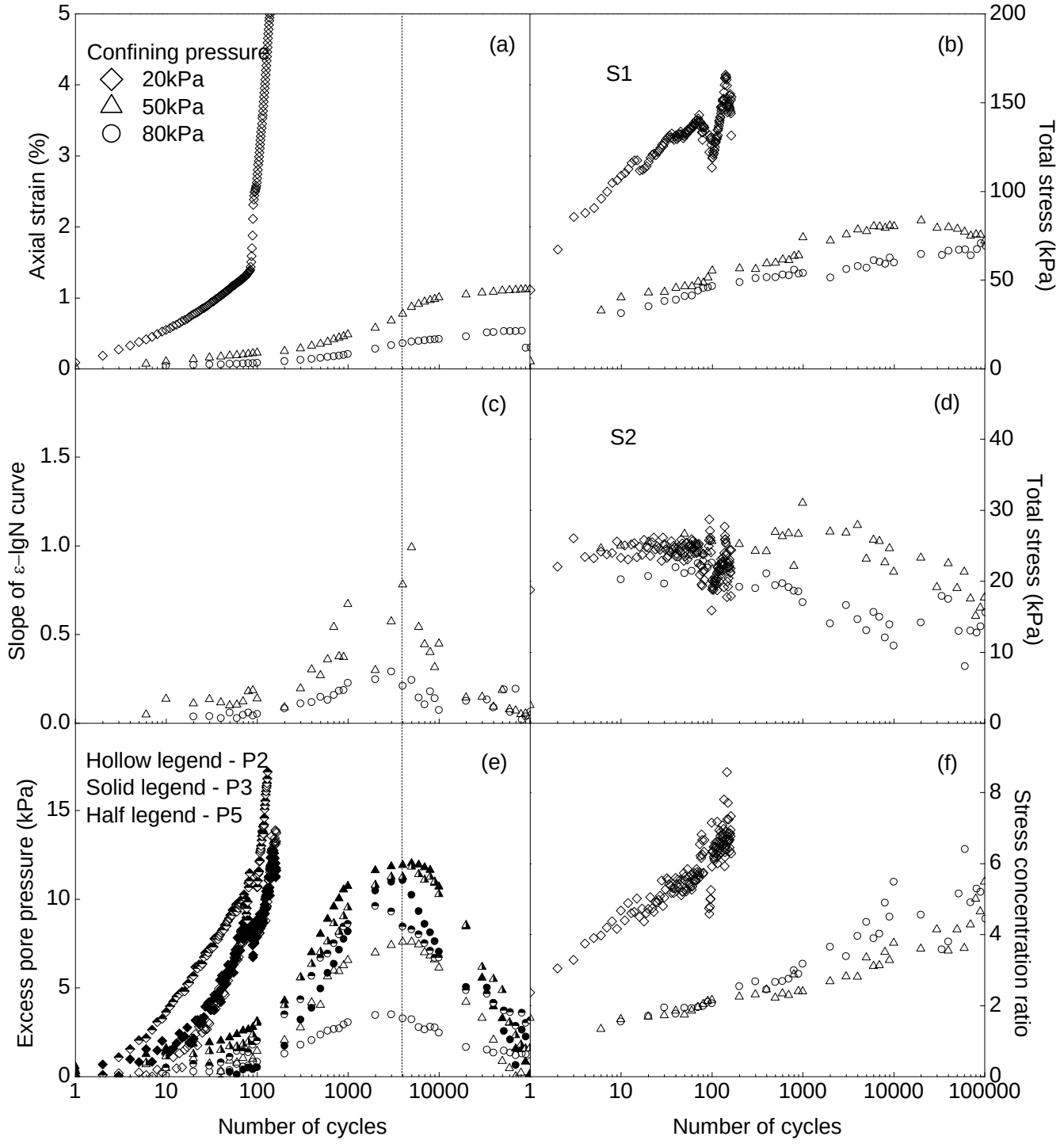

Figure 5.12 Cyclic performance of stone column under different confining pressure: (a) axial strain; (b) total stress S1; (c) slope of ε_a–logN curve; (d)total stress S2; (e) pore pressure P2, P3 and P5; (f) stress concentration ratio

The measured vertical strains (Figure 5.12(a)) reduced under a high confining pressure.

The sample failed within 100 cycles when under 20 kPa of effective cell pressure,

corresponding to a CCSR below 0.75. For confining pressure of 20 kPa, the stress on top of the column is much higher than the cases with the application of higher confining pressure, as a result of sample failure (Figure 5.12(b)). A sample under higher confining pressure would expect to increase the stiffness of surrounding clay and further reduce the stress on the column. However, the stress on top of the clay remains at the same level despite the difference in confining pressure (Figure 5.12(d)), and therefore, the stress concentration ratio is much higher (up to 9) for a lower confining pressure (Figure 5.12(f)).

The data from pore pressure sensors P2, P3, and P5 are shown in Figure 5.12(e); note that the same cyclic loading under a higher confining pressure generates a lower excess pore pressure.

For the samples that did not fail, Figure 5.12(c) and (e) show that the peak excess pore water pressure appeared at the same time when the slope of axial strain rate curve (versus cycle number in log10 scale) reached the maximum.

This series of tests indicate that a stone column in the field would fail in shallow depth because the vertical stress generated from cyclic loading decreases with depth while the confining pressure increases with depth. Therefore, in the design stage, it is crucial to consider the necessity to reinforce the shallow part of a stone column.

5.7 Performance of stone column experienced rest periods

An additional test with multi-stage cyclic loading, C18, was also carried out, such that at each stage the sample experienced a cyclic loading of 10^5 cycles. The cyclic deviator stress gradually increased from 30 kPa to 120 kPa which corresponds to CSR from 0.3

to 1.2 in four stages. There was a 24-hour period between the increases of cyclic deviator stress to dissipate the accumulated pore pressure.

A comparison between the previous individual tests (C2-C5) and this consecutive test is presented in Figure 5.13. It is shown that the vertical strain induced by cyclic loading after a rest period is much lower than the vertical strain of a sample which has never experienced cyclic loading under the same cyclic loading. According to the previous section, the critical CSR should be between 0.7 and 0.8, but even a CSR of 1.2 could not fail the sample in the consecutive test. It seems the strength of the sample was increased by the previous loading and rest period, which will be an advantage if stone columns are used to enhance the foundation of transportation infrastructure because the stability of foundation can be enhanced after experiencing traffic loadings followed by rest periods.

The total stresses on top of the sample are similar compared to the samples loaded with no rest period (Figure 5.13(b) (d)), whereas the comparison in Figure 5.13(f) indicates that if failure happens, relatively heavier stress will tend to concentrate on the column. Moreover, the magnitude of excess pore water pressure decreases due to consolidation during the rest period after cyclic loading, as shown by the response of selected Sensor P2 in Figure 5.13(e). Furthermore, the accumulation of excess pore water pressure is also delayed after previous cyclic loading. Also, through the comparison between Figure 5.13(c) and (e), the relationship between peak excess pore pressure and maximum slope of axial strain curve seems to be validated as well for the case where rest periods were included.

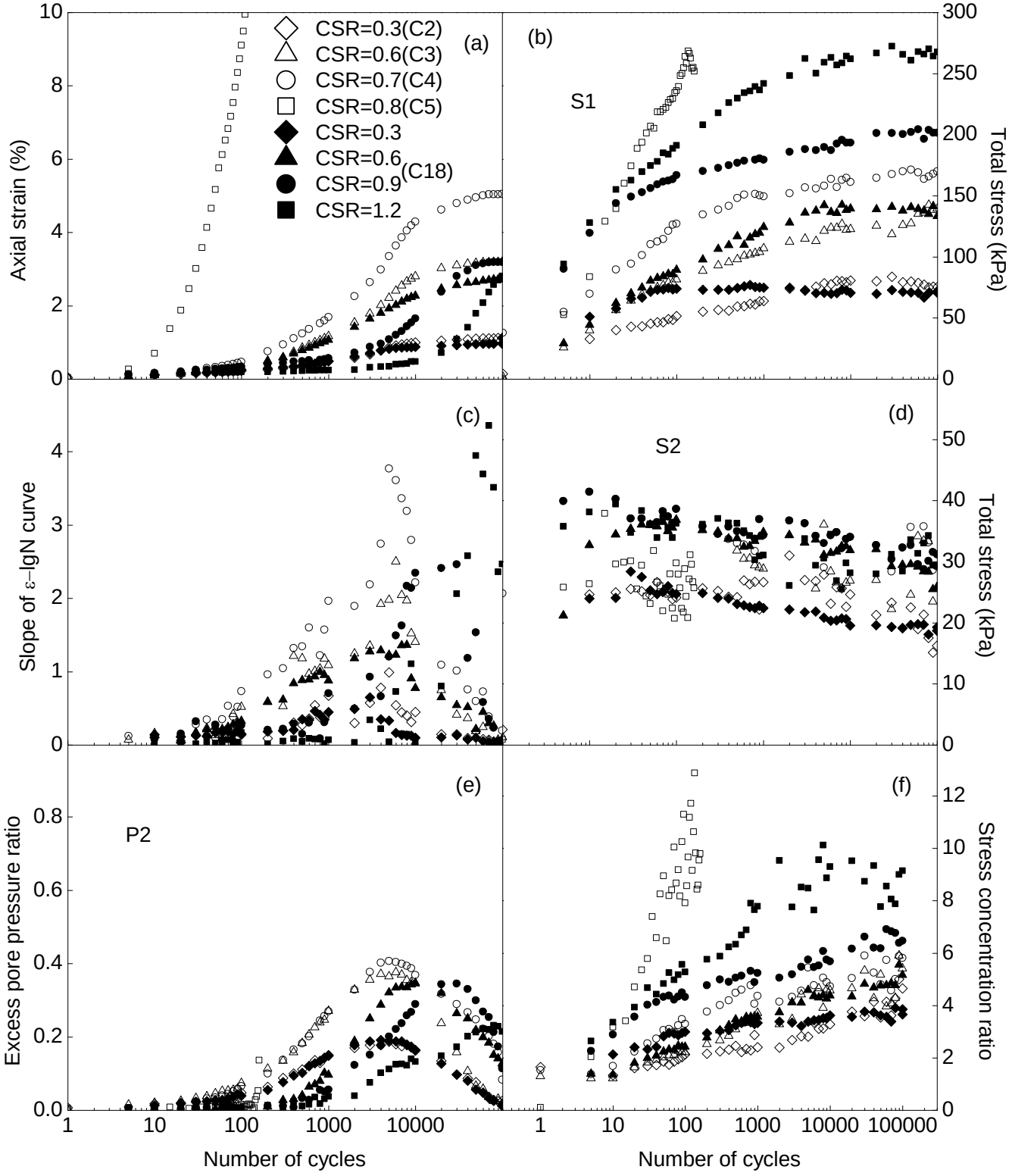

Figure 5.13 Effect of rest periods: (a) axial strain; (b) total stress S1; (c) slope of ε_a−logN curve; (d) total stress S2; (e) pore pressure P2; (d) stress concentration ratio

The phenomenon mentioned above occurs because the sample behaves like an "over-consolidated" soil such that the column is also densified and the void ratio of surrounding clay decreases compared to the sample that experienced no loading. As a result, the sample becomes stiffer and can bear higher vertical stress. When a new sequence of cyclic loading begins, negative pore water pressure and dilatancy may be observed due to "over-consolidated" nature of the samples, and therefore the corresponding axial strain and excess pore water pressure may become smaller.

5.8 Critical cyclic stress ratio (CCSR)

The critical cyclic stress ratio (CCSR) is defined as a CSR where the sample starts to experience failure. For a particular soil, it could vary due to the change of the loading frequency, confining pressure, initial deviator stress, drainage conditions and so on.

As stated in Section 5.6.1, the CCSR is between 0.7-0.8 for a loading frequency of 5Hz and confining pressure of 50kPa.

Tests C7-C9 indicate that for a loading frequency of 1Hz and confining pressure of 50kPa, the CCSR remains between 0.6-0.8 and the corresponding axial strain for are shown in Figure 5.14(a).

For a loading frequency of 10Hz and confining pressure of 50kPa, the CCSR is between 0.6-0.8, as indicated by Tests C10-C12. The axial strain response is presented in Figure 5.14(b) below, but unfortunately the response of total stress sensors and pore pressure sensors in test C11 did not give much useful information due to unexpected and excessive reading noise.

When the frequency is in the range of 1-10Hz, its effect on CCSR is almost negligible, and the resulting critical CSR is between 0.6-0.8.

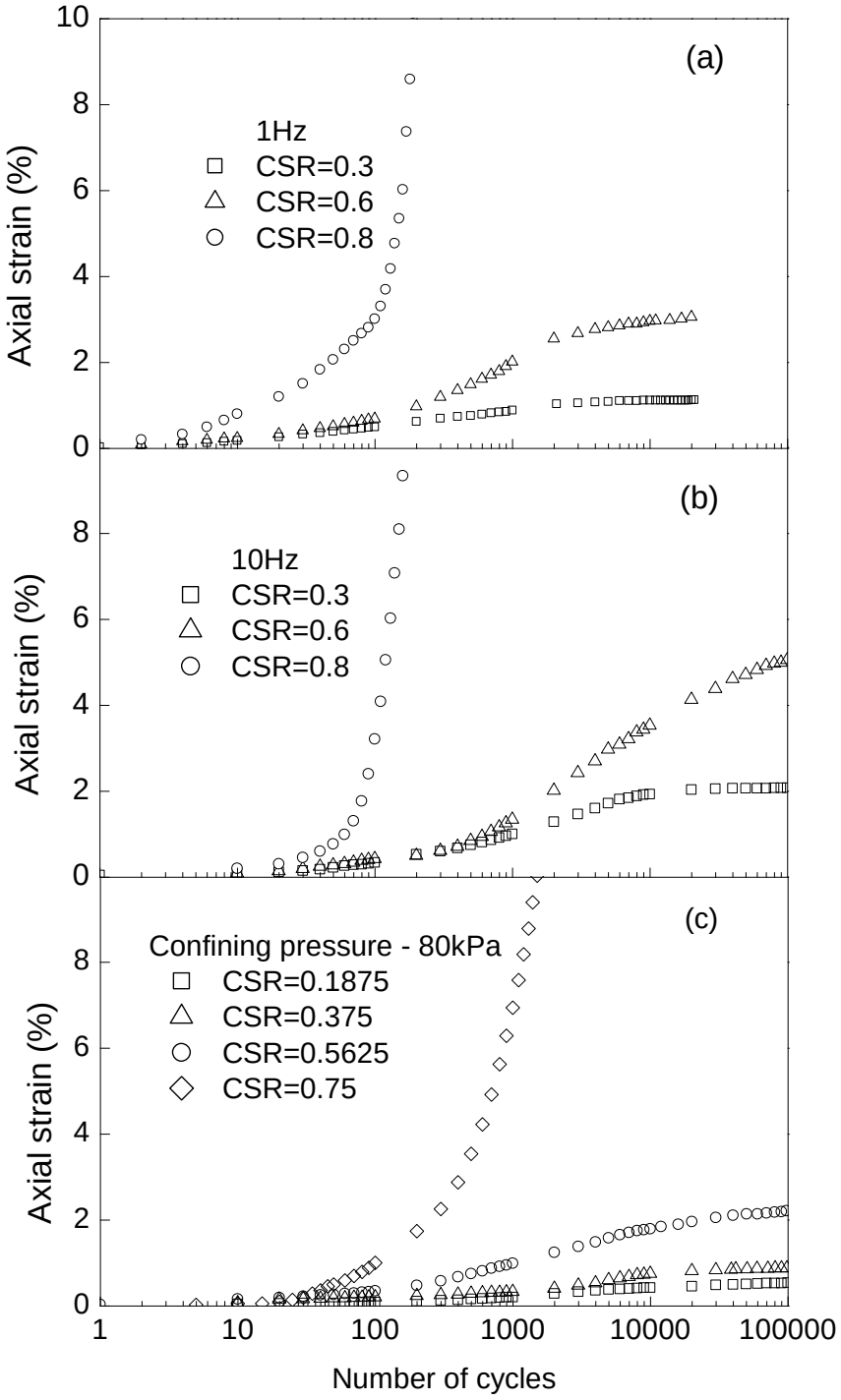

Figure 5.14 Effect of CSR on performance of stone column: (a) under 1Hz cyclic loading; (b) under 10Hz cyclic loading; (c) under 80kPa confining pressure

Test C13 (CSR of 0.75) indicates that for a confining pressure of 20kPa and loading frequency of 5Hz, the axial strain of the model sample failed within 1000 cycles. Another test C1 (CSR of 0.46) had the same loading frequency (5 Hz) but larger

confining pressure (24 kPa) and the sample survived after 10^5 cycles of loading. It appears that the CCSR under 20 kPa confining pressure is between 0.46 and 0.75.

When the confining pressure increased to 80 kPa and the loading frequency remained at 5 Hz (C14-C17), the cyclic deviator stress is varied from 30 kPa to 120 kPa (corresponding to CSR from 0.1875 to 0.75) to find a CCSR value, as interpreted in Figure 5.14(c); this showed that the critical CSR under 80kPa confining pressure is between 0.56 and 0.75.

For model tests with different confining pressures varying from 20kPa to 80kPa, it shows that the CCSR value lies between roughly 0.5 and 0.8. Therefore, based on all model tests conducted in this section, the CCSR has an upper limit value of 0.8 for a single column surrounded by kaolin clay. It is suggested that more tests would be needed to support this conclusion.

5.9 Relation between peak excess pore water pressure and maximum slope of axial strain curve

As mentioned earlier in Section 5.6.1, the number of cycles which correspond to peak excess pore pressure coincides with the number of cycles where the peak axial strain slope appears in a logarithm scale. The results of all stable tests were listed in Table 5.3 to verify this finding.

Since the peak excess pore pressure responses from different sensors did not emerge at the same time, the average number of cycles for peak excess pore pressure is used to represent each test. The results in Figure 5.15 show that the peak excess pore water pressure and maximum slope of axial strain curve (in log scale) always appear at the same number of cycles, and all the tests landed closely on the 1:1 line. This relationship

is independent of the CSR ratio, the confining pressure, the loading frequency, or the rest period. It also suggests that the generation of excess pore water pressure is related to the rate at which the tested samples deformed during the partially drained test.

Table 5.3 Peak excess pore pressure versus peak strain slope (log10 scale)

Test No.	$\overline{N}$ - peak r_u	N - peak strain slope (log10)	Test details (frequency-CSR- cell pressure)
C1	3750	4000	5 Hz - 0.458 - 24 kPa
C2	4500	5000	5 Hz - 0.3 - 50 kPa
C3	6000	6000	5 Hz - 0.6 - 50 kPa
C4	5000	5000	5 Hz - 0.7 – 50 kPa
C6	230	300	0.1 Hz - 0.3 – 50 kPa
C7	950	1000	1 Hz - 0.3 - 50 kPa
C8	1667	1000	1 Hz - 0.6 – 50 kPa
C10	6750	6000	10 Hz - 0.3 - 50 kPa
C11	3000	2000	10 Hz - 0.6 – 50 kPa
C14	2500	3000	5 Hz - 0.1875 - 80 kPa
C15	4750	5000	5 Hz - 0.375 – 80 kPa
C16	6500	6000	5 Hz - 0.5625 - 80 kPa
C18-1	4333	4000	5 Hz - 0.3 – 50 kPa
C18-2	9000	8000	5 Hz - 0.6 - 50 kPa (after C18-1)
C18-3	30000	30000	5 Hz - 0.9 – 50 kPa (after C18-2)
C18-4	70000	70000	5 Hz - 1.2 - 50 kPa (after C18-3)

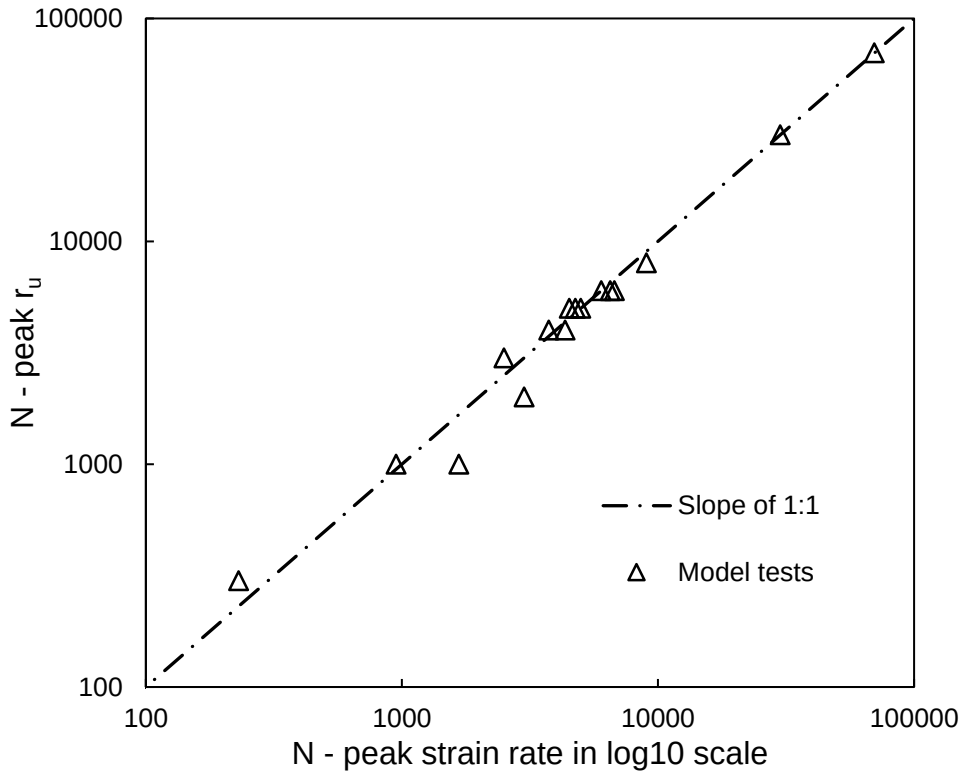

Figure 5.15 Relation between peak excess pore water pressure and peak axial strain slope

These model tests were conducted with top drainage open, but there was excess pore water pressure accumulated due to the low permeability of kaolin clay. The excess pore water pressure can be divided into two parts, transient pore pressure and additional pore pressure (also known as residual pore pressure). During a cycle of loading, the transient pore pressure follows the change of applied loading, and the pore water pressure should disappear if there is no volumetric strain happens. However, the vertical strain did happen in these tests, so there will be additional positive pore pressure generated to resist compression. At the end of each cycle, the loading as well as the transient pore pressure comes to zero, but the additional pore pressure related to deformation remains. This additional pore pressure is closely related to the deformation rate, for example, if the frequency of cyclic loading is low enough, then the model tests becomes totally drained, there will be no excess pore water pressure generated.

5.10 Summary

In this chapter, a series of model tests where a stone column and its surrounding clay were subjected to cyclic loading was presented. After a similarity analysis, these model tests were designed so that the essential dimensionless parameters stay in the range of typical values of field stone columns. During each model test, several miniature sensors were installed at various locations to record the changes of total stress and pore water pressure in specific positions.

The results of two model tests under same circumstances were compared; the comparison showed that the procedure used has good repeatability. Regarding stress on top of the unit cell, the stress on top of the column increased with the number of cycles while the stress on the surrounding clay decreased slightly; the stress concentration gradually increased within the range of 2 to 6. This observation agrees with the statement made by Han and Ye (2001). The excess pore water pressure generated by cyclic loading increased with depth as well as the distance to the column, and there was no build-up of pore pressure inside the model stone column.

The potential for using stone columns to improve foundations under cyclic loading was observed, and the results were compared with previous tests where the ground was either unimproved or improved with PVD (Indraratna et al. 2009). The comparison indicated that stone column reduces the settlement considerably compared to the original ground and ground improved with PVD. Moreover, the stone column also serves well as drainage to prevent excess pore water pressure from accumulating.

The factors which affect the performance of ground improved by stone column under cyclic loading were also investigated, including CSR, loading frequency, and confining pressure.

There is a CCSR value beyond which a sample would quickly fail. The CCSR in the current tests has an upper limit of 0.8; the stress on top of the column increases as the CSR increases, while the stress on top of the clay remains the same; the peak excess pore water pressure also increases as the CSR increases.

When the loading frequency is less than 5Hz, there is a slight change in settlement or other sensor readings if plotted in the time domain. While this finding agrees with previous studies (Jiang et al., 2010; Mortezaie and Vucetic, 2013), it also shows that when the frequency increases to 10Hz, the axial strain (settlement) and the excess pore water pressure increases considerably compared to tests at low frequency.

The tests under varying confining pressure show that settlement would increase and more excess pore water pressure would accumulate if the confining pressure decreases; in practice, this indicates that possibility of shallow failure needed to be considered.

The individual loading tests were compared to a consecutively loading test with rest period under the same loading. The sample was densified and behaves as a kind of "overconsolidated" soil after experiencing loading and rest period. Compared to individual loading test, the final vertical strain becomes smaller; the CCSR value also increases; the emergence of peak pore pressure also delayed.

Finally, in those tests which failed under a low number of cycles, it may be inappropriate to treat an abrupt rise of excess pore water pressure as an indication of failure because there may be a time lag. If plotting the results of all the model tests that were stable after cyclic loading, then the number of cycles corresponding to the peak excess pore water pressure always matches the number of cycles when the peak slope of axial strain curve (versus cycles in log10 scale) appears. It means that there is a

relationship between generating excess pore water pressure and accumulating deformation, both of which need more tests so they can be verified and clarified.

Chapter 6 Performance of an Embankment Built on Soft Soil Improved by Stone Columns

6.1 General information

There is some concern when building infrastructure over natural soft estuarine along coastlines worldwide because it usually has a low undrained shear strength and high compressibility, and usually consists of organic matter, expansive minerals, pore fluid with electrolytes, as well as weak cementation (Pineda et al., 2016). A proper understanding of the mechanical behaviour of estuarine clays is challenging for both laboratory and in situ-tests. Spatial variation and complexity of geotechnical properties could cause significant problems for future infrastructure projects such as highways. For example, Kelly et al. (2017) reported that during the construction of a motorway near Ballina, Australia, "up to 6.4 m of embankment settlement had occurred over a period of 3 years during construction (maximum 14m high fill) and accurate predictions of settlement, time rate of settlement and lateral soil movements had proved to be difficult". It is also why full-scale tests, although expensive, can be beneficial at verifying the results of soil properties obtained from laboratory and in-situ tests as well as providing extra confidence for the serviceability and safety of geotechnical structures.

Since the Pacific Highway upgrade project between Sydney and Brisbane commenced, approximately 150 km of the motorway has been constructed around the Ballina area, of which 25 km passes through areas of soft soil (Kelly et al., 2017). To help industry improve their design of transport infrastructure on natural soft soil deposits, the Australian Research Council Centre of Excellence for Geotechnical Science and

Engineering (CGSE) established a field testing facility which enables high-quality in-situ testing and monitoring to take place at Ballina.

This field test facility is located north-west of Ballina, as shown in Figure 6.1, on a 6.5-hectare site that was previously part of a sugar cane plantation. The extensive field investigations carried out by Ballina Bypass Alliance revealed the geological setting, geomorphology, and ground conditions (Bishop, 2004). Notably, it was mentioned that there was a soft clay layer with a thickness of more than 10 m underlying most of this test site.

Figure 6.1 Image of the site of Ballina field testing facility (source: https://www.google.com.au/maps)

A linkage project under the auspices of the Australian Research Council was initiated by the Centre for Geomechanics and Railway Engineering of UOW and the Centre for Geotechnical and Material Modelling (UON) to study the field behaviour of soft ground with stone columns installed. In collaboration with an industry partner (Keller Ground Engineering), a group of stone columns were installed in mid-2012 at the south-western corner of the site, adjacent to Flathead Lane, as highlighted by the white rectangle in Figure 6.1. Construction of the embankment was overseen by Dr. Sudip Basack (a former UOW research fellow), while the collection and processing of field data were carried out by the author of this thesis.

6.2 Site conditions

It was stated by Kelly et al. (2017) that the ground surface at this site is even, and its altitude is at 0.5 m Australian height datum (AHD), but the ground level at the northern and eastern part of the site is slightly lower and at 0.3 m AHD.

The geological profile of sediment at Ballina site was given by Bishop (2004), who identified three distinct stages of Quaternary deposition based on an in-situ investigation using core samples. There are different stages being distinguished from the sediment facies which are separated by oxidisation zones and hardened clay. Stage-1 contains 1-2 metre thick dense, sandy gravels deposited to form some deeper channels, beyond which there may be some stiff clay. On top of Stage-1, there are sediments overlying from Stage-2, on top of which are deposits from Stage-3. Both Stage-2 and Stage-3 consist of gravel and sandy-clays at lower levels and dark shelly muds at the upper levels.

Two embankments were built at the National Soft Soil Field Testing Facility (NFTF) to monitor the performance of soft soil improved with prefabricated vertical drains (PVD).

The characteristics of soil under those embankments were studied through in-situ and laboratory tests on tube samples (Pineda et al., 2016). The layout is shown in Figure 6.2 below, where two 13-metre-deep boreholes marked as Inclo-2 and Mex-9 were drilled for sampling, and the location of a CPT test (CPT6) which is close to the current test embankment over stone columns was also marked. Samples of soil from those two boreholes were used to detect the in-situ soil properties, while the results of CPT tests help to interpret the profile of the soil stratum.

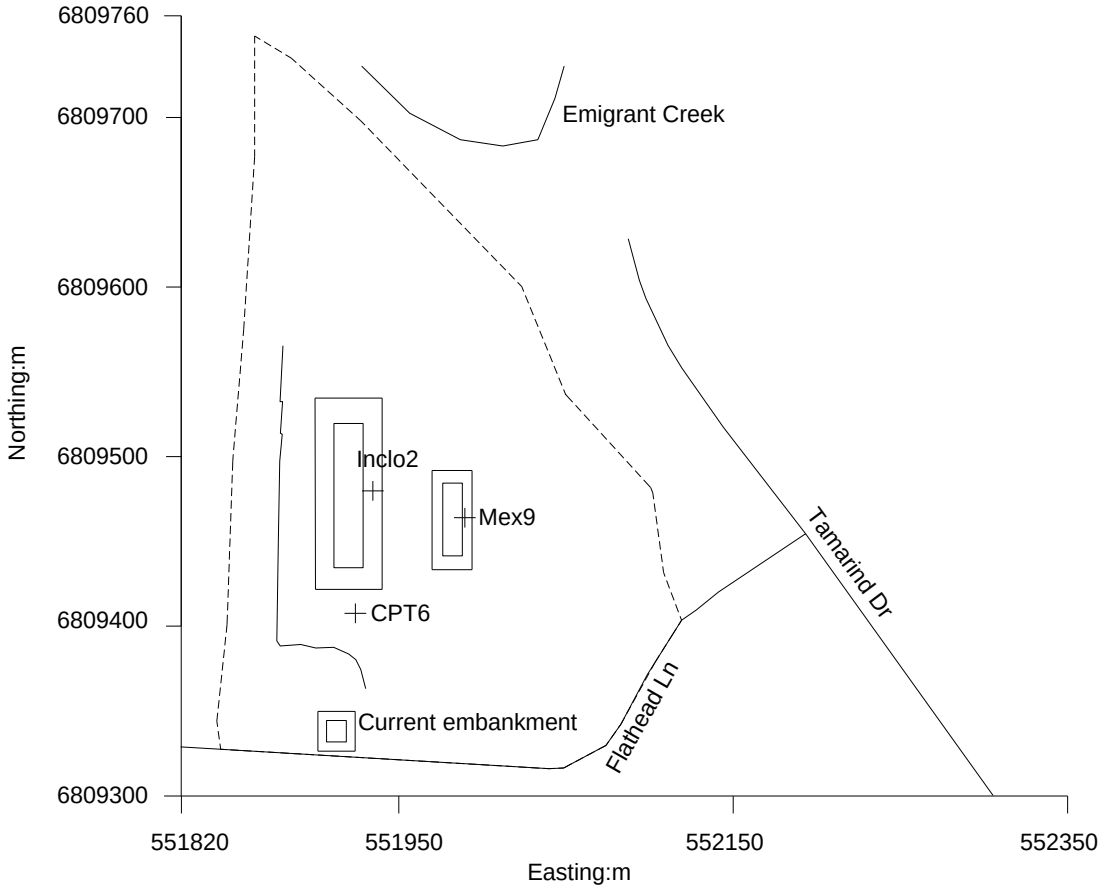

Figure 6.2 Plan-view of test facilities in Ballina site

Another CPT test was also carried out under the current embankment; the variation of undrained shear strength with depth is given in Figure 6.3, which is joined by the results of CPT6 as reported by Kelly et al. (2017).

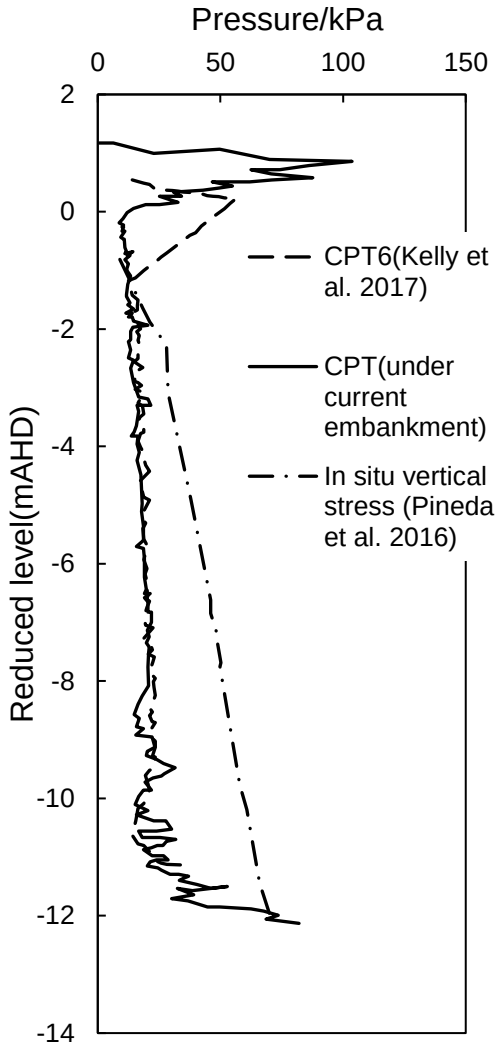

Figure 6.3 Undrained shear strength profile based on CPT tests and in-situ vertical stress

A comparison between these two tests shows good agreement, which indicates that the stratigraphy is quite consistent around the area of the current embankment; this finding agrees with Kelly et al. (2017). Figure 6.3 also suggests that there is a stiff crust existing between the RL (reduced level) +1.0 m AHD and the RL -1.0 m AHD, and then a 10-metre thick layer of soft clay under the crust. Figure 6.3 also interprets the in-situ vertical stress (Pineda et al. 2016), which was calculated by measuring the bulk unit weight of soil samples from the borehole and information regarding the groundwater level.

Four vibrating wire piezometers (VWPs) were installed under the current embankment, and their initial reading indicates that the water table is near the ground surface, as shown in Figure 6.4 below; this will be explained further in the next section.

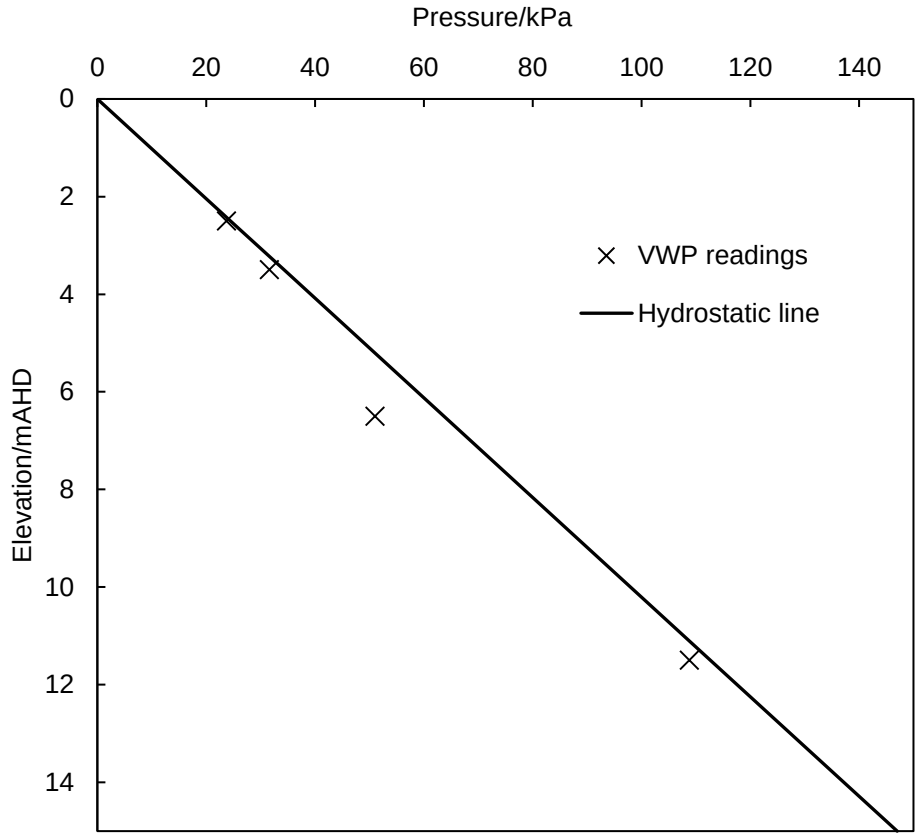

Figure 6.4 Comparison of initial VWP readings and hydrostatic line (water table assuming at ground level)

The properties of Ballina clay were found elsewhere by Pineda et al. (2016); this includes the particle size distribution, salinity of the pore water, mineralogy, organic content, soil plasticity, soil activity, and so on. Constant strain rate (CSR) oedometer tests and conventional triaxial tests were carried out to determine the constrained modulus, M, the consolidation coefficient, c_v, and the permeability, k. Some of the soil properties are shown in Table 6.1 below.

Table 6.1 Properties of Ballina clay (Pineda et al. 2016)

Borehole number	Inclo2	Mex9
Depth	2.1m-10.5m	2.8m-10m
Water content	78%-122%	81%-113%
Liquid limit	87%-128%	87%-127%
Plastic limit	32%-50%	34%-46%
Initial void ratio e_0	2.03-3.31	2.16-2.89
Dry density ρ_d (g/cm^3)	0.62-0.89	0.65-0.87
Coefficient of consolidation c_v (m^2/year)	2.5-285	4.75-23.5
Undrained shear strength s_u (kPa)	11-24	10-26
Permeability k (10^{-9}m/s)	0.65-54	0.5-4.7
Modulus M (kPa)	1140-2561	1587-3120

These saturated clays that correspond to depths of 2-10 metres can be classified as intermediate to high plasticity, and the sand content was almost negligible for the clay layer. The CRS tests by Pineda et al. (2016) also indicated that the natural structure of clay could be observed below depths of 4.5m. The natural water content of these clays approached its liquid limit.

Table 6.1 lists the fundamental characteristics of Ballina clay as having a high water content, high plasticity, low shear strength, low permeability, and high compressibility.

6.3 Test layout and instrumentation

In mid-2012, a total number of 50 stone columns were installed at BFTF in a rectangular area (20m×10m as marked in Figure 6.1), which is adjacent to Flathead Lane at the north of Ballina, NSW. The patterns of installation and the instrumentation are shown in Figure 6.5. The stone columns were installed in a square pattern (5×10) at a spacing of 2-metre. Towards the east, three sets of stone columns with diameters of 1000mm, 800mm, and 1200mm were installed.

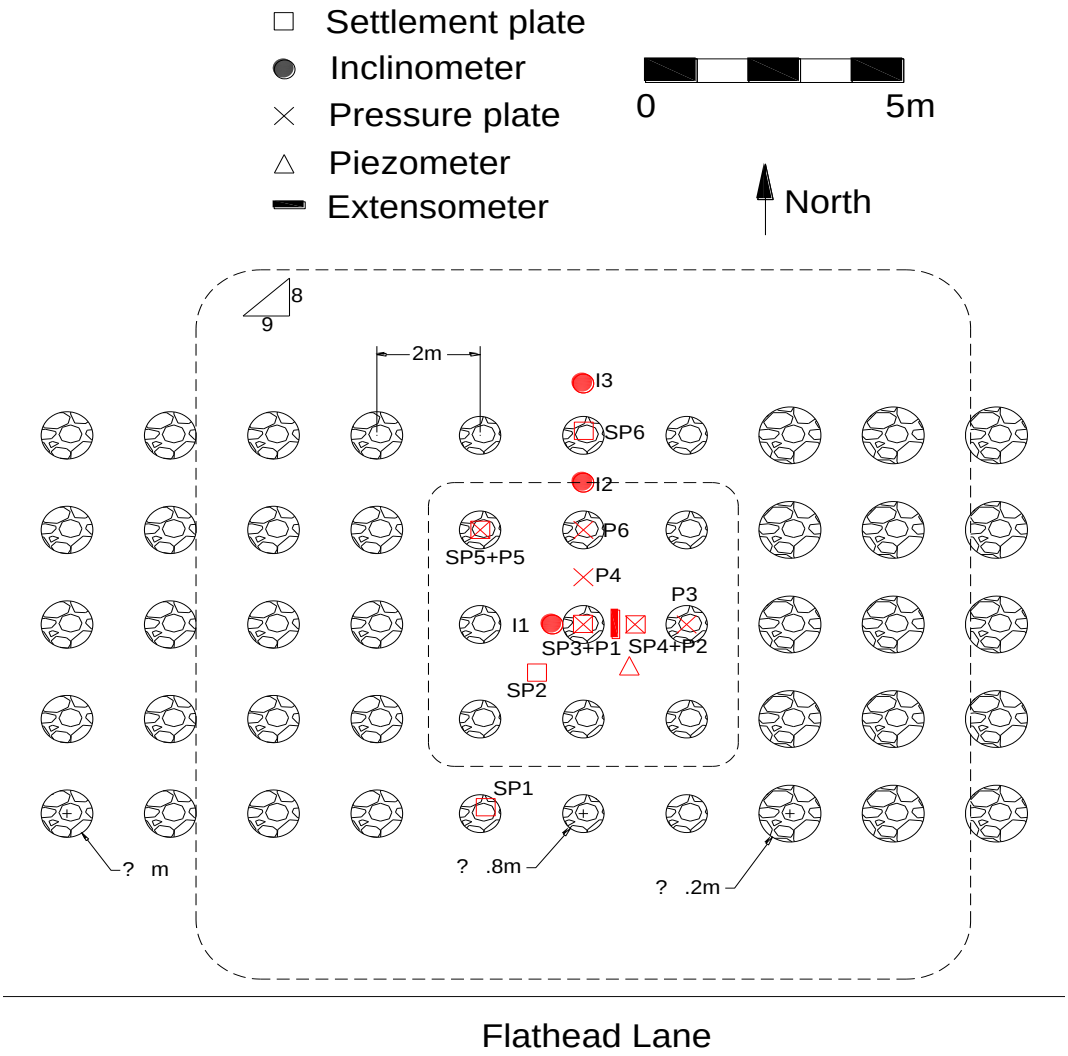

Figure 6.5 Plan view of test embankment

The gradation of material for the stone columns used in this case is given in Figure 6.6. The median diameter, *d50*, is about 22.8 mm, the coefficient of uniformity, C_u, is around 1.4 and the coefficient of curvature, C_c, is about 1.1.

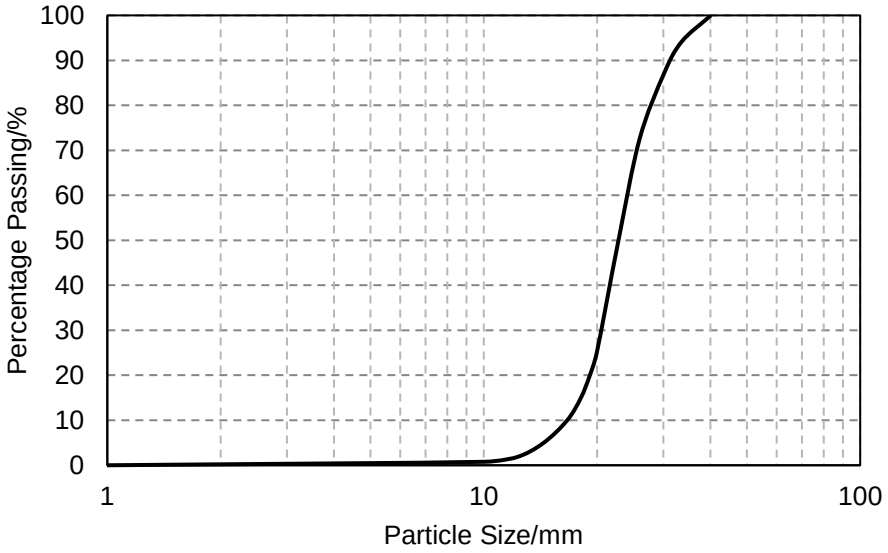

Figure 6.6 Gradation of stone column material in Ballina field

The footprint of the embankment occupied a square area (15m×15m) while the top was reduced to about 6m×6m. The embankment was 4 metres high, so the slope was 1:1.125 (8:9).

To monitor the performance of this trial embankment, an array of instruments were installed in the ground as shown in Figure 6.5, including six settlement plates, three inclinometers, six pressure cells, one magnetic probe extensometer, and four piezometers (at the same position with depths of 2.5m, 3.5m, 6m, and 10.5m).

The settlement plates were used to record the surface settlement on and between the columns at ground level. The extensometer can provide the settlement profile at different depths. The pressure cells could indicate the redistribution of embankment

pressure between the column and the surrounding soils. The piezometers were used to show the change of total water pressure.

Photos of the field before and after the construction of embankment are presented in Figure 6.7.

(a)

(b)

Figure 6.7 Photos of site: (a) before construction of embankment (courtesy of Dr. Sudip Basack); (b) after construction of embankment

The embankment was built in four stages, which lasted for totally 50 days, and the embankment loading was applied for more than six months. The starting date of construction was 24/10/2016, and the sequence of construction is presented in Figure 6.8.

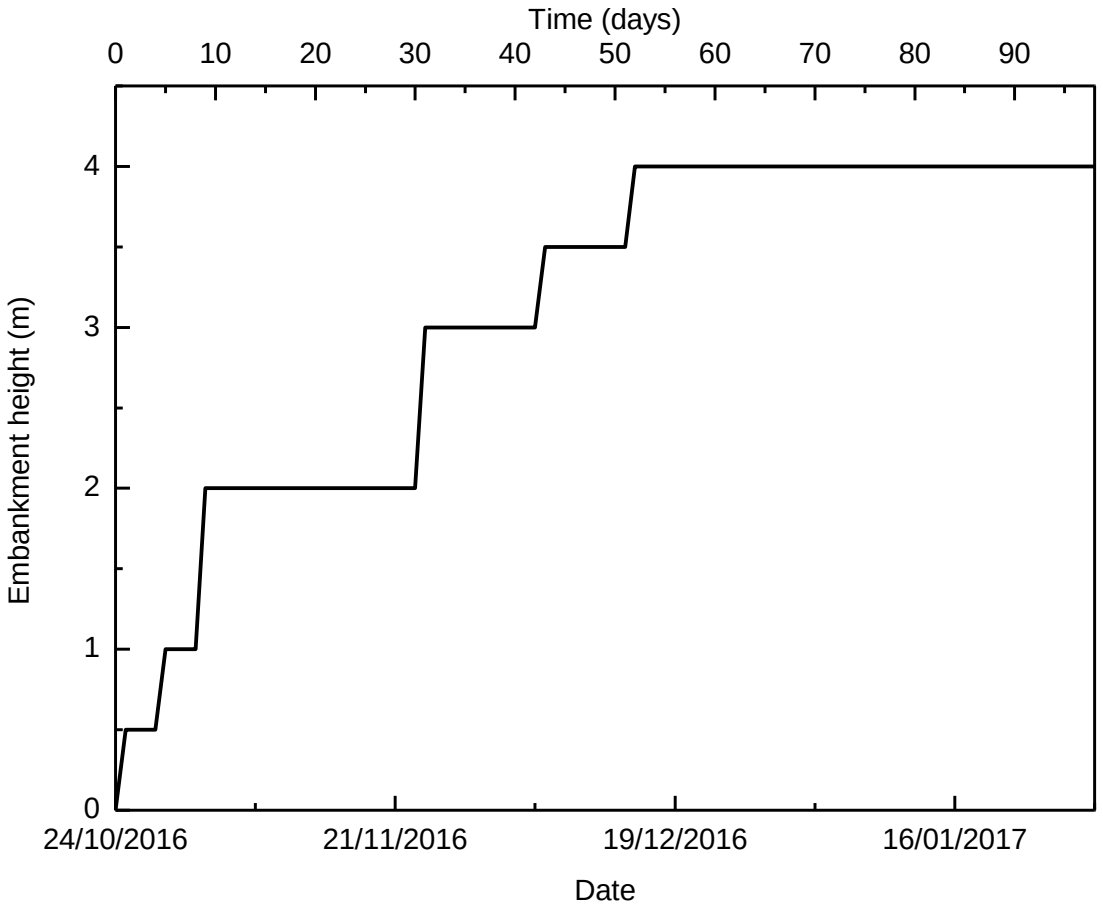

Figure 6.8 Construction sequence of embankment

The first metre of the embankment consisted of rockfill overlain with a layer of geogrid to provide more uniform distribution of stress. Subsequently, the embankment was built to its final height with local soils that can be conveniently obtained. The natural unit weight of embankment fill was between 17.5-20 kN/m^3.

6.4 Field behaviour of the embankment

The performance of the embankment was regularly monitored with an array of instrumentation; the data presented here is up until August 2017.

6.4.1 Settlement

The sets of data of settlement plates were obtained through GPS and settlement plates. The GPS reading was accurate to within 10 mm, albeit very strongly influenced by weather conditions; as a result, the GPS readings of those settlements were not always available, and the recorded data shows some fluctuations. The earliest available GPS data started at the end of November 2016. The response from all six settlement plates (Figure 6.9(a)) has a similar trend, which indicates that surface settlement was about 0.3 m to 0.4 m until August 2017. The abrupt rise in the readings was caused by extensions of the measuring pipe, which is inevitable when constructing an embankment.

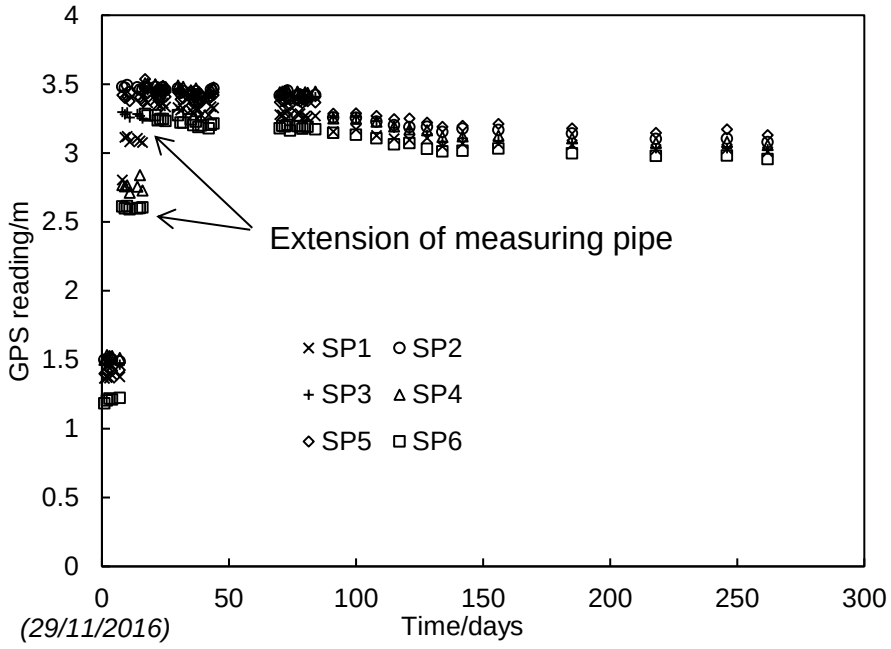

(a)

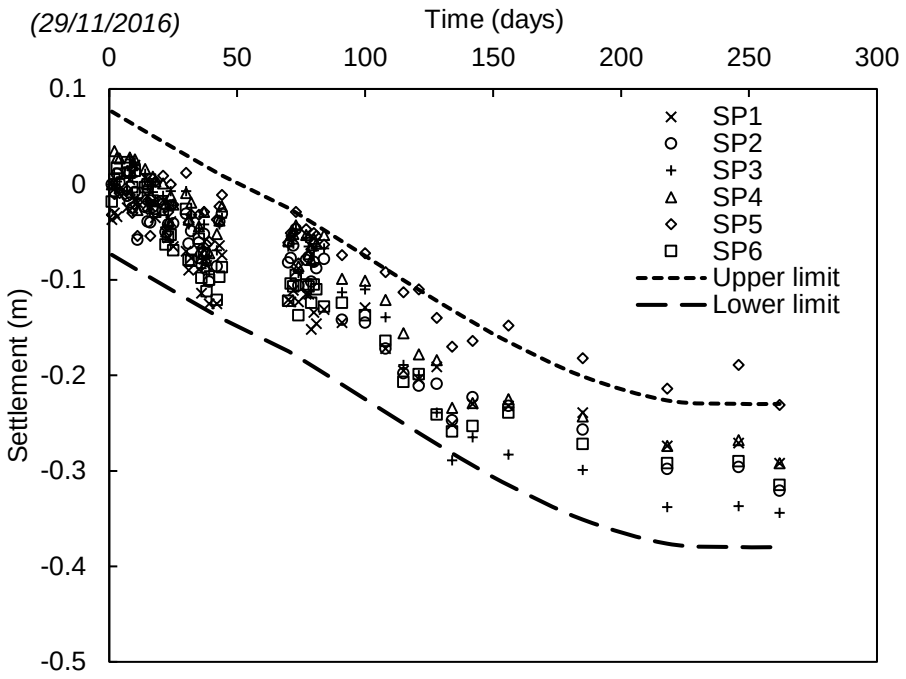

(b)

Figure 6.9 GPS readings of settlement plates: (a) raw data; (b) data after processing

The GPS data after processing in Figure 6.9(b) shows that the settlement at the ground surface was uneven. However, the data from six settlement plates can be confined in a belt zone, where the upper and lower limits are marked as shown in Figure 6.9(b). Note that the maximum differential settlement measured at the ground surface was about 0.1m.

Subsurface settlement can be obtained from the extensometer installed between SP3 and SP4. The accuracy of extensometer is typically within 2 mm. The datum was fixed at a depth of 15m below the original ground surface, and six spider magnets were set at depths of approximately 14 m, 10 m, 6 m, 5 m, 3 m, and 2 m. The data available from the extensometer began recording on 10/11/2016. It is observed that insignificant settlements were recorded at depths below 10 metres, but the datum magnet showed some slight upward displacement. If the differences caused by pipe extension are

excluded and the datum magnet is considered to be fixed, settlements at the extensometer borehole can be calculated. Figure 6.10 shows the variation of settlements with time as recorded by four magnets in the extensometer at depths of 6 m, 5 m, 3 m, and 2 m.

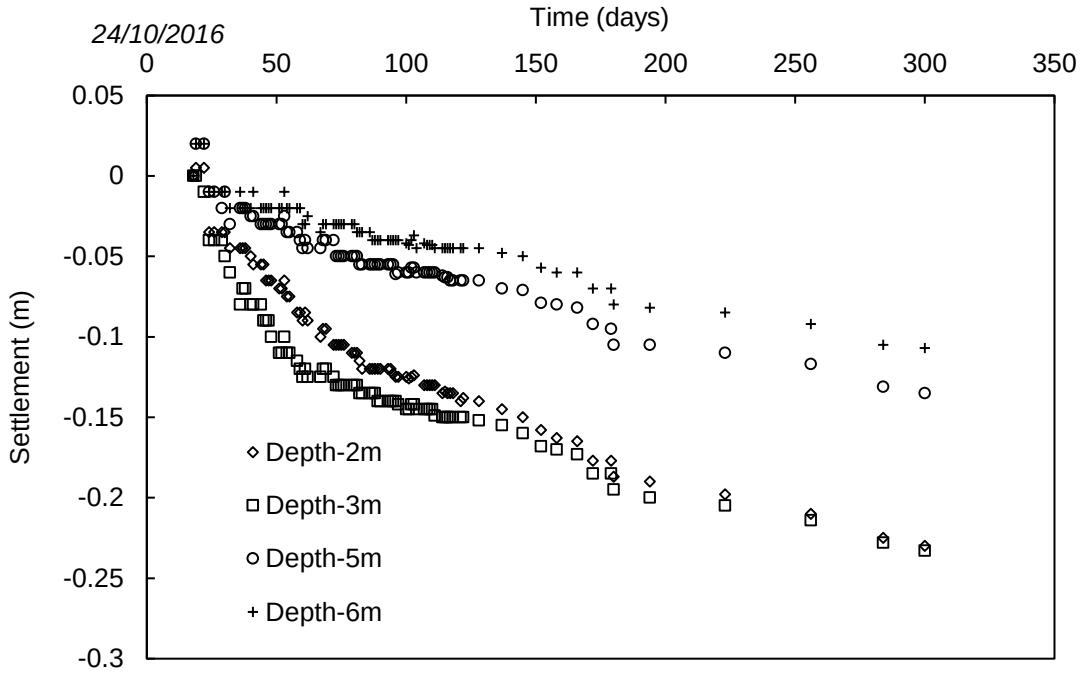

Figure 6.10 Settlement at different depths

Until August 2017, consolidation continued for 300 days, the maximum surface settlement is approximately 0.35 m, and settlement decreased with depth. At depths of 2-3 metres, the settlement was about 23 cm; at depths of 5-6 metres, it was between 10 and 13 cm.

6.4.2 Lateral deformation

The inclinometer probe has two force-balanced servo-accelerometers to measure tilt. One accelerometer measures tilt in the plane of the inclinometer wheels which is called the A-axis. The other one measures tilt in the plane perpendicular to the wheels which is

called the B-axis. An inclinometer casing was installed so that one set of grooves (the A-axis) was aligned to the expected direction of movement, which is away from the embankment centreline. When the probe was tilted in this direction, readings were positive.

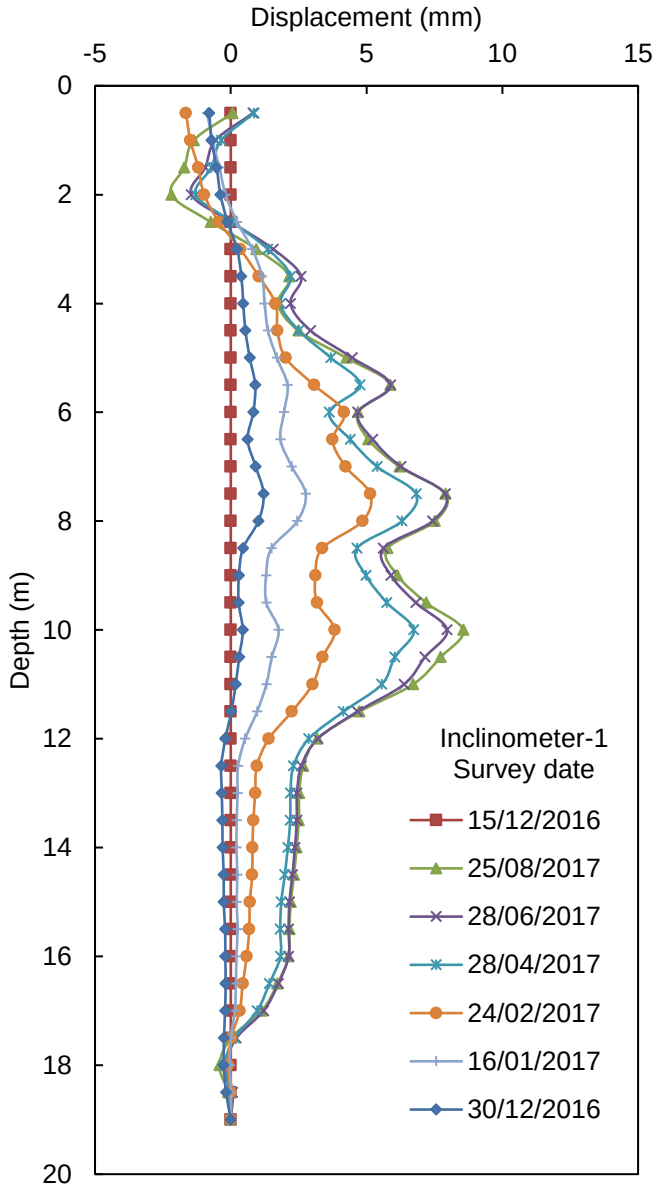

(a)

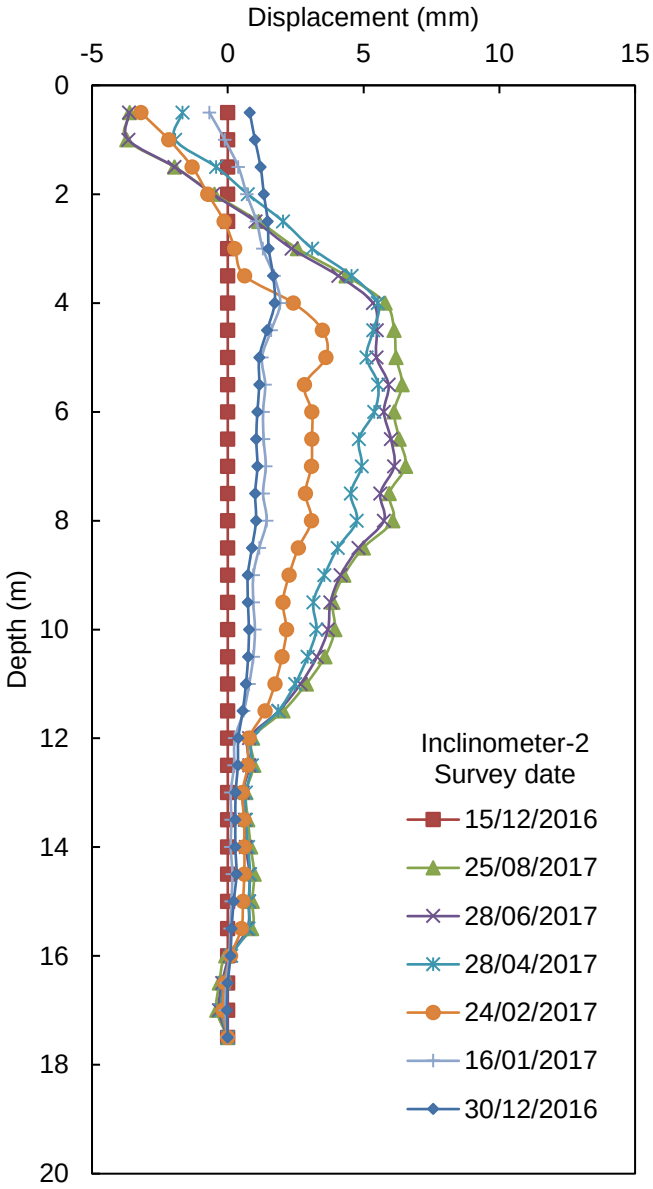
Displacement (mm)
-5
0
5
10
15
Depth (m)
0
2
4
6
8
10
12
14
16
18
20
Inclinometer-2
Survey date
15/12/2016
25/08/2017
28/06/2017
28/04/2017
24/02/2017
16/01/2017
30/12/2016

(b)

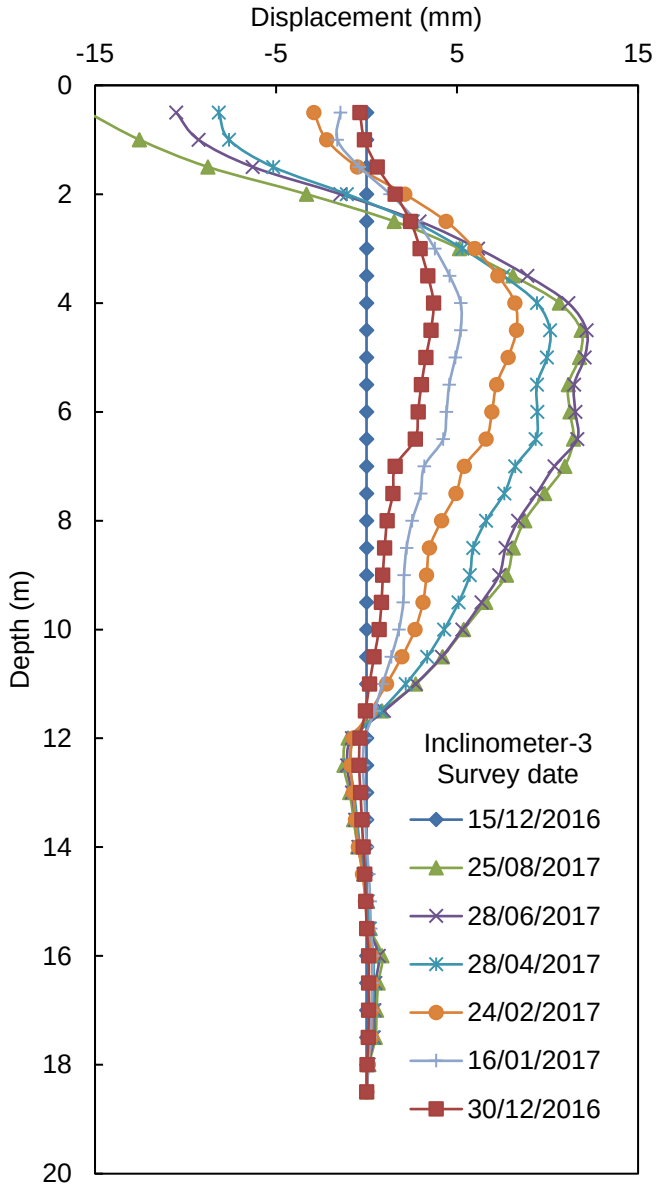

(c)

Figure 6.11 Lateral movement with depth: (a) Inclinometer-1; (b) Inclinometer-2; (c) Inclinometer-3

Figure 6.11 shows that, regardless of the locations of the inclinometers, the crust was always compacted and forces the soil to move inwards. In the layer of soft clay, because of the compression of soil and tendency of a bulged column, the movement was outwards. The magnitude of maximum lateral movement was relatively low (within 20

mm). Compared to the column diameter of 800mm, the lateral strain was less than 2%. Therefore, it is reasonable to assume that stone columns retained their original shapes without noticeable bulging.

6.4.3 Stress concentrations

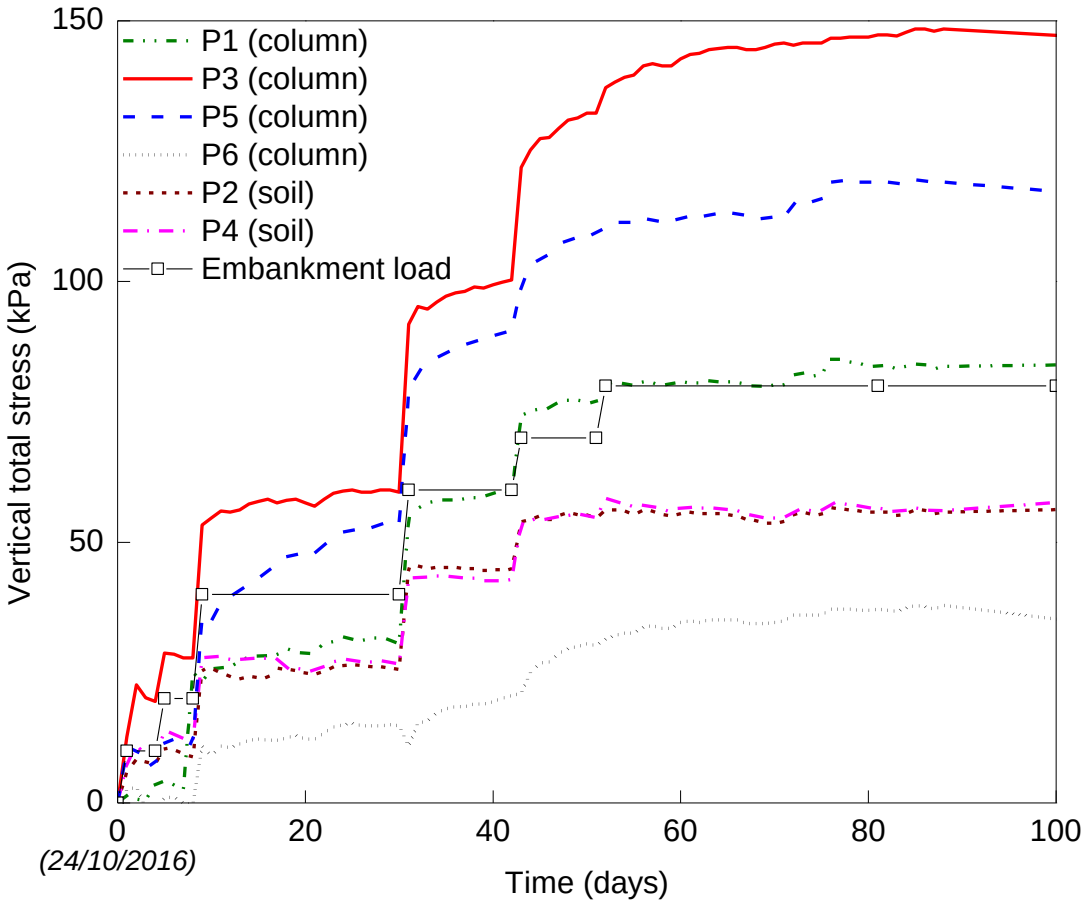

Figure 6.12 Measured total stresses at ground level

The total stress on top of the column and soil at the ground surface was monitored by six pressure cells (P1-P6), but this information was only available for the first 100 days due to sensor faulty.

The load from the 4-metre-high embankment was about 80 kPa. The change of total stress matched the sequence of embankment construction quite well. The maximum total stress on top of four columns varied from 30 kPa to 150 kPa, but the stress on top of the soil between the columns agreed with each other and finally reached 50 kPa. Moreover, the total stress on the column increased during consolidation while the stress on the surrounding soil decreased slightly. The stress concentration ratio calculated from two adjacent sensors (P2 and P3), increased from 2 to 3 during the first 100 days.

6.4.4 Excess pore water pressure

The piezometers placed at different depths recorded that less than 20 kPa of excess pore water pressure was generated by the 80 kPa embankment load; this indicated that the stone columns carried most of the embankment loading, although the pore water pressure could be influenced by evaporation and infiltration induced by rainfall.

The excess pore water pressure induced by the embankment load dissipated rapidly, which confirmed the presence of radial drainage. After 100 days the piezometer readings followed the rainfall data obtained from Bureau of Meteorology, Australian Government. Therefore, it was concluded that the excess pore water pressure had dissipated completely after March 2017.

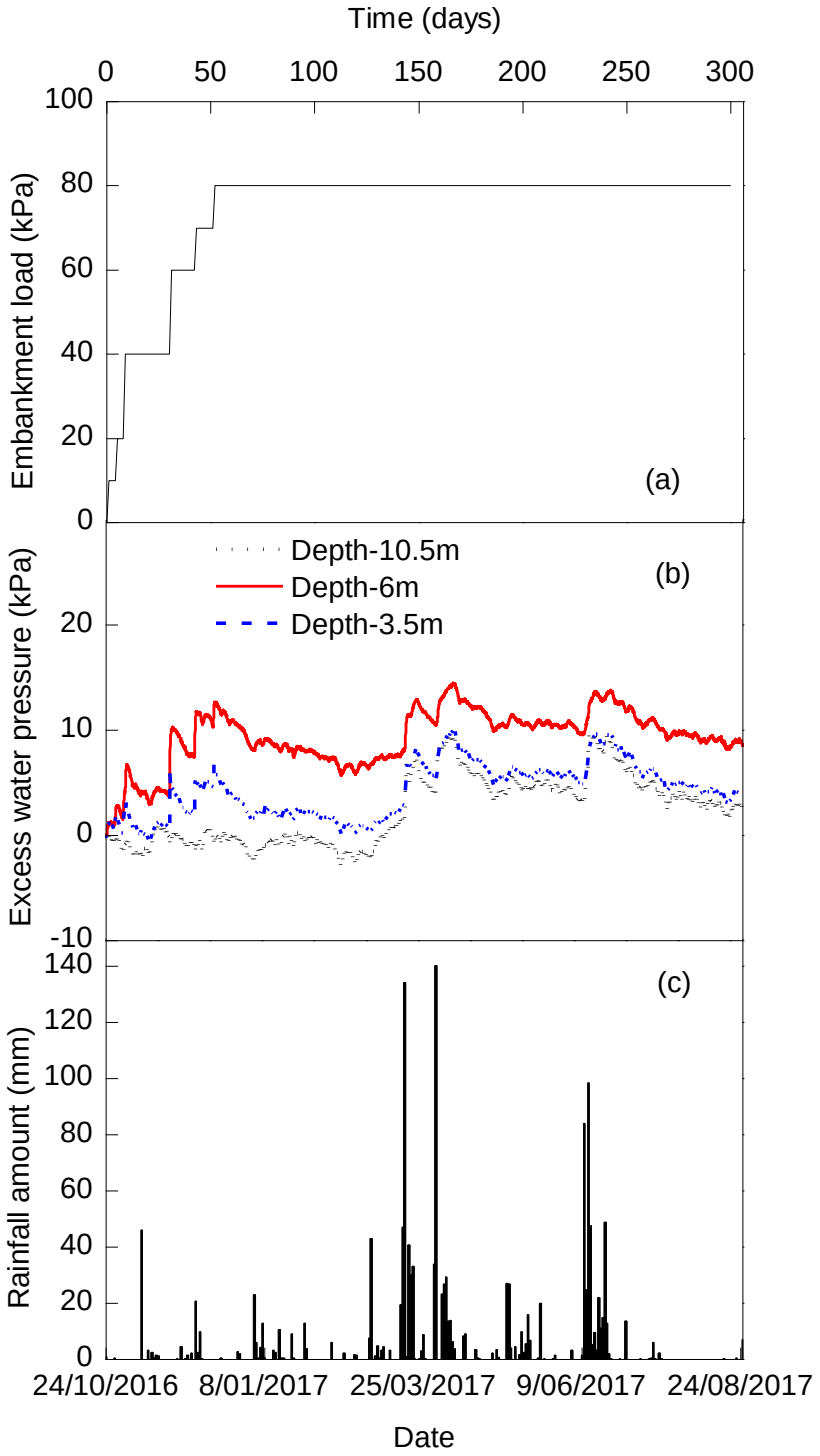

Figure 6.13 Performance of piezometers: (a) embankment load; (b) net pore water pressure; (c) rainfall in Ballina (http://www.bom.gov.au/climate/dwo/IDCJDW2006.latest.shtml)

6.5 Comparison with analytical prediction

The consolidation model proposed in Chapter 4 was used here to predict the performance of the embankment at Ballina. The necessary parameters are presented in Table 6.2 below.

Table 6.2 Parameters used in prediction of field embankment

h(m)	r_s(m)	r_c(m)	r_d/r_c	K(kPa)
10	1.13	0.4	[2]1.15	[2]2000
k_s(m/s)	k_c(m/s)	k_d/k_s	m_{vc}(MPa^{-1})	m_{vs}(MPa^{-1})
[1]10^{-9}	[1]10^{-4}	[2]0.1	[2]0.08	[1]0.67

1. assumed based on test results of Pineda et al. (2016) and Kelly et al. (2017)
2. assumed according to Han and Ye (2001), Indraratna et al. (2013)

The thickness of soft soil was assumed to be 10-metre-thick. The results correspond to the performance of the embankment along its centre. The 2-metre-spacing in a rectangular installation pattern leads to a unit cell with a radius of 1.13m (Wang, 2009).

The prediction of settlement at the ground surface is presented in Figure 6.14, which indicates that the settlement on top of the stone column, S_c, usually is smaller than that on top of the surrounding soil, S_s. The prediction at the first 50 days (start from 29/11/2016) agrees with the measurement, but then the model overestimates the consolidation rate until 150 days. The predicted settlement rate is higher than the measurement after 50 days, because the model used for prediction is simplified but the field condition is much more complicated. Several possible reasons are listed: the soil properties such as coefficient of consolidation is varied spatially while it is assumed to be uniform in the model which could be overestimated; Besides, the effect of clogging is not included in the prediction because the clogging information will be detected after

exhumation of columns, the clogging may considerably reduce the consolidation rate; the top surface is assumed to be free drainage in the model, but in the field there may be some obstruction come from the crest layer. This comparison also shows that the differences between the readings of settlement plates can be captured using this consolidation model which predicted approximately 0.09-0.1m of differential settlement for foundation stiffness of 1MPa.

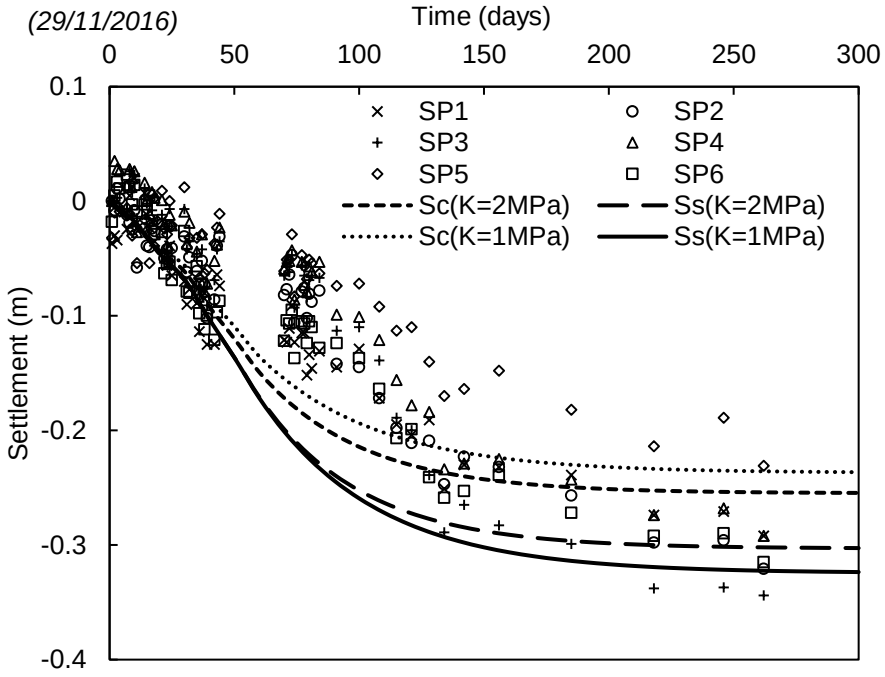

Figure 6.14 Comparison of surface settlement between measurements and predictions

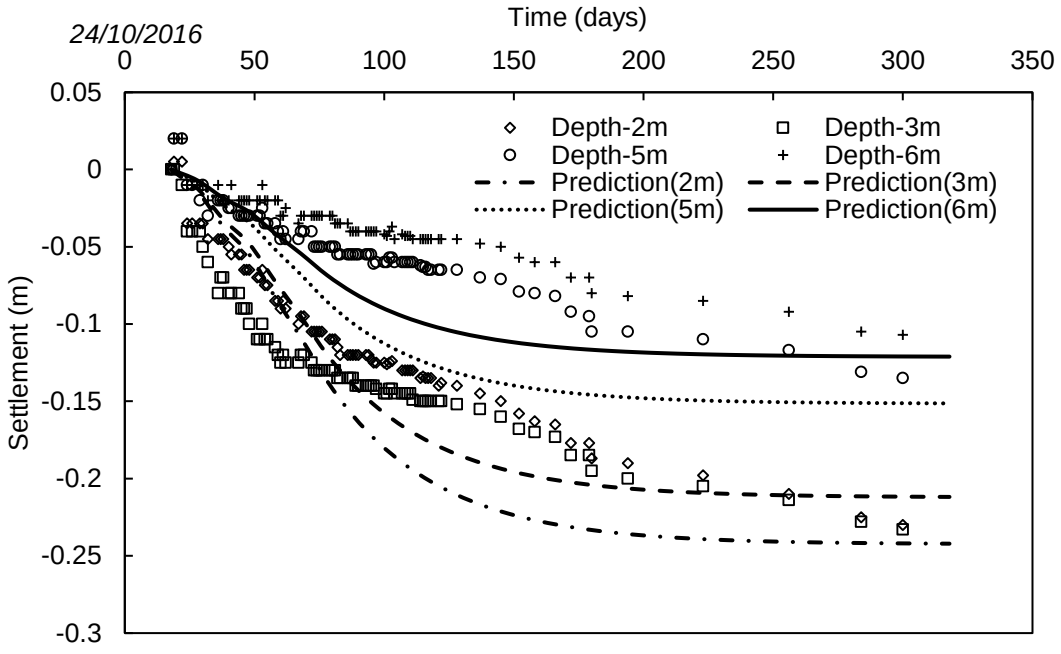

Figure 6.15 Settlement at different depths (measurements and predictions)

The settlement at different depths (obtained from the extensometer) was also calculated using the proposed model. Figure 6.15 shows that the predictions tended to overestimate settlement and the predicted settlement was faster than the measurements. This overestimation is resulted from the assumption about the uniform induced vertical stress in subgrade. In field, the vertical stress in subgrade attenuates with depth, and it could be ignored after a certain depth. However, in the model, it is assumed to always equal to the load intensity. In other words, the vertical stress is overestimated and as a result the calculated settlement becomes higher.

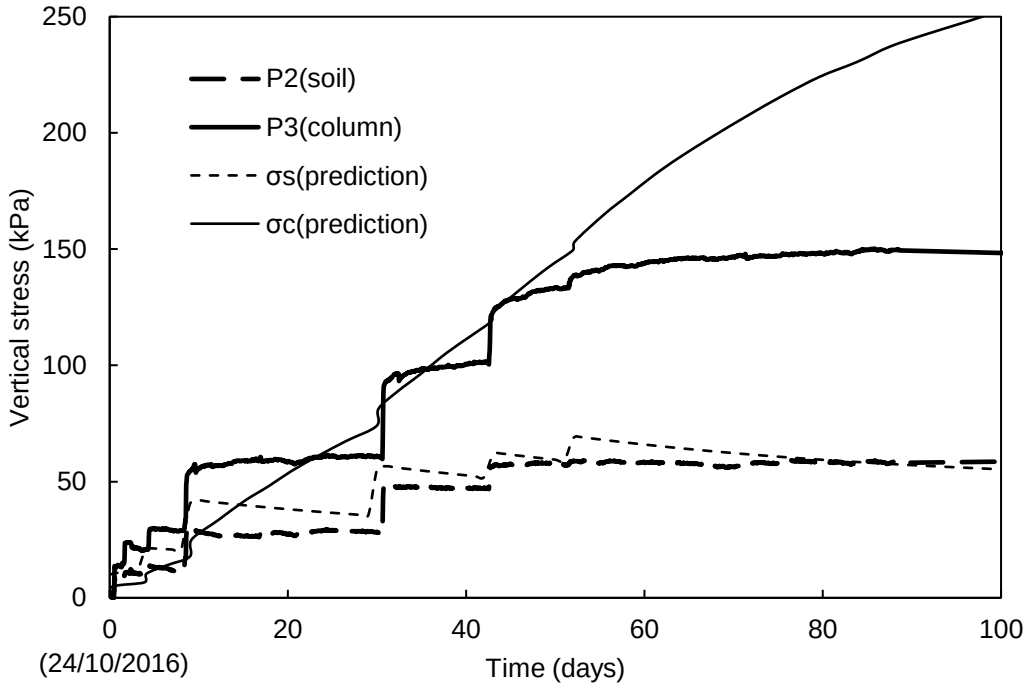

Figure 6.16 Total stress at ground level (measurement versus prediction)

Figure 6.16 shows that the total stress predicted on top of the surrounding soil was slightly higher than the readings taken by the pressure cells, but the calculation of total stress on top of the column does not capture its real behaviour. The measured total stress on top of stone column follows the construction order of embankment, but the calculated stress on the column keeps increasing after the built of embankment, the load transfer process seems to be much more in field. At about 100 days, the calculated stress on the column increased by more than 200kPa, but there is only about 150kPa been recorded in the field. A possible explanation is that the model is established based on unit cell concept, when comes to a group of stone columns, the load transfer mechanism not only depends on the consolidation process, but also on the interaction between columns (group effect).

As for the excess pore water pressure, the analytical model has the same trend as the actual variation of pore pressure in the field, but the magnitude of excess pore water

pressure in the calculation was much higher than measurements (Figure 6.17). As stated before, the vertical stress considered in analytical model is overestimated, that may be the reason why the predicted excess pore pressure is higher than the measurement. The change of excess pore pressure is captured which means the predicted consolidation process is reasonable, and as for the magnitude, the prediction could also be improved if change the basic assumption about induced vertical stress in the future.

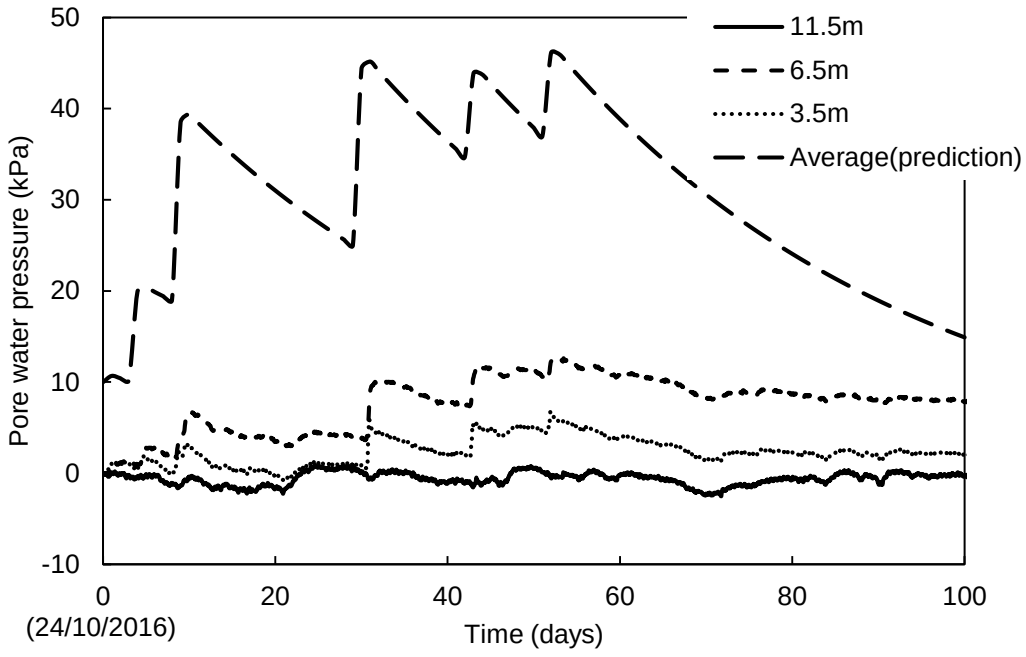

Figure 6.17 Measured and predicted excess pore pressure at different depths in surrounding soil

6.6 Summary

An embankment was built on soft ground improved with stone columns in field test facility located at Ballina, Australia. Instrumentation was set up to monitor the performance of soft ground including inclinometers, extensometer, settlement plates, pressure cells, and piezometers. The measurements show that 4-metre-high embankment leads to surface settlement of around 300 mm; the steady stress concentration ratio increased from 2 to 3; lateral deformation of stone column is within

2%; excess pore water pressure generated by embankment loads was less than 20 kPa, and its variation could be influenced by rainfall.

The predictions are also given using the consolidation model proposed in Chapter 4. A comparison between predictions and measurements shows that this analytical model can capture the development of settlement, the differential settlement at the ground surface, and the variation of total stress in the surrounding soil. The total stress predicted on top of the stone column has a significant deviation. The magnitude of excess pore water pressure predicted was more significant than the readings taken by the piezometers, but the trend of pore pressure dissipation agrees with the field measurements.

Chapter 7 Conclusions and Recommendations

7.1 General summary

The need to build transportation infrastructure carrying increased freight such as highways and heavy haul railways on marginal areas underlain by soft alluvial soil is inevitable in coastal areas. Stone columns, as one of the popular ground improvement methods, has often been used to stabilise the soft ground before the construction of transport structure, due to its ability to shorten the drainage path while increasing the overall stiffness of the ground and its load bearing capacity.

This thesis has made an attempt to deliver outcomes to better understand the long-term behaviour of stone columns under transport infrastructure in regard to the consolidation and deformation behaviour of the composite ground.

A comprehensive literature review and existing issues were presented in Chapters 1 and 2. In Chapter 3, clogging phenomenon in stone column was modelled mathematically and experimentally, and its effect on the consolidation of stone column unit cell was quantified. The influence of foundation stiffness was included in a proposed consolidation model to describe the more realistic state of consolidation which should be between “equal strain” and “free strain” condition (Chapter 4). In Chapter 5, the behaviour of soft ground improved with stone column under cyclic loading was studied via a series of laboratory model tests based on the unit cell concept. A full-scale embankment built on soft ground improved with stone columns was reported in Chapter 6 and its performance was monitored through detailed instrumentation.

7.2 Clogging in stone column

The clogging phenomenon in stone column was confirmed by Weber et al. (2010) through centrifuge tests. Although some effort has already been made to reflect the effect of clogging on consolidation (Indraratna et al. 2013, Deb and Shiyamalaa 2015), to the best of the author's knowledge, the quantification of clogging is still lacking. A model test was carried out to quantify the extent of clogging, where a unit cell including a single stone column and its surrounding soil was one-dimensionally compressed. CT scanning revealed that the clogged zone varies with depth, such that it could occupy up to 20% of the outer area of the model column at the top, and then it decreased rapidly along the column length. The porosity of the model column was calculated, and the clogging related parameters were determined.

These findings were used to develop a consolidation model to capture the effect of initial clogging and time-dependent clogging. The model was verified by comparison with existing models, but between those results with and without clogging, there was some apparent discrepancy; it appears that "no clogging" and "initial clogging" would give the upper and lower limit of predictions if this model was used to predict the response based on the concept of unit cell. Another interesting finding is that besides reducing the permeability of soil in the clogged zone, clogging could also lead to an increase in compressibility because of the intrusion of clay particles into the clean stone column. Consequently, the overall settlement may increase, compared to cases without clogging. This observation may cause some contradiction with the more commonly accepted belief or impression that clogging could normally impede the dissipation of excess pore water pressure, after which a reduced rate of soil consolidation would occur.

7.3 Between equal strain and free strain

Traditional consolidation theories of vertical drains usually follow two basic assumptions given by Barron (1948), “equal strain” and “free strain”. Equal strain means that vertical strain is homogeneous while free strain means there is no redistribution of vertical stress at the top of the unit cell. However, in practice, differential settlement and stress concentration on stone column can be compromised between those two assumptions. To capture this salient feature, a revised consolidation model for ground improved with stone column was proposed by combining the stiffness of the foundation. Shear stress is generated in the foundation layer due to differential settlement, and it can be determined by following a similar method as “trapdoor” theory (Terzaghi, 1943). With the shear resistance provided by the foundation, the distribution of stress on top of the unit cell can be updated.

The proposed model was solved using the variable separation method, and a general closed-form series solution was derived. This solution can also be converted to special solutions which correspond to either “equal strain” or “free strain” condition. The results were validated by previous studies. It shows that the degree of consolidation at the initial stage of consolidation under free strain condition is higher than that under equal strain, but the consolidation rate under equal strain condition is higher at the later stage; this observation was in accordance with a much higher initial dissipation of excess pore pressure in the column under free strain condition. More general cases between equal strain and free strain were modelled as well, and the effects of foundation stiffness on the consolidation rate, stress concentration ratio and differential settlement were studied. As the foundation stiffness increases, the consolidation rate and stress concentration ratio increase while the differential settlement decreases. The

influences of foundation stiffness under various radius ratio of the unit cell to column, the modulus ratio and permeability ratio of the column to surrounding soil were also presented. A special index is also used to indicate the influence of these factors on consolidation which is the time needed to achieve 90% of consolidation degree. The results show that this crucial time decreases as modulus ratio increases, or radius ratio decreases, or permeability ratio increases.

This model was also used to predict a 4-metre-high embankment built over soft ground improved with stone columns at Ballina, Australia. Extensive instrumentation scheme, including inclinometers, extensometer, settlement plates, pressure cells, and piezometers were set up at this embankment to monitor the variations of the settlements, pore water pressures, total stresses and lateral displacements with time. After about 300 days, the measurements indicated that: (a) the settlement at ground surface was around 300mm, and the maximum difference among the readings obtained from settlement plates was about 100mm; (b) the steady stress concentration ratio was in the range of 2 to 3; (c) the lateral displacement of stone column was within 20mm which means no notable bulging occurred; and (d) the excess pore pressure generated by embankment loads was less than 20kPa, and it flucuated considerably by the rainfall. With appropriate parameters, the proposed model could capture the behaviour of settlement at the centreline (the total and differential settlement) and the variation of total stress on top of the surrounding soil. The trend of dissipation of excess pore pressure could also be predicted very well, however, the predictions of total stress on top of the column and the magnitude of excess pore pressure were not as accurate. The difference between prediction and field measurement mainly originates from the simplification in the proposed model which cannot reflect the complicated field condition. For example, the

assumption of uniform induced vertical stress in subgrade, the homogeneous soil properties, the neglect of clogging phenomenon, and so on.

7.4 Performance of stone column under cyclic loading

If stone column is used to improve soft ground under transportation infrastructure, traffic loading can become a significant influencing factor in the performance of this composite ground. This problem was examined via a series of laboratory model tests based on the unit cell concept. These model tests were designed to maintain the important dimensionless parameters in the typical field values using similarity analysis. This series of model tests under cyclic loading was carried out under partially drained condition; miniature sensors were installed to monitor the change of total stresses on top of the sample and excess pore water pressures at different positions.

Repeatability of model tests was satisfactory, as indicated by a comparison between the results of two repeated model tests. Several patterns that were consistent in most model tests were also generalised as follows: the total stress on top of the column increased with the number of cycles while the total stress on surrounding soil decreased slightly; the stress concentration ratio was in the range of 2 to 6 during cyclic loading; the excess pore water pressure increased with depth and the distance to the column; the build-up of pore pressure in stone column was negligible because the permeability of column material was much higher than the surrounding clay.

The ability of stone column to improve soft ground under cyclic loading was examined by a comparison with similar model tests where the soft ground was either not improved or improved with PVD (Indraratna et al. 2009). This comparison showed that stone column could dissipate excess pore pressure and further reduce total settlement compared to the ground that was not improved or improved by PVD.

Several factors related to on the performance of stone column unit cell under cyclic loading were investigated through model tests, such as the cyclic stress ratio (CSR), the loading frequency, and the confining pressure.

- The peak excess pore pressure and total stress on top of the column increased as CSR increased, whereas the total stress on surrounding soil barely changes. The critical CSR is defined as a value beyond which a sample would fail rapidly in a model test. The CCSR in the current model tests had an upper limit of 0.8.
- Previous research of soft soil under cyclic loading (Jiang et al., 2010; Mortezaie and Vucetic, 2013) showed that varying the loading frequency at a low level has minor influence on the behaviour of soft soil. When the loading frequency was below 5 Hz, the current model tests agreed with this finding, and there would only be a slight change in the vertical strain, pore pressure, and total stress if plotted in the time domain. However, the settlement and peak excess pore pressure would increase considerably if the loading frequency increases to 10 Hz.
- The vertical strain and excess pore pressure decreased with an increase in the effective confining pressure; this finding also implied that the failure is likely to occur at shallow depth in the field.
- A comparison between an individual loading test and a consecutive loading test with rest periods showed that: the vertical strain under the same loading decreased due to previous loading experience; the CCSR value also increased in the consecutive test; the emergence of peak pore pressure was also delayed after a previous loading and rest period, and the sample was likely to be densified and showed “overconsolidated” behaviour.

In relation to the failed samples, the vertical strain exceeded 20% at a low number of cycles, and it was inappropriate to treat an abrupt rise in the pore pressure as a sign of imminent failure because there may be a time lag between the developments of pore pressure and vertical strain.

The results of all stable model tests indicated that the number of cycles corresponding to the peak excess pore pressure matched with the number of cycles when the peak slope of axial strain curve (versus cycle number in log10 scale).

7.5 Recommendations for future research

To extend the work presented in this thesis, future research could be undertaken in the following areas.

1. In this study, the development of clogging in stone column was based on simplified assumptions made in Chapter 3. Although the influence factors were listed, a rational mathematical description of the mechanism of time-dependent clogging is yet to be formulated. The evolution of clogging may be explained through the micro mechanics aspect, i.e. particle mitigating theory. A combination of micro study may lead to a more accurate estimation of permeability and compressibility of soil in the clogged zone.
2. As pointed out in Chapter 4, the ideal free strain condition would unlikely to occur within a unit cell due to the existence of shear resistance at the column-soil interface. If the shear stress at the interface is included, a more realistic model could be established. The calculation of the shear stress in the foundation layer in Chapter 4 is primarily simplified using the “trapdoor” theory. In the future, sophisticated arching theories may be adopted to refine the current solution.

3. The performance of stone column under cyclic loading was studied experimentally. A theoretical model that focuses on its long-term behaviour could be useful for design. To establish such a model, a theoretical or empirical equation which describes the generation of excess pore water pressure under cyclic loading is crucial. Undrained tests may be useful for establishing and calibrating a cyclic excess pore water pressure generation model. Also, through other test equipment such as large-scale physical model box or centrifuge test combined with cyclic loading actuator, the group effect should be considered, because the behaviour of stone column acting in group may be largely changed compared to unit cell tests.
4. The laboratory work could also be extended by focusing on the geometry of stone columns, such as the ratio of column length to diameter (L/d), area replacement ratio, and partially penetrating stone columns. The performance of a group of stone columns under cyclic loading could also be studied through model tests in large-scale triaxial apparatus.

Chapter 8 References

ABOSHI, H., ICHIMOTO, E., ENOKI, M. & HARADA, K. The compozer—a method to improve characteristics of soft clays by inclusion of large diameter sand columns. Proceedings of International Conference on Soil Reinforcement, 1979. 211-216.

ADALIER, K. & ELGAMAL, A. 2004. Mitigation of liquefaction and associated ground deformations by stone columns. *Engineering Geology,* 72**,** 275-291.

ADALIER, K., ELGAMAL, A., MENESES, J. & BAEZ, J. I. 2003. Stone columns as liquefaction countermeasure in non-plastic silty soils. *Soil Dynamics and Earthquake Engineering,* 23**,** 571-584.

AL-KHAFAJI, Z. A. & CRAIG, W. H. 2000. Drainage and reinforcement of soft clay tank foundation by sand columns. *Géotechnique,* 50**,** 709-713.

AL-TABBAA, A. & WOOD, D. M. 1987. Some measurements of the permeability of kaolin. *Géotechnique,* 37**,** 499-514.

ALEM, A., AHFIR, N.-D., ELKAWAFI, A. & WANG, H. 2015. Hydraulic operating conditions and particle concentration effects on physical clogging of a porous medium. *Transport in Porous Media,* 106**,** 303-321.

AMBILY, A. P. & GANDHI, S. R. 2007. Behavior of Stone Columns Based on Experimental and FEM Analysis. *Journal of geotechnical and geoenvironmental engineering,* 133**,** 405-415.

ANDERSEN, K. H., KLEVEN, A. & HEIEN, D. 1988. Cyclic Soil Data for Design of Gravity Structures. *Journal of Geotechnical Engineering*.

ANSAL, A. M. & ERKEN, A. 1989. Undrained behavior of clay under cyclic shear stresses. *Journal of Geotechnical Engineering*.

ARULRAJAH, A., ABDULLAH, A., BO, M. & BOUAZZA, A. 2009. Ground improvement techniques for railway embankments. *Proceedings of the Institution of Civil Engineers-Ground Improvement,* 162**,** 3-14.

ASAOKA, A., KODAKA, T. & NOZU, M. 1994. undrained shear strength of clay improved with sand compaction piles. *Soils and foundations,* 34**,** 23-32.

ASHFORD, S., ROLLINS, K., BRADFORD V, S., WEAVER, T. & BAEZ, J. 2000. Liquefaction mitigation using stone columns around deep foundations: Full-scale test results. *Transportation Research Record: Journal of the Transportation Research Board***,** 110-118.

ASTM 2004. Standard Test Method for Load Controlled Cyclic Triaxial Strength of Soil. *ASTM D5311.* Annual Book of ASTM Standards.

ASTM 2011. Standard Test Method for Consolidated Undrained Triaxial Compression Test for Cohesive Soils. *ASTM D4767-11.* West Conshohocken, PA.

BALAAM, N. P. 1978. *Load settlement behaviour of granular piles.* Doctor of Philosophy, University of Sidney.

BALAAM, N. P. & BOOKER, J. R. 1981. Analysis of Rigid Rafts supported by Granular Piles. *International Journal for Numerical and Analytical Methods in Geomechanics,* 5**,** 379-403.

BARKSDALE, R. D. & BACHUS, R. C. 1983. Design and Construction of Stone Column. *No. FHWA-RD-83-026 Final Rpt.*

BARRON, R. 1948. The influence of drain wells on the consolidation of fine-grained soils. *Diss., Providence, US Eng. Office*.

BASACK, S., SIAHAAN, F., INDRARATNA, B. & RUJIKIATKAMJORN, C. Influence of clogging on the performance of stone column improved soft ground. 15 th PanAmerican Conference on Soil Mechanics and Goetechnical Engineering, 2015.

BISHOP, D. A proposed geological model and geotechnical properties of a NSW estuarine valley: A case study. Proc., 9th ANZ conference on geomechanics, 2004. New Zealand Geotechnical Society, Auckland, New Zealand, 261-267.

BLACK, J., SIVAKUMAR, V. & MCKINLEY, J. D. 2007. Performance of clay samples reinforced with vertical granular columns. *Canadian Geotechnical Journal,* 44**,** 89-95.

BLACK, J. A., SIVAKUMAR, V. & BELL, A. 2011. The settlement performance of stone column foundations. *Géotechnique,* 61**,** 909-922.

BOUASSIDA, M. 2016. *Design of Column-Reinforced Foundations,* FL, USA, J. Ross Publishing.

BOUASSIDA, M., BUHAN, P. D. & DORMIEUX, L. 1995. Bearing capacity of a foundation resting on a soil reinforced by a group of columns. *Géotechnique,* 45**,** 25-34.

BOUASSIDA, M. & CARTER, J. P. 2014. Optimization of Design of Column-Reinforced Foundations. *International Journal of Geomechanics***,** 04014031.

BROMS, B. & CASBARIAN, A. 1965. Effects of rotation of the principal stress axes and of the intermediate principal stress on the shear strength. *Proceedings of the 6th ICSMFE, Montreal,* 1**,** 179-183.

BROWN, S. 1996. Soil mechanics in pavement engineering. *Géotechnique,* 46**,** 383-426.

BROWN, S. F., LASHINE, A. K. F. & HYDE, A. F. L. 1975. Repeated load triaxial testing of a silty clay. *Géotechnique*.

CARRIER III, W. D. 2003. Goodbye, hazen; hello, kozeny-carman. *Journal of geotechnical and geoenvironmental engineering,* 129**,** 1054-1056.

CARRILLO, N. 1942. Simple two and three dimensional cases in the theory of consolidation of soils. *Journal of Mathematics and Physics,* 21**,** 1-5.

CASACRANDE, A. & WILSON, S. 1951. Effect of rate of loading on the strength of clays and shales at constant water content. *Géotechnique,* 2**,** 251-263.

CASTRO, J. & KARSTUNEN, M. 2010. Numerical simulations of stone column installation. *Canadian Geotechnical Journal,* 47**,** 1127-1138.

CASTRO, J., KARSTUNEN, M. & SIVASITHAMPARAM, N. 2014. Influence of stone column installation on settlement reduction. *Computers and Geotechnics,* 59**,** 87-97.

CHARLES, J. & WATTS, K. Compressibility of soft clay reinforced with granular columns. Proceedings of the 8th European conference on soil mechanics and foundation Engineering, Helsinki, 1983. 347-352.

CHRISTOULAS, S., BOUCKOVALAS, G. & GIANNAROS, C. 2000. An experimental study on model stone columns. *Soils and foundations,* 40**,** 11-22.

CIMENTADA, A., DA COSTA, A., CA IZAL, J. & SAGASETA, C. 2011. Laboratory study on radial consolidation and deformation in clay reinforced with stone columns. *Canadian Geotechnical Journal,* 48**,** 36-52.

DEB, K. & SHIYAMALAA, S. 2015. Effect of Clogging on Rate of Consolidation of Stone Column–Improved Ground by Considering Particle Migration. *International Journal of Geomechanics***,** 04015017.

DELEO, P. 1995. Microbial clogging of saturated soils and aquifer materials: Evaluation of mathematical models. *Water Resources Research,* 31**,** 2173-2180.

DHEERENDRA BABU, M. R., NAYAK, S. & SHIVASHANKAR, R. 2012. A Critical Review of Construction, Analysis and Behaviour of Stone Columns. *Geotechnical and Geological Engineering,* 31**,** 1-22.

FATAHI, B., BASACK, S., PREMANANDA, S. & KHABBAZ, H. 2012. Settlement prediction and back analysis of Young's modulus and dilation angle of stone columns. *Australian Journal of Civil Engineering,* 10**,** 67-79.

GRAHAM, J., CROOKS, J. H. A. & BELL, A. L. 1983. Time effects on the stress-strain behavior of natural soft clays. *Géotechnique,* 33**,** 327-340.

GREENWOOD, D. 1975. Vibroflotation: rationale for design and practice. *Methods of treatment of unstable ground***,** 189-209.

GREENWOOD, D. & KIRSCH, K. Specialist ground treatment by vibratory and dynamic methods. Proceedings of the International Conference on Advances in Piling and Ground Treatment for Foundations, 1983. 17-45.

GUETIF, Z., BOUASSIDA, M. & DEBATS, J. M. 2007. Improved soft clay characteristics due to stone column installation. *Computers and Geotechnics,* 34**,** 104-111.

HAN, J. & YE, S. L. 2001. Simplified Method for Consolidation Rate of Stone Column Reinforced Foundations. *Journal of Geotechnical and Geoenvironmental Engineering,* 127**,** 597-603.

HAN, J. & YE, S. L. 2002. A Theoretical Solution for Consolidation Rates of Stone Column-Reinforced Foundations Accounting for Smear and Well Resistance Effects. *The International Journal Geomechanics,* 2**,** 135-151.

HANSBO, S., JAMIOLKOWSKI, M. & KOK, L. 1981. Consolidation by vertical drains. *Géotechnique,* 31**,** 45-66.

HU, W. 1995. *Physical modellings of group stone columns.* Doctor of Philosophy, University of Glasgow.

HUANG, C., SUI, Z., WANG, L. & LIU, K. 2016. Mitigation of Soil Liquefaction Using Stone Columns: An Experimental Investigation. *Marine Georesources & Geotechnology,* 34**,** 244-251.

HUGHES, J. M. O. & WITHERS, N. J. 1974. Reinforcing of soft cohesive soils with stone columns. *Ground Engineering,* 7.

HUGHES, J. M. O., WITHERS, N. J. & GREENWOOD, D. A. 1975. A field trial of the reinforcing effect of a stone column in soil. *Géotechnique,* 25**,** 31-44.

HUSTON, D. L. & FOX, J. F. 2015. Clogging of fine sediment within gravel substrates: Dimensional analysis and macroanalysis of experiments in hydraulic flumes. *Journal of Hydraulic Engineering,* 141**,** 04015015.

HYDE, A. & WARD, S. 1986. The effect of cyclic loading on the undrained shear strength of a silty clay. *Marine Georesources & Geotechnology,* 6**,** 299-314.

HYODO, M., YAMAMOTO, Y. & SUGIYAMA, M. 1994. Undrained cyclic shear behaviour of normally consolidated clay subjected to initial static shear stress. *Soils and foundations*.

INDRARATNA, B., ATTYA, A. & RUJIKIATKAMJORN, C. 2009. Experimental Investigation on Effectiveness of a Vertical Drain under Cyclic Loads. *Journal of Geotechnical and Geoenvironmental Engineering*.

INDRARATNA, B., BALASUBRAMANIAM, A. & BALACHANDRAN, S. 1992. Performance of test embankment constructed to failure on soft marine clay. *Journal of Geotechnical Engineering,* 118**,** 12-1.

INDRARATNA, B., BASACK, S. & RUJIKIATKAMJORN, C. 2013. Numerical Solution of Stone Column–Improved Soft Soil Considering Arching, Clogging, and Smear Effects. *Journal of Geotechnical and Geoenvironmental Engineering,* 139**,** 377-394.

INDRARATNA, B., IONESCU, D. & CHRISTIE, H. 1998. Shear behavior of railway ballast based on large-scale triaxial tests. *Journal of geotechnical and geoenvironmental Engineering,* 124**,** 439-449.

INDRARATNA, B., SALIM, W. & RUJIKIATKAMJORN, C. 2011. Advanced rail geotechnology-ballasted track.

INDRARATNA, B., THAKUR, P. K. & VINOD, J. S. 2010. Experimental and Numerical Study of Railway Ballast Behavior under Cyclic Loading. *International Journal of Geomechanics*.

INDRARATNA, B. & VAFAI, F. 1997. Analytical model for particle migration within base soil-filter system. *Journal of Geotechnical and Geoenvironmental Engineering,* 123**,** 100-109.

INDRARATNA, B., WIJEWARDENA, L. & BALASUBRAMANIAM, A. 1993. Large-scale triaxial testing of grey wacke rockfill. *Géotechnique,* 43**,** 37-51.

ISHIBASHI, I. & HAZARIKA, H. 2010. *Soil mechanics fundamentals*, CRC Press.

ISHIHARA, K. & TOWHATA, I. 1983. Sand response to cyclic rotation of principal stress directions as induced by wave loads. *Soils and foundations,* 23**,** 11-26.

JIANG, M., CAI, Z., CAO, P. & LIU, D. Effect of Cyclic Loading Frequency on Dynamic Properties of Marine Clay. Soil Dynamics and Earthquake Engineering, 2010. ASCE, 240-245.

JURAN, I. & GUERMAZI, A. 1988. Settlement response of soft soils reinforced by compacted sand columns. *Journal of geotechnical engineering,* 114**,** 930-943.

KELLER. 2017. *Deep Vibro Techniques* [Online]. Keller Websites Worldwide. Available: http://www.kellerholding.com/deep-vibro-techniques.html [Accessed May, 2018.

KELLY, P. 2014. *Soil Structure Interaction and Group Mechanics of Vibrated Stone Column Foundations.* University of Sheffield.

KELLY, R. B., MUTTUVEL, T. & CHAN, K. F. 2011. Lateral Displacements in Soft Soil Due to Installation of Vibro-Stone Columns Using the Dry Method. *Geo-Frontiers 2011@ sAdvances in Geotechnical Engineering***,** 549-556.

KELLY, R. B., PINEDA, J. A., BATES, L., SUWAL, L. P. & FITZALLEN, A. 2017. Site characterisation for the Ballina field testing facility. *Géotechnique,* 67**,** 279-300.

KIRSCH, F. 2006. Vibro stone column installation and its effect on ground improvement. *Int. Conf. on" Numerical Simulation of Construction Processes in Geotechnical Engineering for Urban Environment*.

KOLEKAR, Y. A., MIR, O. S. & DASAKA, S. M. 2012. Laboratory Studies on the Behavior of Floating Stone Column Under Cyclic Loads. *ICGI Wollongong 2012*. Wollongong.

KUMRUZZAMAN, M. & YIN, J. H. 2010. Influences of principal stress direction and intermediate principal stress on the stress-strain-strength behaviour of completely decomposed granite. *Canadian Geotechnical Journal,* 47**,** 164-179.

LACKENBY, J., INDRARATNA, B., MCDOWELL, G. & CHRISTIE, D. 2007. Effect of confining pressure on ballast degradation and deformation under cyclic triaxial loading. *Géotechnique,* 57**,** 527-536.

LAREW, H. & LEONARDS, G. A strength criterion for repeated loads. Highway Research Board Proceedings, 1962.

LEE, F. H., JUNEJA, A. & TAN, T. S. 2004. Stress and pore pressure changes due to sand compaction pile installation in soft clay. *Géotechnique,* 54**,** 1-16.

LEFEBVRE, G. & LEBOEUF, D. 1987. Rate effects and cyclic loading of sensitive clays. *Journal of Geotechnical Engineering,* 113**,** 476-489.

LEI, G., FU, C. & NG, C. 2016. Vertical-drain consolidation using stone columns: An analytical solution with an impeded drainage boundary under multi-ramp loading. *Geotextiles and Geomembranes,* 44**,** 122-131.

LEI, G., ZHENG, Q., NG, C., CHIU, A. & XU, B. 2015. An analytical solution for consolidation with vertical drains under multi-ramp loading. *Géotechnique,* 65**,** 531-547.

LEKHA, K., KRISHNASWAMY, N. & BASAK, P. 1998. Consolidation of clay by sand drain under time-dependent loading. *Journal of Geotechnical and Geoenvironmental engineering,* 124**,** 91-94.

LEO, C. J. 2004. Equal strain consolidation by vertical drains. *Journal of Geotechnical and Geoenvironmental engineering,* 130**,** 316-327.

LIN, H. & PENUMADU, D. 2005. Experimental investigation on principal stress rotation in Kaolin clay. *Journal of Geotechnical and Geoenvironmental engineering,* 131**,** 633-642.

LIU, J. K. & XIAO, J. H. 2010. Experimental Study on the Stability of Railroad Silt Subgrade with Increasing Train Speed. *Journal of Geotechnical and Geoenvironmental engineering,* 136**,** 833-841.

LU, M. M., XIE, K. H. & GUO, B. 2010. Consolidation theory for a composite foundation considering radial and vertical flows within the column and the variation of soil permeability within the disturbed soil zone. *Canadian Geotechnical Journal,* 47**,** 207-217.

MADHAV, M. R. & ARLEKAR, J. N. 2000. Dilation of granular piles in mitigating liquefaction of sand deposits. *12th World Conference Earthquake Engineering.*

MATSUBARA, K., MIHARA, M. & TSUJITA, M. 1988. Analysis of gravel drain against liquefaction and its application to design. *ANALYSIS,* 4**,** 3-12.

MCCABE, B. A., EGAN, D. & NIMMONS, G. J. 2009. A review of field performance of stone columns in soft soils. *Proceedings of the ICE - Geotechnical Engineering,* 162**,** 323-334.

MCCABE, B. A., MCNEILL, J. A. & BLACK, J. A. 2007. Ground Improvement VibroStone ColumnTechnique. *Joint meeting of Engineers Ireland West Region and the Geotechnical Society of Ireland*.

MCKELVEY, D. 2002. *The performance of vibro stone column reinforced foundations in deep soft ground.* Queen's University of Belfast.

MCKELVEY, D., SIVAKUMAR, V., BELL, A. & GRAHAM, J. 2004. Modelling vibrated stone columns in soft clay. *Proceedings of the ICE-Geotechnical Engineering*.

MESRI, G. 1975. New design procedure for stability of soft clays. *Journal of Geotechnical and Geoenvironmental Engineering,* 101.

MILLER, G. A., TEH, S. Y., LI, D. & ZAMAN, M. M. 2000. Cyclic Shear Strength of Soft Railroad Subgrade. *Journal of Geotechnical and Geoenvironmental engineering*.

MITCHELL, J. K. Soil improvement-state of the art report. Proc., 11th Int. Conf. on SMFE, 1981. 509-565.

MITCHELL, J. K. & HUBER, T. R. 1985. Performance of a Stone Column Foundation. *Journal of Geotechnical Engineering,* 111**,** 205-223.

MOREAU, N. & MOREAU, M. 1935. Foundations. Emploi du Sable. *Annales des ponts et chausses. Memoires***,** 171-214.

MORTEZAIE, A. R. & VUCETIC, M. 2013. Effect of frequency and vertical stress on cyclic degradation and pore water pressure in clay in the NGI simple shear device. *Journal of Geotechnical and Geoenvironmental Engineering,* 139**,** 1727-1737.

NI, J. 2012. *Application of geosynthetic vertical drains under cyclic loads in stabilizing tracks.* Doctoral dissertation, University of Wollongong.

OTSU, N. 1975. A threshold selection method from gray-level histograms. *Automatica,* 11**,** 23-27.

PARIHAR, A. K., MIR, B. A. & JUNEJA, A. 2011. Effects of sand compaction pile installation in model clay beds. *International Journal of Geotechnical Engineering,* 5**,** 199-209.

PILLAI, R. J., ROBINSON, R. & BOOMINATHAN, A. 2011. Effect of microfabric on undrained static and cyclic behavior of kaolin clay. *Journal of Geotechnical and Geoenvironmental Engineering,* 137**,** 421-429.

PINEDA, J. A., SUWAL, L. P., KELLY, R. B., BATES, L. & SLOAN, S. W. 2016. Characterisation of Ballina clay. *Géotechnique,* 66**,** 556-577.

PRIEBE, H. J. 1995. The Design of Vibro Replacement. *Ground engineering,* 28**,** 31.

PROCTER, D. C. & KHAFFAF, J. H. 1984. Cyclic triaxial tests on remoulded clays. *Journal of Geotechnical Engineering,* 110**,** 1431-1445.

RANDOLPH, M. F. & WROTH, C. 1979. An analytical solution for the consolidation around a driven pile. *International Journal for Numerical and Analytical Methods in Geomechanics,* 3**,** 217-229.

RAYAMAJHI, D., ASHFORD, S. A., BOULANGER, R. W. & ELGAMAL, A. 2016a. Dense Granular Columns in Liquefiable Ground. I: Shear Reinforcement and Cyclic Stress Ratio Reduction. *Journal of Geotechnical and Geoenvironmental Engineering***,** 04016023.

RAYAMAJHI, D., BOULANGER, R. W., ASHFORD, S. A. & ELGAMAL, A. 2016b. Dense Granular Columns in Liquefiable Ground. II: Effects on Deformations. *Journal of Geotechnical and Geoenvironmental Engineering,* 142**,** 04016024.

REDDI, L. N., MING, X., HAJRA, M. G. & LEE, I. M. 2000. Permeability reduction of soil filters due to physical clogging. *Journal of Geotechnical and Geoenvironmental engineering,* 126**,** 236-246.

RICHART, F. E. 1959. Review of the theories for sand drains. *Transactions of the American Society of Civil Engineers,* 124**,** 709-736.

RUJIKIATKAMJORN, C. & INDRARATNA, B. 2015. Analytical Solution for Radial Consolidation Considering Soil Structure Characteristics. *Canadian Geotechnical Journal*.

SANGREY, D., HENKEL, D. & ESRIG, M. 1969. The effective stress response of a saturated clay soil to repeated loading. *Canadian Geotechnical Journal,* 6**,** 241-252.

SASAKI, Y. & TANIGUCHI, E. 1982. Shaking table tests on gravel drains to prevent liquefaction of sand deposits. *Soils and Foundations,* 22**,** 1-14.

SCHOFIELD, A. & WROTH, P. 1968. *Critical state soil mechanics,* McGraw-Hill London.

SEED, H. B. & BOOKER, J. R. 1977. Stabilization of potentially liquefiable sand deposits using gravel drains. *Journal of Geotechnical and Geoenvironmental Engineering,* 103.

SHAHU, J. T., MADHAV, M. R. & HAYASHI, S. 2000. Analysis of soft ground-granular pile-granular mat system. *Computers and Geotechnics,* 27**,** 45-62.

SHAHU, J. T. & REDDY, Y. R. 2011. Clayey soil reinforced with stone column group: model tests and analyses. *Journal of Geotechnical and Geoenvironmental Engineering,* 137**,** 1265-1274.

SHEAHAN, T. C., LADD, C. C. & GERMAINE, J. T. 1996. Rate-dependent undrained shear behavior of saturated clay. *Journal of Geotechnical Engineering,* 122**,** 99-108.

SIMPSON, D. C. & EVANS, T. M. 2016. Behavioral thresholds in mixtures of sand and kaolinite clay. *Journal of Geotechnical and Geoenvironmental Engineering,* 142**,** 04015073.

SIRIWARDENE, N., DELETIC, A. & FLETCHER, T. 2007. Clogging of stormwater gravel infiltration systems and filters: Insights from a laboratory study. *Water research,* 41**,** 1433-1440.

SIVAKUMAR, V., MCKELVEY, D., GRAHAM, J. & HUGHES, D. 2004. Triaxial tests on model sand columns in clay. *Canadian Geotechnical Journal,* 41**,** 299-312.

TAI, P., INDRARATNA, B. & RUJIKIATKAMJORN, C. 2017. Experimental Simulation and Mathematical Modelling of Clogging in Stone Column. *Canadian Geotechnical Journal*.

TAKAHASHI, M., HIGHT, D. & VAUGHAN, P. Effective stress changes observed during undrained cyclic triaxial tests on clay. Proceedings of the International Symposium on Soils under Cyclic and Transient Loading, Swansea, 1980. 201-209.

TANG, X. W. & ONITSUKA, K. 1998. CONSOLIDATION OF GROUND WITH PARTIALLY PENETRATED VERTICAL DRAINS. *Geotechnical Engineering*.

TAYLOR, D. 1948. *Fundamentals of soil mechanics,* Chapman And Hall, Limited.; New York.

TERZAGHI, K. 1943. *Theoretical soil mechanics,* New York, Wiley.

TORISU, S., PEREIRA, J.-M., DE GENNARO, V., DELAGE, P. & PUECH, A. 2012. Strain-rate effects in deep marine clays from the Gulf of Guinea. *Géotechnique,* 62**,** 767-775.

VALDES, J. R. & SANTAMARINA, J. C. 2006. Particle clogging in radial flow: Microscale mechanisms. *SPE Journal,* 11**,** 193-198.

VUCETIC, M. & DOBRY, R. 1988. Degradation of marine clays under cyclic loading. *Journal of Geotechnical Engineering,* 114**,** 133-149.

WALKER, R. & INDRARATNA, B. 2006. Vertical drain consolidation with parabolic distribution of permeability in smear zone. *Journal of Geotechnical and Geoenvironmental Engineering,* 132**,** 937-941.

WANG, C. & CHEN, Y.-M. 2007. Study on effect of traffic loading induced static deviator stress on undrained cyclic properties of saturated soft clay. *Chinese Journal of Geotechnical Engineering,* 29**,** 1742-1747.

WANG, G. 2009. Consolidation of Soft Clay Foundations Reinforced by Stone Columns under Time-Dependent Loadings. *Journal of Geotechnical and Geoenvironmental engineering,* 135**,** 1922-1931.

WATABE, Y., YAMADA, K. & SAITOH, K. 2011. Hydraulic conductivity and compressibility of mixtures of Nagoya clay with sand or bentonite. *Géotechnique,* 61**,** 211-219.

WEBER, T. M., PESCHKE, G., LAUE, J., PL TZE, M. & SPRINGMAN, S. M. 2010. Smear zone identification and soil properties around stone columns constructed in-flight in centrifuge model tests. *Géotechnique,* 60**,** 197-206.

WHITE, D. J., PHAM, H. T. & HOEVELKAMP, K. K. 2007. Support mechanisms of rammed aggregate piers. I: Experimental results. *Journal of Geotechnical and Geoenvironmental Engineering,* 133**,** 1503-1511.

WOOD, D. M., HU, W. & NASH, D. F. T. 2000. Group Effects in Stone Column Foundation-Model Tests. *Géotechnique,* 50**,** 689-698.

XIE, K.-H., LU, M.-M., HU, A.-F. & CHEN, G.-H. 2008. A general theoretical solution for the consolidation of a composite foundation. *Computers and Geotechnics,* 36**,** 24-30.

XIE, K. H., LU, M. M. & LIU, G. B. 2009. Equal strain consolidation for stone columns reinforced foundation. *International Journal for Numerical and Analytical Methods in Geomechanics,* 33**,** 1721-1735.

YASUHARA, K. Consolidation and settlement under cyclic loading. Proceedings of the international symposium on compression and consolidation of clayey soils. Hiroshima, 1995.

YASUHARA, K., YAMANOUCHI, T. & HIRAO, K. 1982. Cyclic strength and deformation of normally consolidated clay. *Soils and foundations*.

YONG, C. F., MCCARTHY, D. T. & DELETIC, A. 2013. Predicting physical clogging of porous and permeable pavements. *Journal of Hydrology,* 481**,** 48-55.

ZHANG, Y., XIE, K. & WANG, Z. 2006. Consolidation analysis of composite ground improved by granular columns considering variation of permeability coefficient of soil. *Geotechnical Special Publication,* 152**,** 135.

ZHOU, J. & GONG, X. 2001. Strain degradation of saturated clay under cyclic loading. *Canadian Geotechnical Journal,* 38**,** 208-212.

ZHU, G. & YIN, J.-H. 2001. Consolidation of soil with vertical and horizontal drainage under ramp load. *Géotechnique,* 51**,** 361-367.

ZHU, G. & YIN, J.-H. 2004a. Consolidation analysis of soil with vertical and horizontal drainage under ramp loading considering smear effects. *Geotextiles and Geomembranes,* 22**,** 63-74.

ZHU, G. & YIN, J. H. 2004b. Accuracy of Carrillo's formula for consolidation of soil with vertical and horizontal drainage under time‐dependent loading. *Communications in numerical methods in engineering,* 20**,** 721-735.

ZHU, J.-G. & YIN, J.-H. 2000. Strain-rate-dependent stress-strain behavior of overconsolidated Hong Kong marine clay. *Canadian Geotechnical Journal,* 37**,** 1272-1282.